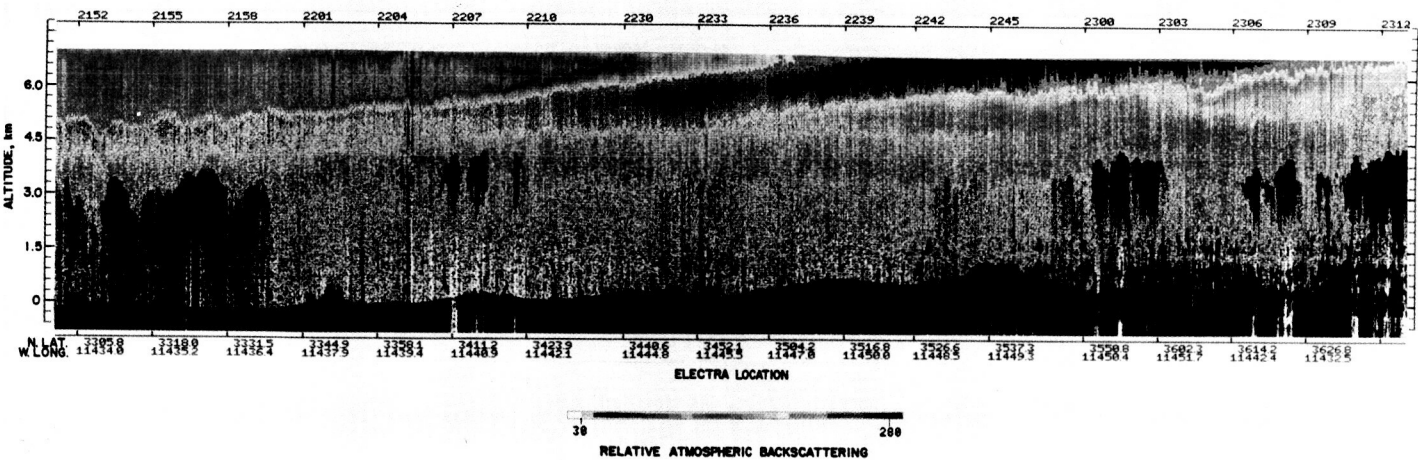


ORIGINAL PAGE IS  
OF POOR QUALITY

CHAPTER

# STRAT-TROP EXCHANGE

AIRBORNE DIAL AEROSOL MEASUREMENT OF TROPOPAUSE FOLD EVENT  
APRIL 20, 1984  
TIME, GMT



## Panel Members

A.F. Tuck, Chairman

- |                |              |
|----------------|--------------|
| E.V. Browell   | D. Kley      |
| E.F. Danielsen | A.J. Krueger |
| J.R. Holton    | G. Megie     |
| B.J. Hoskins   | R.E. Newell  |
| D.R. Johnson   | G. Vaughan   |

## CHAPTER 5

### STRATOSPHERE-TROPOSPHERE EXCHANGE

#### TABLE OF CONTENTS

5.0 INTRODUCTION .....	151
5.1 EXCHANGE IN THE TROPICS .....	152
5.1.1 Meteorological Processes .....	152
5.1.2 Cumulonimbus Clouds .....	164
5.1.3 Aircraft Studies near Cumulonimbus Anvils in Panama .....	168
5.1.4 Discussion of Tropical Exchange .....	172
5.1.5 Summary of Tropical Exchange .....	173
5.2 EXTRATROPICAL EXCHANGE .....	174
5.2.1 Meteorological Processes .....	174
5.2.2 A Theoretical View of Mid-latitude Exchange .....	181
5.2.2.1 Deductions from Two-dimensional Models .....	181
5.2.2.2 Deductions from Three-dimensional Models .....	183
5.2.2.3 Diabatic Processes .....	184
5.2.3 A View Based on Isentropic FGGE Analyses .....	186
5.2.3.1 Systematic Meridional Exchange by Geostrophic Modes of Isentropic Mass Transport .....	188
5.2.3.2 Geostrophic Modes of Mass Transport and Quasi-horizontal Stratospheric- Tropospheric Exchange Within Middle Latitudes .....	190
5.2.3.3 Some Additional Aspects of Stratospheric-Tropospheric Exchange in Mid- latitudes .....	194
5.2.3.4 Summary of Isentropic Analyses .....	196
5.2.4 A Review of Past Work on Exchange in Mid-latitudes .....	197
5.2.5 Recent Aircraft Studies near the British Isles .....	202
5.2.6 Recent Aircraft Studies over the South Western United States .....	210
5.2.6.1 Analyses and Measurements at and below the Jet .....	212
5.2.6.2 Analyses and Measurements above the Jet .....	218
5.2.7 Ground Based Studies over France .....	222
5.2.8 Global Coverage: TOMS Ozone Column Measurements .....	227
5.2.8.1 Brewer Circulation/ITCZ Exchange/Stratospheric Fountain .....	228
5.2.8.2 Tropopause Folding near Jet Streams .....	228
5.2.8.3 Cut-off Lows .....	229
5.3 LARGE SCALE NUMERICAL MODELLING OF STRATOSPHERE-TROPOSPHERE EXCHANGE .....	230
5.3.1 General Circulation Models .....	230
5.3.2 Operational Weather Forecasting Models .....	235
5.4 ASSESSMENT OF STRATOSPHERE-TROPOSPHERE EXCHANGE .....	235
5.4.1 Unresolved Problems .....	238
5.4.2 Recommended Future Studies .....	239

## 5.0 INTRODUCTION

Exchange between the stratosphere and troposphere is important to the chemical composition of both regions; the export of ozone from the stratosphere provides the troposphere with a means of initiating photochemistry (Levy, 1971), and the precursor molecules originating from the planetary surface provide the stratosphere with its chemical feedstock from which the ozone-controlling  $\text{HO}_x$ ,  $\text{NO}_x$  and  $\text{Cl}_x$  photochemistries are driven (Hampson, 1965, Crutzen, 1971, Molina and Rowland, 1974).

The coarsely characterized morphology of the meteorological circulation governing the ingress of tropospheric air to the stratosphere in the tropics was deduced from the dryness apparent in mid-latitude measurements of stratospheric water vapour by Brewer (1949); the egress of air in mid-latitudes via tropopause folding during upper frontogenesis was demonstrated by Reed (1955), Reed and Danielsen (1959) and Staley (1960) using isentropic potential vorticity as a tracer for stratospheric air.

There have been several estimates of the annual mass exchange between the stratosphere and the troposphere. Reiter, (1975) has written a review, and has also (Reiter, 1979) emphasized the interannual variability which could exist as a result of fluctuations in the intensity of the Inter Tropical Convergence Zone. The annual average of the exchange of air for one hemisphere of the stratosphere was 89%, distributed as follows: Hadley Cell 43%, large scale eddies near jet stream regions 20%, seasonal changes in tropopause height 10%, horizontal exchange with the other hemispheric stratosphere 16%. These numbers were largely obtained by diagnostic studies using meridional stream functions relative to isobaric coordinates, combined with a cyclogenesis index and statistics of the conventionally defined (thermal) tropopause.

Such studies however do not provide a great deal of insight into the cross-tropopause flux of trace molecules, such as ozone and water vapour, which have their own particular distributions of sources and sinks. Some of the problems were outlined in an earlier report (WMO, 1982), pages 2-91 to 2-99. In particular, the laminar, correlated structure in ozone and water vapour profiles in the lower mid-latitude stratosphere, and the detailed physics and scale of the desiccation mechanism near the tropical tropopause are not well understood. It follows that quantitative estimates of the global distribution of cross-tropopause flux for specific molecules remains elusive.

A further unresolved issue is the extent of exchange associated with steady jet streams, i.e., those not involved in rapid upper cyclogenesis. Krishnamurti (1961) suggested that a thermally direct transverse circulation existed for the northern winter subtropical jet stream, while Mahlman (1973) drew a similar conclusion for a composite analysis of a polar front jet stream over North America, averaged relative to the flow. These transverse circulations imply upward air motion on the anticyclonic (equatorward) side and at the jet core, and downward motion on the cyclonic (poleward) side. If such circulations transfer air across the tropopause, there is a limited usefulness to estimates of exchange using cyclogenetic indices, a conclusion supported by the study of radioactive fallout by Mahlman (1969a).

An important result was the discovery of the "hygropause" in the tropics (Kley *et al.*, 1979); the existence of a decrease in water vapour mixing ratio above the tropopause in mid-latitudes had been evident from the first measurements (Dobson, Brewer and Cwiling, 1946; Brewer, 1949) and confirmed by higher and more frequent measurements (Foot, 1984). Water vapour mixing ratios decrease from the tropopause by a factor of 20 or 30 in mid-latitudes over an altitude of a half to one pressure scale height, and by a factor of 2 or 3 in the tropics over a similar depth. These facts, and the frequent occurrence of the layered structure in vertical profiles of ozone for at least two scale heights above the mid-latitude

## STRAT-TROP EXCHANGE

tropopause, suggest that for some purposes it may be necessary to draw a distinction between this transition region and the middle and upper stratosphere above it.

Indeed, if one assumes a mixing ratio of 2.5 and 6.5 ppmv at the hygropause and tropopause, respectively, between 30°N and 30°S, and of 4 and 25 ppmv poleward of these latitudes, it is a simple matter to show that something like a quarter to a half of all stratospheric water vapour is between the tropopause and the hygropause. Of course, in the mean this fraction probably has a much lower residence time than the remaining amount above it.

It has become apparent during the last decade that the transport of mass and tracers by the general circulation is conceptually simplified by using entropy (potential temperature) as the vertical coordinate. This point of view, originated by Shaw (1942), has been revived by Dutton (1976) and Johnson (1980) for the troposphere, by Tung (1982) for the stratosphere and consistently advocated by Danielsen (1961, 1968; Danielsen and Hipskind, 1980) for studies at tropopause level. The isentropic perspective suggests that past estimates of global cross-tropopause mass flux, made by zonal mean Eulerian streamline calculations relative to pressure surfaces, may not be particularly reliable.

It is necessary to obtain good data on the covariance of mass and the mixing ratio of species whose transport across the tropopause is of interest. This is so because while potential vorticity  $P_\theta$  may in future be calculable from the global analyses produced by high resolution primitive equation numerical weather prediction models, it will still be necessary to know the correlation between  $P_\theta$  and the various chemical species in order to compute fluxes; such knowledge is derived currently from a small number of high quality case studies using aircraft and balloons. At present, global estimates of downward cross-tropopause fluxes rely on a very crude count of upper tropospheric cyclogenetic events to give the case study data a global dimension. The estimates of the upward flux in the tropics are even cruder, since the knowledge of the detailed physical characteristics and scale of the meteorological processes responsible is less secure, although substantial progress has been made recently. It remains true that almost all local, high quality knowledge of cross-tropopause flux is confined to the Northern Hemisphere, in the North American and British Isles/Western European sectors. Most of these data, moreover, have been obtained in the March-May period.

In this chapter, the tropopause is defined both statistically and in a local, synoptic sense by the value  $P_\theta = 1.6 \times 10^{-5} \text{ K m}^2\text{kg}^{-1}\text{s}^{-1}$ , taken from an objective analysis of 8 years of zonal, temporal mean cross-sections of potential temperature, wind and potential vorticity by Danielsen (1984), see Figure 5-1. The definition applies from the pole to within 5° latitude of the equator, where  $P_\theta$  changes sign, and is coincident with the conventionally defined tropopause. The analyses are consistent with those obtained in the FGGE year by the ECMWF analyses, see Figure 5-2. A difficulty of isentropic coordinates for work on longer time scales is that the motion of  $\theta$  surfaces with respect to geometric heights has to be established.

### 5.1 EXCHANGE IN THE TROPICS

#### 5.1.1 Meteorological Processes

There is a wide spectrum of circulation features in the tropical troposphere which involve vertical motions and which may be of importance in the transfer of air from the troposphere to the stratosphere and therefore in the ozone budget. The long-term mean motions are dominated by the planetary scale Hadley and Walker circulations, which are essentially statistical entities; temporal variability occurs on a wide

STRAT-TROP EXCHANGE

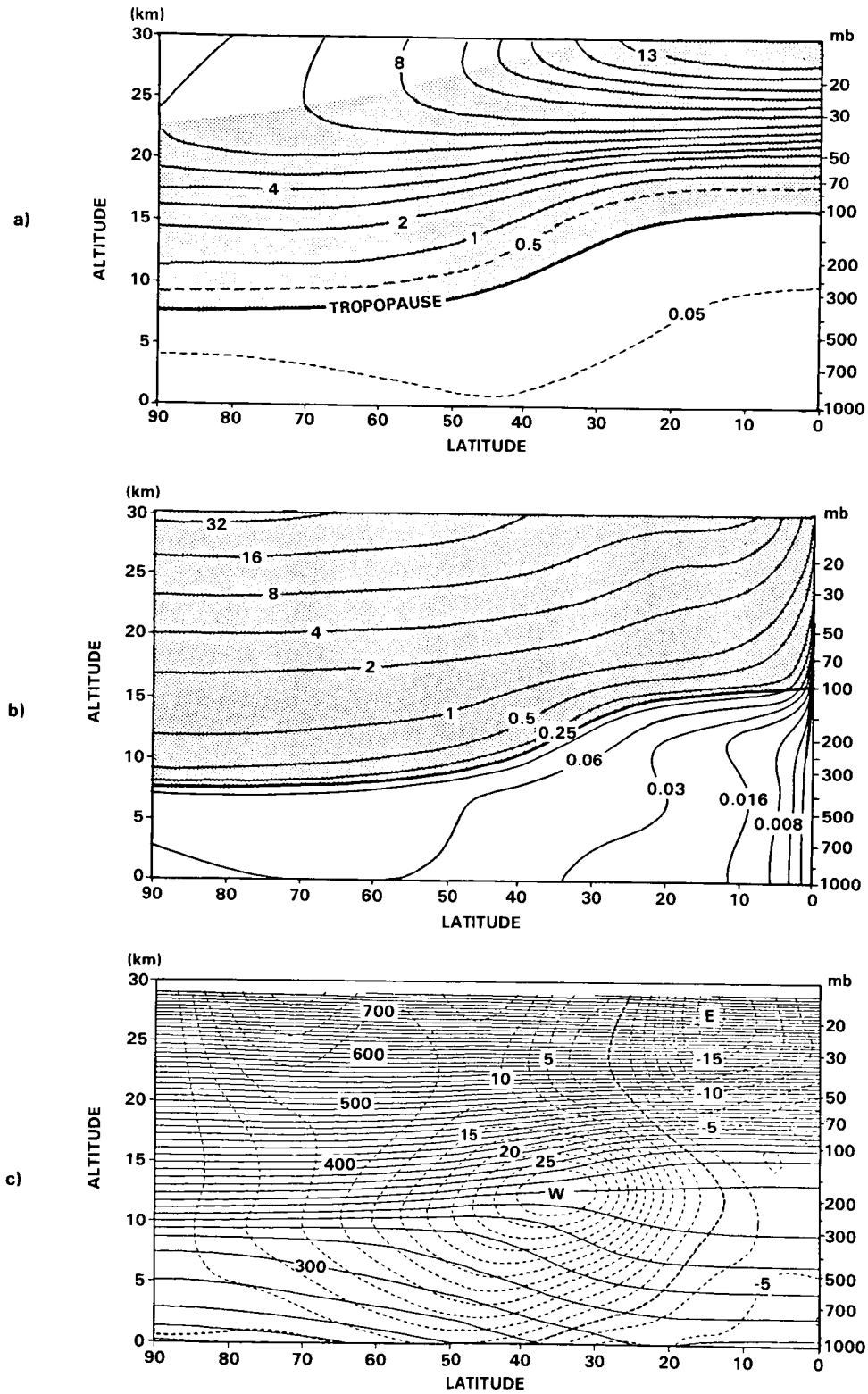
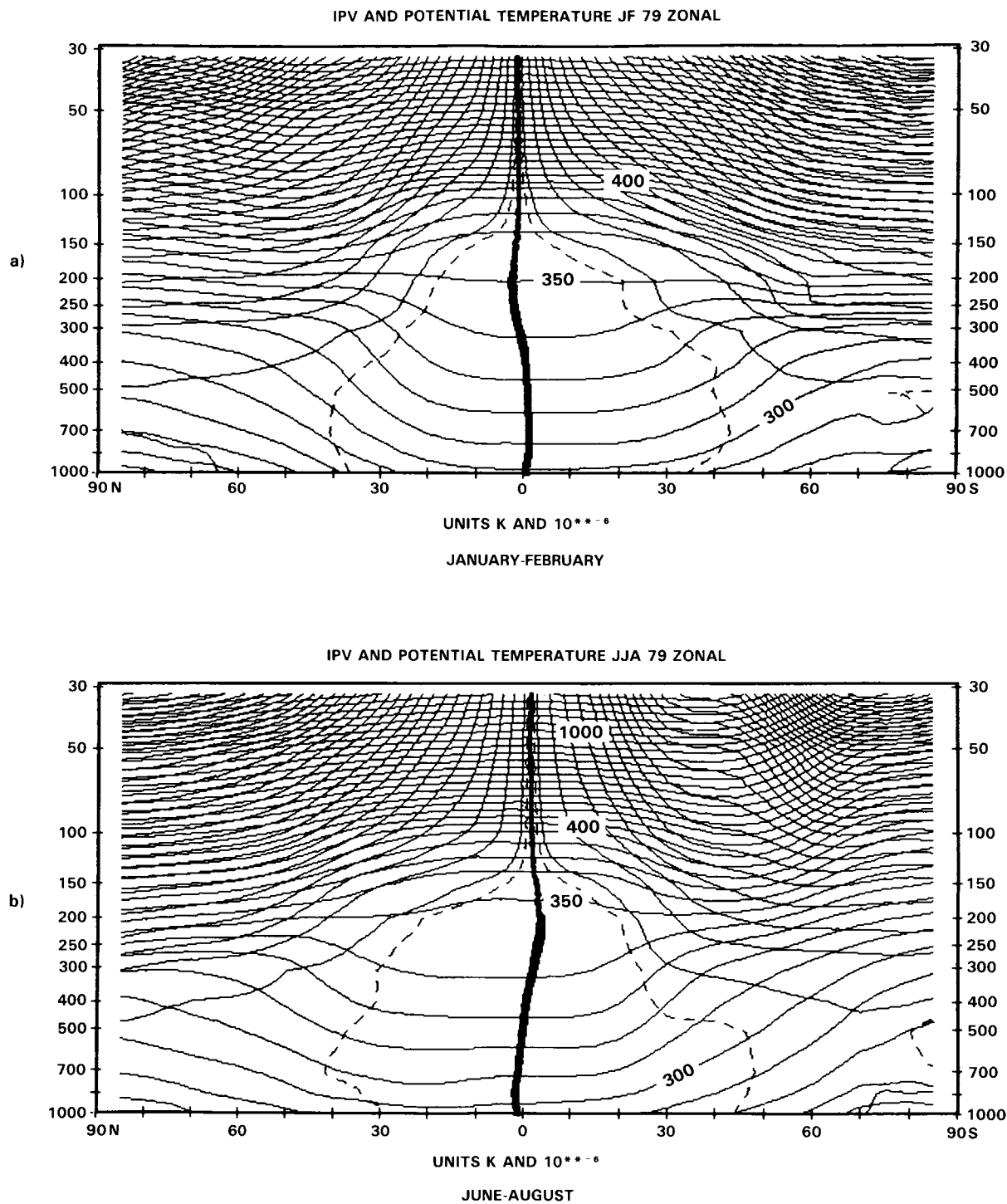


Figure 5-1. Zonal-annual mean distributions of: (a) ozone mixing ratio, ppmv; (b) potential vorticity,  $10^{-4} \text{ cm}^2 \text{ s}^{-1} \text{ K g}^{-1}$ ; (c) potential temperature, K, and westerly wind velocity,  $\text{m s}^{-1}$ .

# STRAT-TROP EXCHANGE



**Figure 5-2.** Zonal mean distributions of  $\theta$  and isentropic potential vorticity (IPV), ECMWF Analyses, FGGE year, 1979. Compare with Figures 5-1 b, c and 5-17. Data are (a) January and February, (b) June, July and August. The potential vorticity contours are 0,  $\pm 0.5$ ,  $\pm 1$ ,  $\pm 2 \dots$  in units of  $10^{-6} \text{ m}^2 \text{ s}^{-1} \text{ K kg}^{-1}$ ,  $\theta$  is contoured at 10 K up to 400 K and at 50 K when  $\theta > 400 \text{ K}$ . The 300 K contour touches the surface in the tropics.

variety of time and space scales down to the scale of the individual cumulonimbus clouds embedded in the larger circulation features. The annual cycles of the Hadley circulation and to a lesser extent the Walker circulation are evident in the north-south and east-west excursions of the tropical convergence zones which accompany the Asian and Australian monsoons as well as the cycles of rainy and dry weather elsewhere in the tropics.

Over much of the tropics, the nonseasonal variability of the Hadley and Walker circulations is primarily associated with the Southern Oscillation which is an interannual phenomenon although it is becoming apparent that there are prominent circulation changes at the subseasonal time scale of 40-50 days as well (Madden and Julian, 1971, 1972a; Anderson and Rosen, 1983; Lorenc, 1984). Synoptic scale disturbances in the tropical convergence zones include easterly waves and monsoon depressions which modulate the large-scale environment for the development of tropical storms and hurricanes and mesoscale disturbances such as squall lines and mesoscale cloud clusters. There are also important mesoscale circulations tied to localized interactions between the diurnal variation of solar heating and surface features; these include, for example, cloud clusters in the winter monsoon region and sea breeze circulations.

The long-term mean global scale flow in the upper tropical troposphere is well represented by the winds at the 150 mb level. Figure 5-3 shows the horizontal winds for January-February and June-August for the FGGE year 1979. The cross-equatorial flow in the western Pacific and the Indonesian region during northern winter and in the eastern Indian ocean in northern summer are the most important local contributions to the zonally symmetric meridional overturning known as the Hadley circulation. The zonal mean pattern of rising motion shifts from south of the equator in January-February to north of the equator in June-August.

Vertical motion is an extremely difficult quantity to estimate. At the synoptic scale it can be estimated kinematically from the divergence of the observed wind field; operational analyses now make use of reports from commercial airliners as well as cloud motion vectors to augment the conventional upper air network. Satellite measurements of tropical outgoing longwave radiation have also proved useful in identifying the spatial and temporal variability of the occurrence of the cold cloud tops associated with deep convection.

The zonal variability of rising motion in the tropics is part and parcel of a set of east-west overturnings which are known collectively as the Walker circulation. These overturnings are most easily seen in the divergent wind field and it has become customary to display the divergent winds in terms of the velocity potential from which it is derived. Figure 5-4 displays the fields of 150 mb velocity potential  $\chi$  for the northern winter and summer of 1979 derived from ECMWF analyses of the FGGE data set. Negative values of  $\chi$  may loosely be associated, in the large scale temporal mean, with rising motion, but should not be identified with vertical velocity. Relative minima in these maps correspond to regions of widespread rising motion; in January the negative center in the Indonesian and west Pacific region is associated with winter monsoon convection and in July the center over southern Asia is evidence of the rising motion due to the summer monsoon. It is worth noting that, as the contribution to the velocity potential from each wave component is inversely proportional to its squared wavenumber, a velocity potential field emphasizes the larger scale patterns of divergence and attendant rising motion; thus in these maps the Pacific-Indian Ocean Walker cells dominate.

The global wind analyses necessary to derive the transport potential fields implied in Figure 5-4 depend to a great extent on high level cloud motion estimates which are nominally applied to a single level only in the upper troposphere; unambiguous identification of penetration of the tropical tropopause in regions

STRAT-TROP EXCHANGE

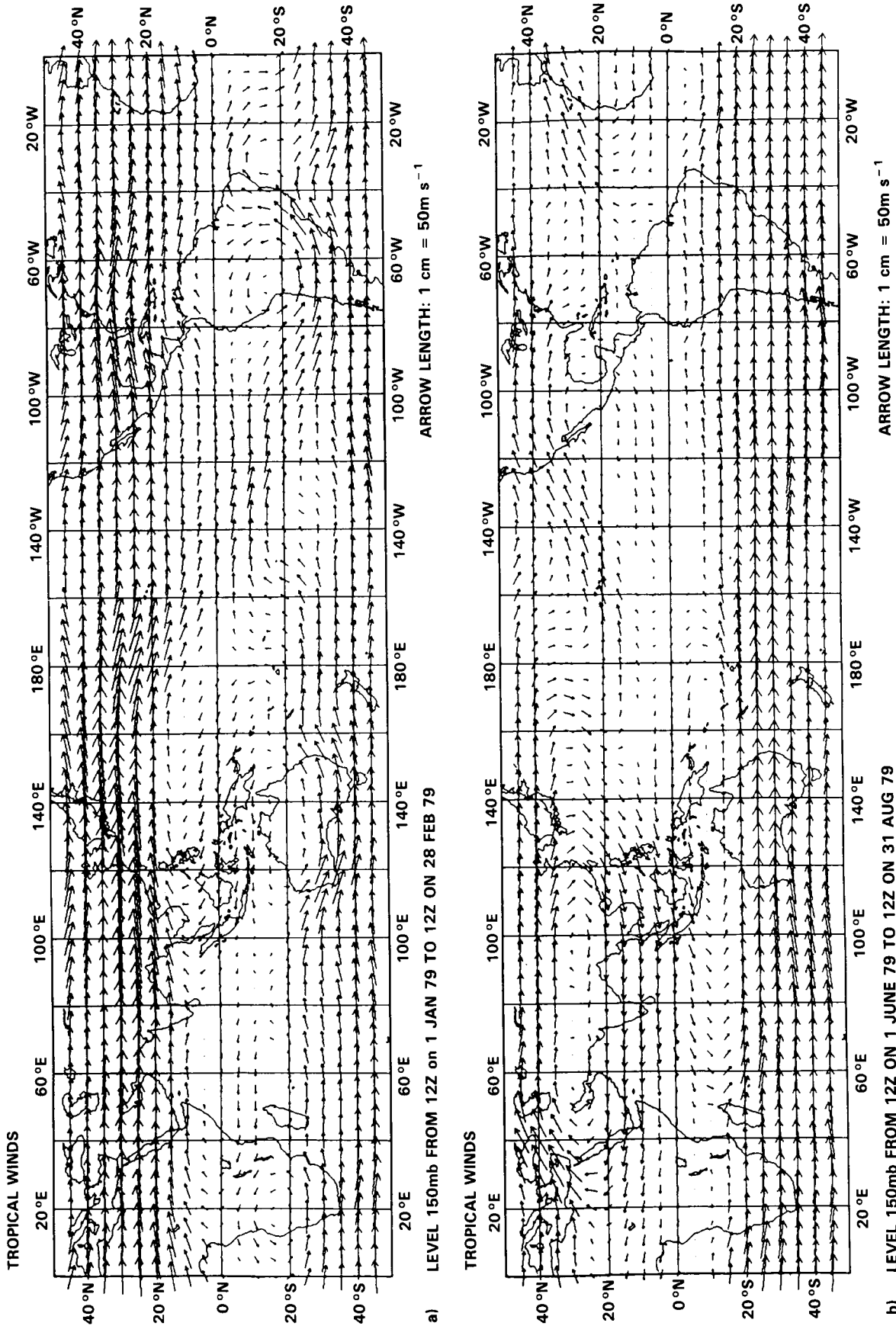
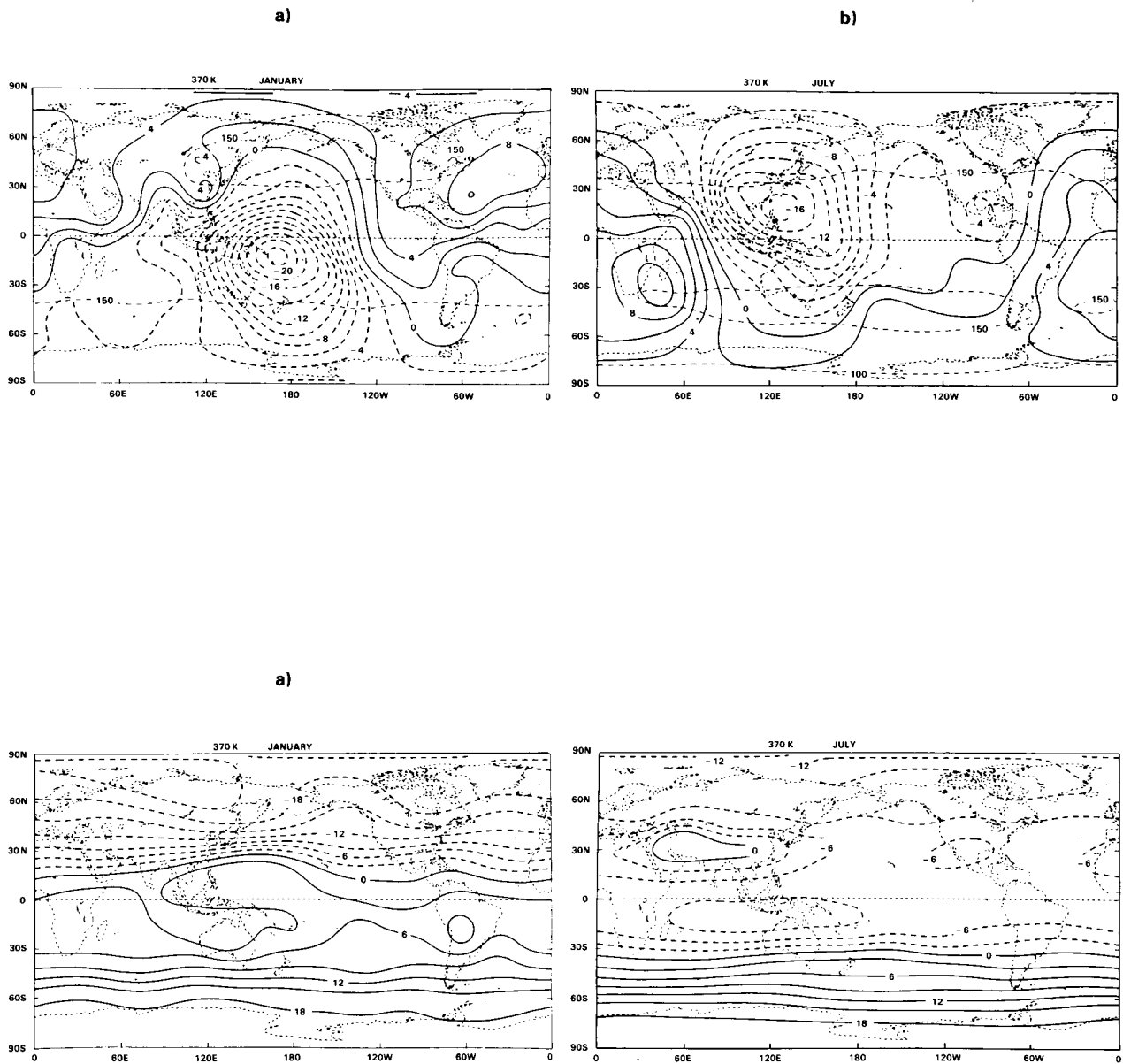


Figure 5-3. Streamlines of 150 mb winds in the tropics, ECMWF analyses, FGGE year, 1979. (a) January and February, (b) June, July and August. Note that some other analyses tend to show stronger cross-equatorial flow than those from ECMWF.

# STRAT-TROP EXCHANGE



**Figure 5-4.** Contours of velocity potential  $\chi$  (upper) and stream function  $\psi$  (lower) 370-380 K Level IIIb analyses, FGGE year, 1979.  $\mathbf{v} = \nabla\chi + \mathbf{k} \times \nabla\psi$ . Note that this decomposition of the velocity field accentuates the largest scales, particularly in  $\chi$ . Irrotational component of isentropic mass transport,  $\chi$ , is normal to contours in upper figures, from lower to higher values. Rotational component of isentropic mass transport,  $\psi$ , is parallel to contours in lower figures, with lower values on the left. (a) January, (b) July.

## STRAT-TROP EXCHANGE

of inferred vertical motion requires higher vertical resolution than is available in the conventional analyses.

Other indicators may suggest the passage of air upwards into the stratosphere. One readily available indicator is radiosonde temperature; cold temperatures are maintained at the tropical tropopause by the adiabatic expansion of air rising from below in deep convection. In the time mean the most vigorous convection is in longitudes 80°E to 180°E, as shown by the monthly 100 mb temperatures for 1979 in Figure 5-5, which was plotted for this report from radiosonde data. A study of 100 mb monthly mean temperatures by Newell and Gould-Stewart (1981) showed that these longitudes in November-February were cold enough to account for the dryness of the stratosphere, although this leaves open the question of the fate of the necessary ice crystals; in July the coldest areas are associated with the Indian monsoon although the 100 mb temperatures in this season are somewhat warmer than those in January. Temperatures at 100 mb below -82.4°C are low enough that the saturation moisture content is  $2 \times 10^{-6}$  mmr such as is observed in the stratosphere (see Chapter 9). Frederick and Douglass (1983) and Atticks and Robinson (1983) have come to the same general conclusion from studies of daily radiosonde data but find a considerably larger areal extent of the region of potential exchange.

As a means of measuring high cloud amount, outgoing longwave radiation measurements suffer from contamination with radiation from lower levels in the atmosphere; Barton (1983) has estimated high cloud frequency using two channels from the NIMBUS 5 radiometer data which are preferentially sensitive to high clouds. His results from the period December 1972 through February 1975 are shown in Figure 5-6. The main tropical regions where high clouds occur are the monsoon areas of the west Pacific and India with secondary regions over South America and Africa. From the three Januaries sampled, Barton found that the cloud was less confined to the west Pacific during the El Nino January of 1973. A similar El Nino dependence was found for rainfall (Rao, 1984), velocity potential (Climate Analysis Center, 1983, 1984) and outgoing longwave radiation (Lau and Chan, 1983), all pointing to a concentration of vertical motion in the west Pacific during cold periods.

Finally, another indicator of large-scale motion that influences the stratosphere is total ozone; this will clearly be lower where ozone-poor tropospheric air enters the lower stratosphere. The ozone data from the Nimbus 7 TOMS for the FGGE year 1979, January and July are shown in Figure 5-7. Lowest values occur in January in the west Pacific and South America with generally higher values occurring everywhere in the tropics in July. Ghazi (1980) has presented a series of total ozone maps that show a minimum in January in the west Pacific and over India in July, essentially in accordance with the findings of Newell and Gould-Stewart, and consistent with the annual cycles of tropopause temperature and total ozone at Gan (1°S, 73°E), Figure 5-8.

The network of upper air and surface stations in the tropics at best provides a grid of data that resolves motions on scales of several hundreds of kilometers; this data source as well as evidence from rainfall, cloud and total ozone measurements can be used to identify regions in which rising motion is occurring but they fall short of defining the scales on which the vertical motions are organized. Nevertheless, the contoured radiosonde data show coherent temperature structure on large scales at 100 mb (Figure 5-5). At the level of the tropical tropopause in particular a number of mechanisms for an exchange of air across the statistical boundary between the stratosphere and troposphere have been proposed to account for the dehydration which must occur as air becomes dry enough to be considered 'stratospheric'. Is penetrative vertical motion organized at the scale of individual overshooting cumulonimbus turrets? Or are there mesoscale regions of moderate ascent, driven by cloud heating from below and cooling at the top? Or is there gentle rising motion over a large area? With these questions in mind, and the fact that many scales

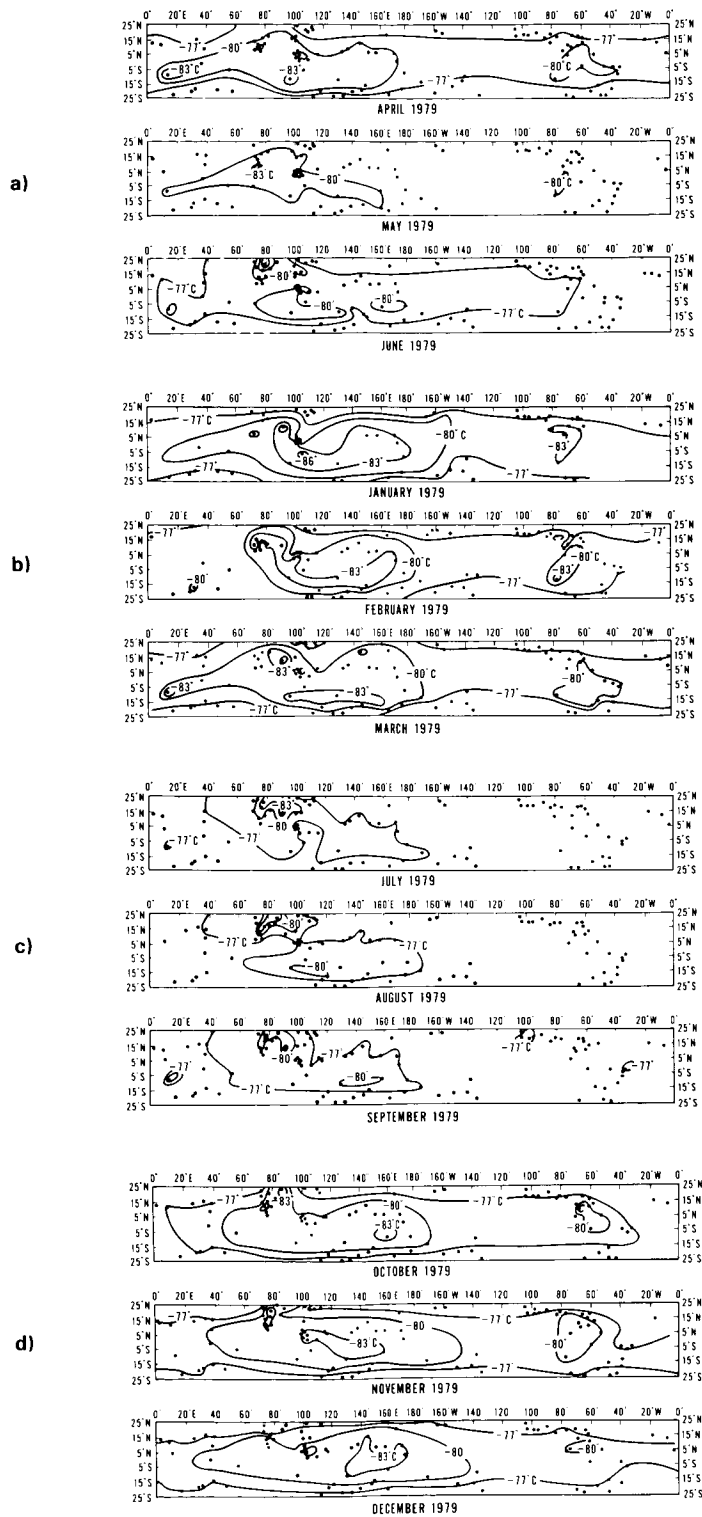
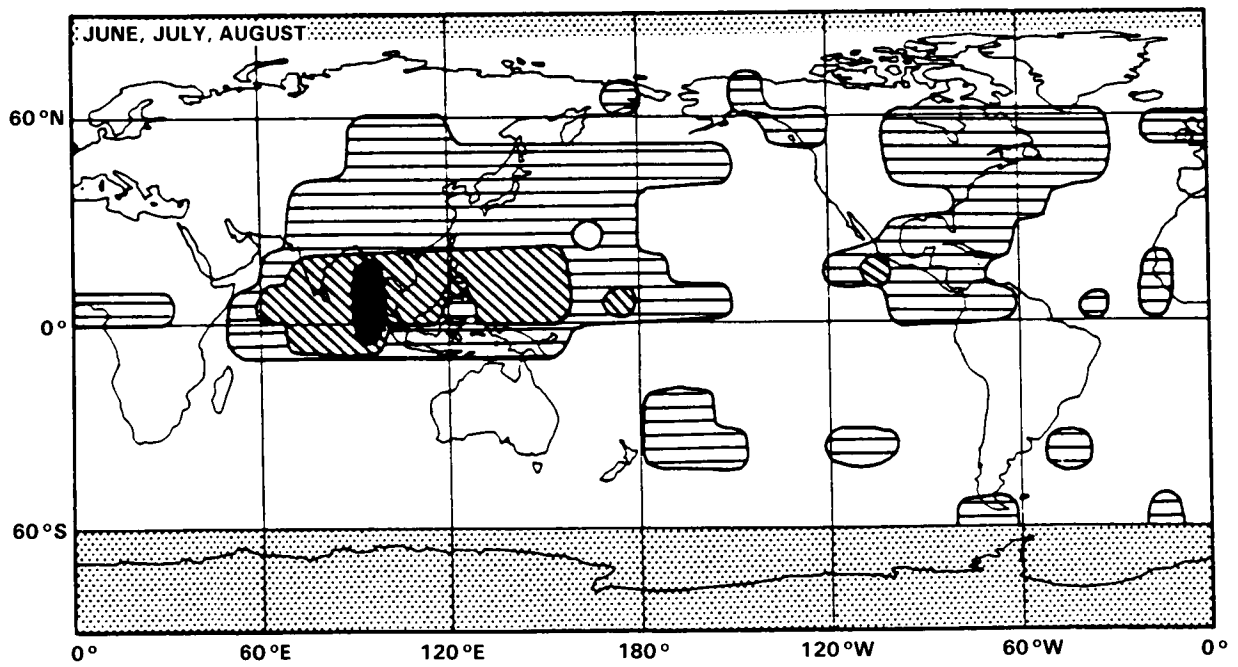
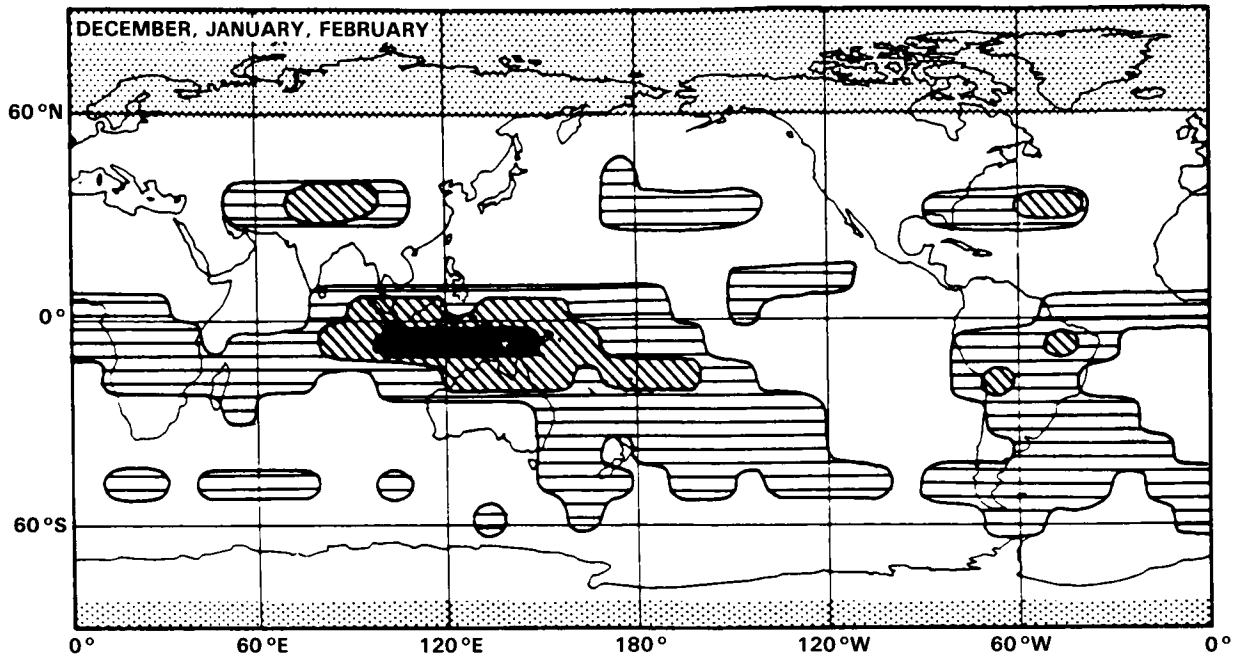


Figure 5-5. 100 mb tropical monthly mean temperatures for the FGGE year (1979), radiosonde data. (a) JFM, (b) AMJ, (c) JAS, (d) OND. Dots are radiosonde stations. Note especially the fluctuation of the area enclosed by the  $-80^{\circ}\text{C}$  contour over the year.

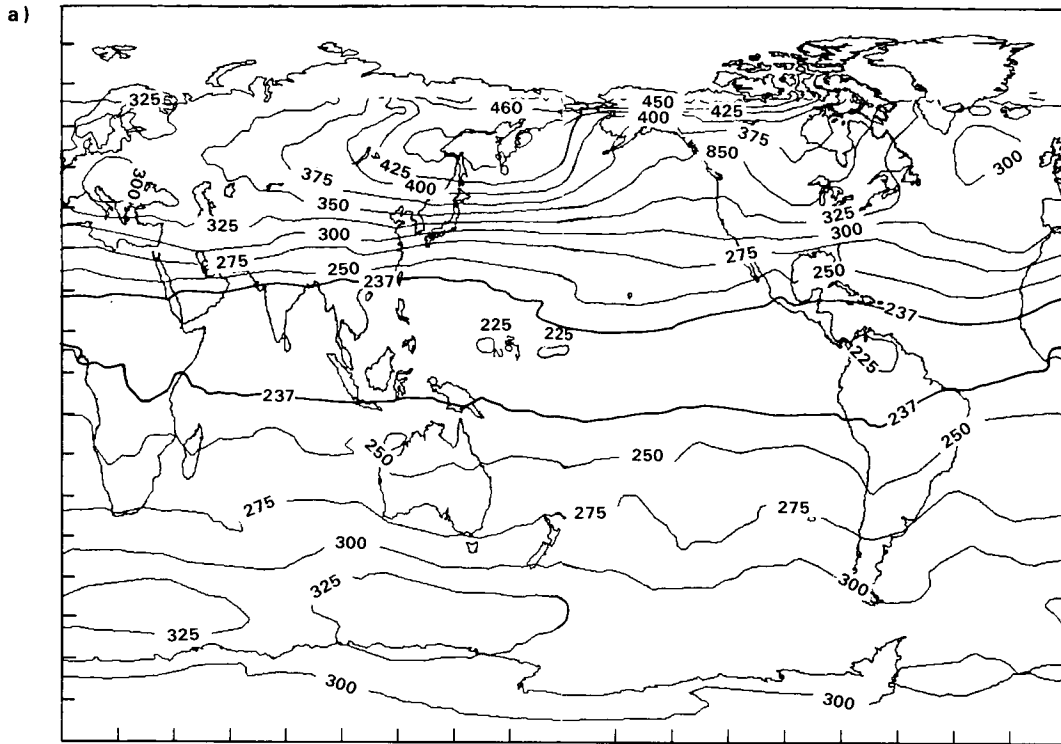
STRAT-TROP EXCHANGE



**Figure 5-6.** Frequencies of high clouds for the period January 1973-May 1975 from Barton (1983) for the seasons December-February (top) and June-August (bottom). Dark area is greater than 60% cloud cover; diagonal lines greater than 40%; horizontal lines, greater than 20%; clear, less than 20%; shaded, no observations.

STRAT-TROP EXCHANGE

JANUARY 1979



JULY 1979

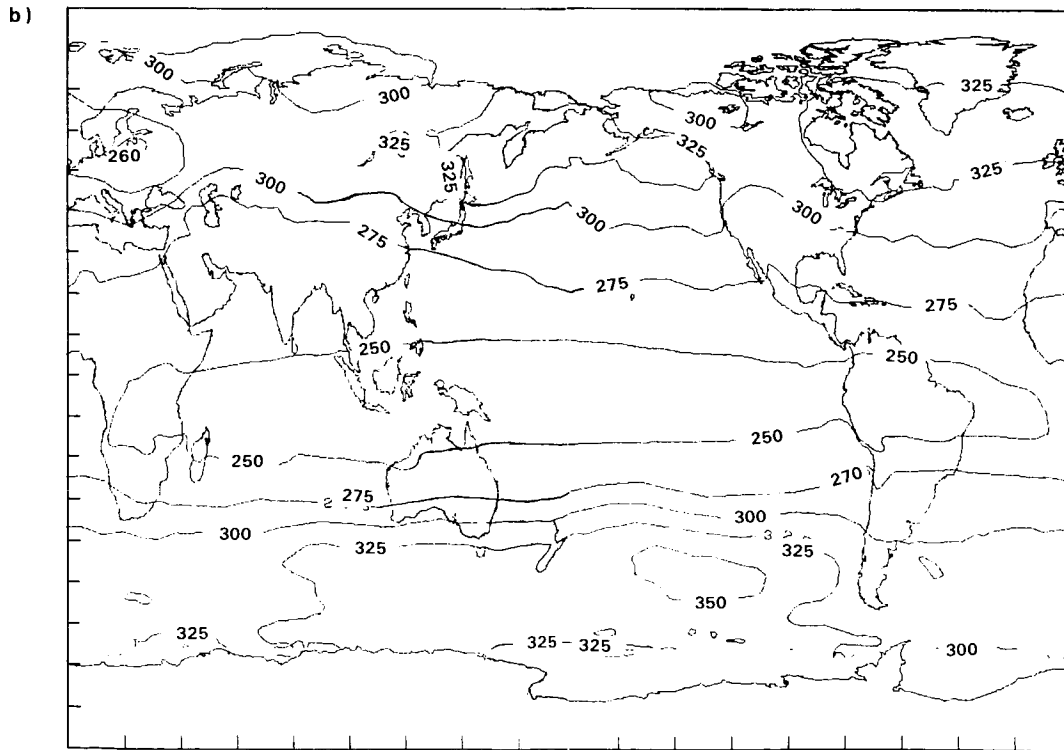
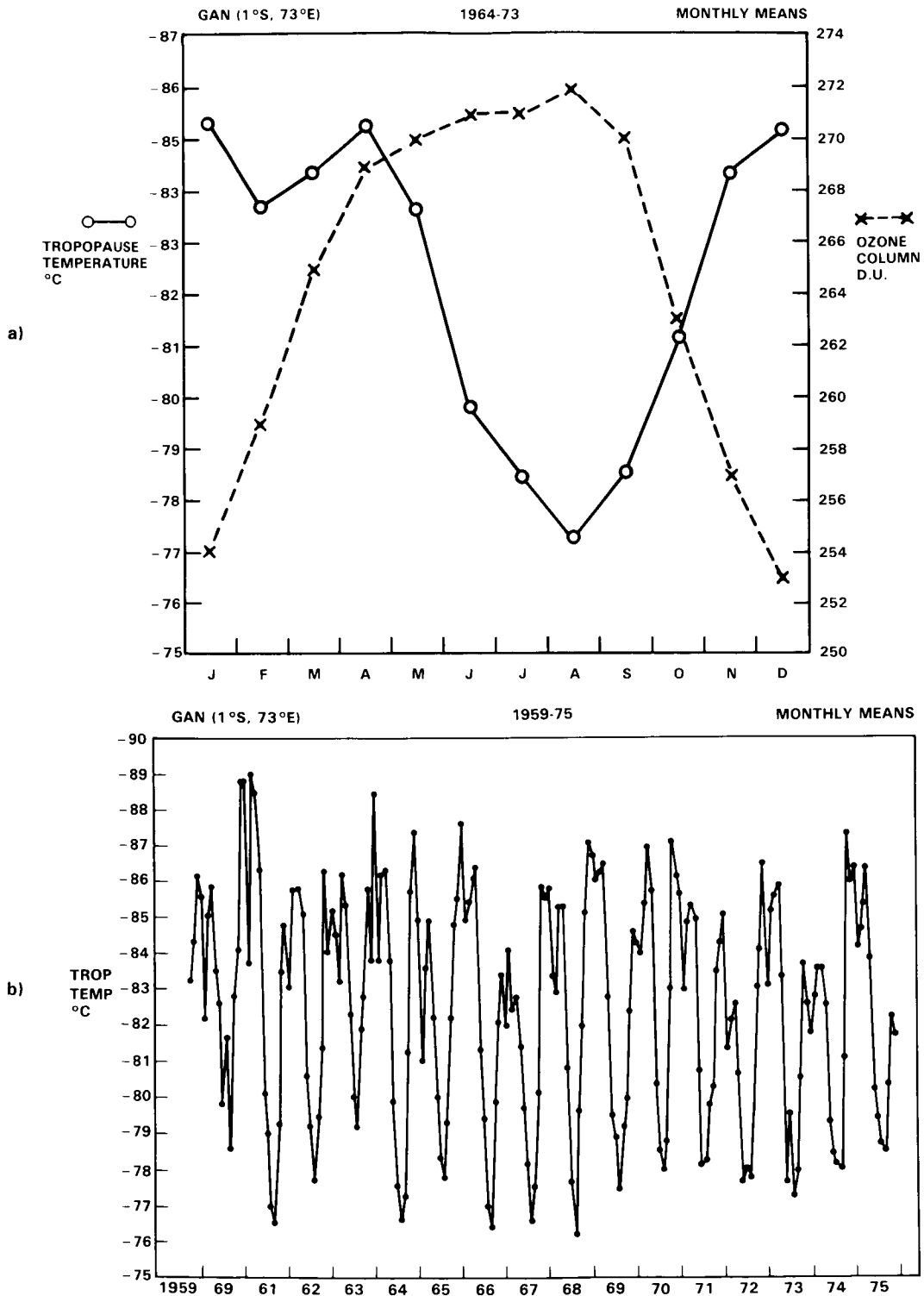


Figure 5-7. Monthly mean O<sub>3</sub> column observations, FGGE year, 1979. Data are from the Nimbus 7 TOMS instrument; (a) January, (b) July.

# STRAT-TROP EXCHANGE



**Figure 5-8.** (a) Annual cycle of tropopause temperature and ozone column density at Gan (1°S, 73°E). Data are monthly means, 1964-73. (b) Time series of monthly mean tropopause temperature, Gan, 1959-75. Note that there is a reproducible warming in February/March between cold peaks in December/January and April/May (on average). August is usually the warmest month.

of motion will have contained within them cumulonimbus clouds we proceed to discuss motions on scales other than the global circulation.

A whole series of synoptic-scale weather systems are present in the tropics, examples of which have been discussed by Riehl (1979). What is relevant here is whether these systems contribute to stratosphere-troposphere exchange. One such system is the easterly wave (Malkus, 1968); these seem to originate over Africa and propagate westward into the tropical Atlantic and Caribbean. Easterly waves are a feature also of the Pacific ITCZ. In some of these waves there is upper level divergence offset by rising motion from the lower troposphere and by sinking motion through the tropical tropopause as shown by Reed, *et al.* (1977). There are no statistics available on how many of these systems are accompanied by significant vertical motions at the level of the tropical tropopause.

Tropical storms are another major feature that may involve stratosphere-troposphere exchange. Gray (1968) has surveyed the region in which they occur and the criteria necessary for their development. Their structure is dealt with at length in Riehl (1979) and Palmen and Newton (1969). It is noteworthy that tropical cyclones in the western Pacific have a higher tropopause than those in the Atlantic; up to 8 °C colder than the average hurricane tropopause (Keenan and Templeton, 1983). It was pointed out above that the background temperature was also different in the same sense. But there is little direct evidence of vertical motion near the tropical tropopause in these severe tropical disturbances. Some of the schematic diagrams in Palmen and Newton (1969), imply subsidence in the eye and Riehl (1979) quotes some evidence from tritium measurements that stratospheric air is drawn down into the hurricane but there have been no systematic studies of this point.

Hurricanes have long been considered to be potential drivers of exchange but with little evidence. Penn (1964) observed the structure of the tropopause with aircraft flights. More recently, Rogers, Stout, and Nunez at Goddard Space Flight Center have analysed the TOMS data over Atlantic hurricanes and find low amplitude total ozone modulations (5 Dobson Units) in a partial ring surrounding the storm, together with larger scale features associated with the trough-ridge structure which steers the storm (Stout *et al.*, 1985). This study also made use of VAS 6.7 micrometer water vapour data to show that the region of higher total ozone in the forward sector of the storm was accompanied by dry air. These characteristics are evidence for tropopause deformation if not actual exchange of air. Evidence for very intense deformation of the tropopause (Holland *et al.*, 1984) is not supported by TOMS observations, which should show a localized ozone maximum. The event may, however, have been so short-lived that it had disappeared by the time that TOMS overflew the storm on the next day. The analyses of satellite observations of tropical storms are only beginning and the full extent of their value is still unknown.

It is essentially the moist static energy acquired near the surface that determines how high an air parcel can reach. This quantity is defined as  $c_p T + Lq + gz$  where  $c_p$  is the specific heat of air,  $T$  its temperature,  $L$  the latent heat of vaporization,  $q$  the specific humidity and  $gz$  the geopotential. Maps of moist static energy are shown in Hsiung and Newell (1985, paper in preparation); again some of the largest values occur in the west Pacific. As the latent heat is released within the rising parcel the air becomes warmer than the environment and therefore buoyant. This process operates on both the hurricane scale and that of the individual cumulonimbus. Parcels with moist static energy values of about  $350 \times 10^3$  J/kg can easily reach 16 km where they will have a temperature of about  $-83$  °C. The important point is that the tropical troposphere is potentially unstable to vertical motion. Roach and James (1973) show that parcel theory applied to soundings in the Bay of Bengal region in May can result in the rising air reaching altitudes of 21 km, with minimum temperatures of  $-90$  °C. Ludlam (1980) points out that dynamical forcing also plays a role in establishing the depth of cumulonimbus convection in this monsoon regime.

## STRAT-TROP EXCHANGE

Mesoscale cloud clusters have been observed in the tropics which seem to form independently of synoptic scale disturbances; over the South China Sea during Winter MONEX disturbances formed offshore in the early hours of each day apparently in response to convergence tied to a combination of local topographic features and the diurnal cycle of solar heating (Houze, *et al.*, 1981). Johnson and Kriete (1982) have shown that forced mesoscale vertical motions are associated with these systems. Similar mesoscale convective zones were observed during the wet season over Panama (Danielsen, 1982). These clusters tend to form extensive anvils and stratus decks at middle levels that may spread over several hundred kilometers. Radiative calculations by Webster and Stephens (1980), Doherty *et al.* (1984) and others indicate that these extensive cloud layers should experience IR warming from below and cooling above to space; the net heating could drive a number of processes including mesoscale ascent and turbulent overturning. These processes are enhanced by the release of latent heat associated with the precipitation observed from these cloud decks which often show a radar bright band similar to those seen in middle latitude stratiform precipitation (see Houze and Betts, 1981).

Radiative destabilization may operate also in other extensive high clouds; in fact although individual cumulonimbus clouds reach up to the tropopause many of the anvils are found well below the tropopause. The origin of some common cirrus clouds near the tropopause is not known; examples have been given by Platt (1983) for the region of northern Australia. Potential sources are synoptic scale motions or some type of radiative instability, both of which may be triggered by cumulonimbus activity.

### 5.1.2 Cumulonimbus Clouds

It is appropriate to discuss the individual cumulonimbus, a scale on which there seems to be a good potential for troposphere-stratosphere exchange as proposed by Danielsen (1982). This section is designed to set the stage for the case studies of Section 5.1.3. The mechanisms involved in cumulonimbus convection are discussed extensively in the textbooks of Riehl (1979) and Ludlam (1980). From the points of view of the present report it is desirable to know if this process can carry air into the stratosphere and if so, where and when. There is no question that large masses of air from the boundary layer are carried aloft to the upper troposphere by the cumulonimbus process. Although vertical motions in individual cells may range up to 30 m/sec, overall it takes an hour or more for significant quantities of air to be transferred to the upper troposphere. Whether the physical processes in the anvil then lead to penetration, as suggested by Danielsen, (1982) and reviewed by Holton (1984b) is an unsolved problem which is soon to be examined experimentally in NASA's STEP project. For the present discussion it is assumed that there is association between penetration and anvils. Frequency of occurrence of cumulonimbus is shown in Figure 5-9 for two seasons and may be compared with that of cirrus from the same marine data set down in Figure 5-10. The two are clearly related, especially in the west Pacific and the Indian Ocean. Cumulonimbus distribution thus matches the large-scale motion distribution discussed earlier. The release of latent heat that maintains the tropical circulation occurs primarily within these phenomena, termed by Malkus (1968), the "firebox of the circulation". If it turns out that experiments verify Danielsen's hypothesis, the correspondence between the most extensive cumulonimbus activity and the greatest large-scale vertical motion may allow stratosphere-troposphere exchange in the tropics to be monitored by means of the large-scale observables as we have discussed above.

We now consider some results of a case study which was designed to see how actual observations of large cumulonimbus tops compared with established climatologies. Airborne radar and cameras combined with horizon gyroscopes were used by Cornford and Spavins (1973) to study cumulonimbus tops during the April-June period in NE India. They concluded that tops extended to at least 20 km, and noted that Burnham (1970) had established that turbulence may extend into the clear air for 25-30 km around

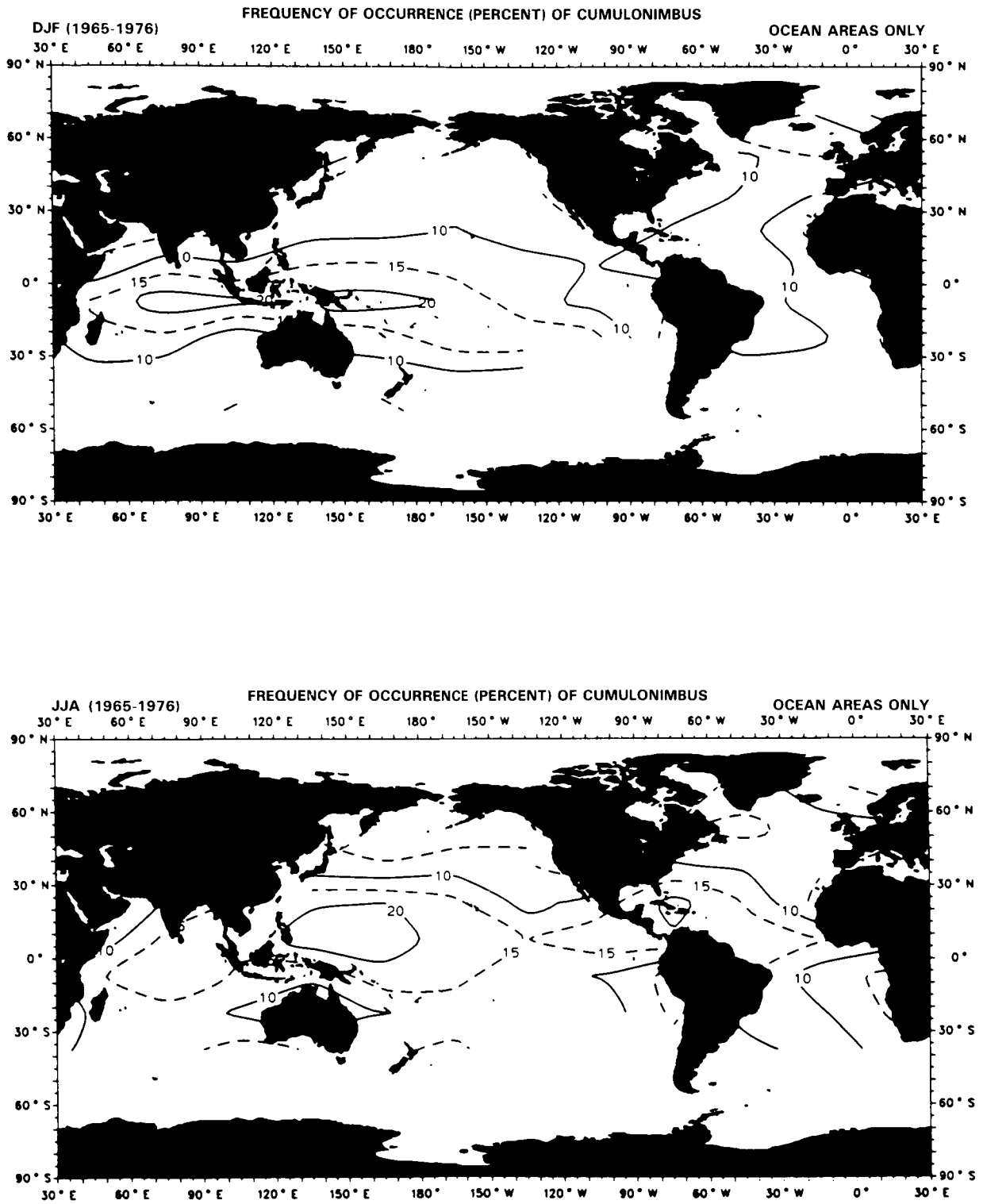


Figure 5-9. Frequencies of observation of cumulonimbus clouds over the ocean from Hahn, *et al.* (1982) for December-February (top) and June-August (bottom).

STRAT-TROP EXCHANGE

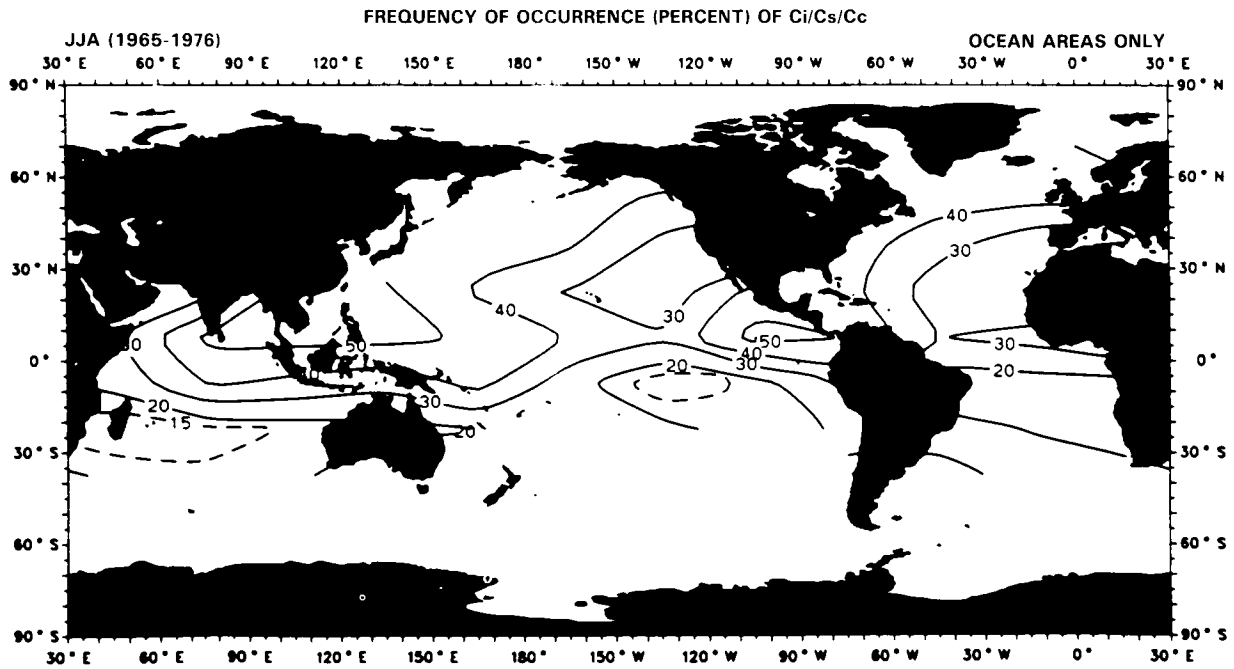
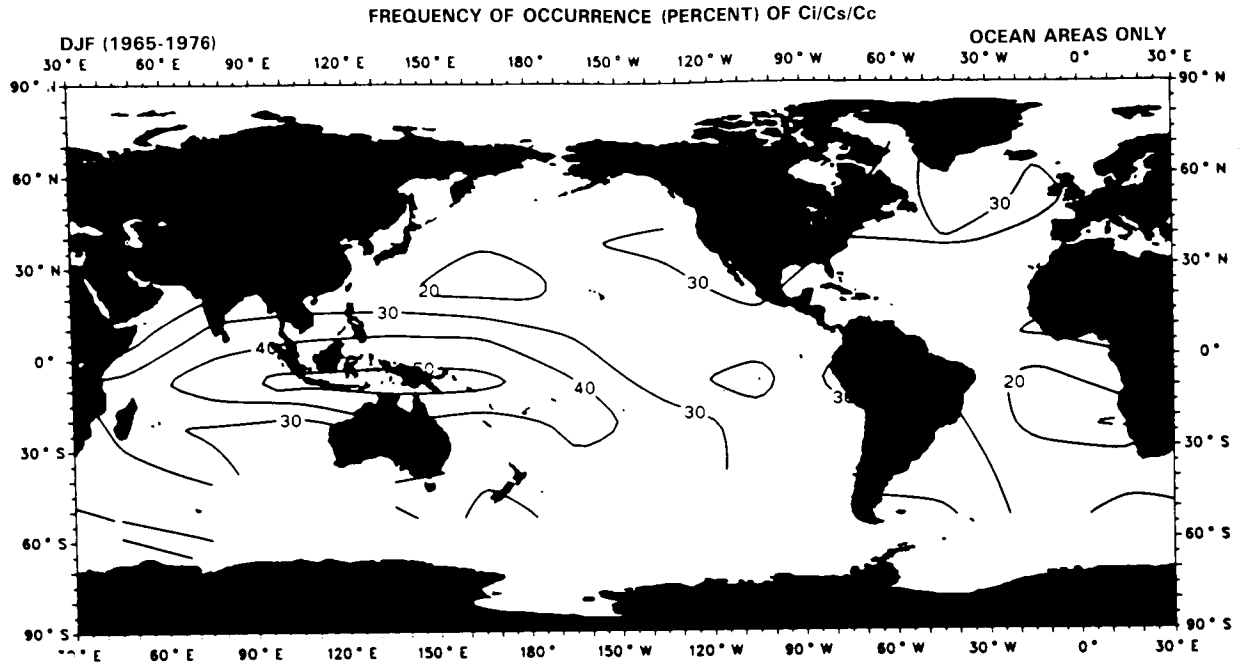


Figure 5-10. As in Figure 5-9 but for cirrus/cirrostratus/cirrocumulus.

a visible storm, and up to 1½-3 km above its top. Since parcel theory was the best statistical predictor of the observed top heights (although it was not reliable on a day to day basis), it is clear that near-surface air may be carried, on a time scale of hours, largely undiluted to up to 20 km, with potential for further mixing above this altitude. Mattingly (1977) noted a statistically significant tendency for the vertical extent of tops penetrating the tropopause in the Cornford and Spavins data to be correlated with the horizontal dimension: the bigger storms penetrated further, as shown in Figure 5-11.

It should be noted that upper level windshear frequently plays an important role in cumulonimbus development (Ludlam 1980), and the possibility of horizontal winds at the level of cumulonimbus tops and their associated anvils transporting water vapour and small ice crystals downwind must be considered. Aircraft studies in mid-latitudes (Barrett *et al.*, 1973) have apparently shown that this can occur.

Shipborne radiosonde launches during the winter MONEX experiment have also shown mesoscale temperature structure just above the tropopause near Borneo which was sufficiently cold to be compatible with the low mixing ratio associated with the stratosphere at and above the hygropause (Johnson and Kriete 1982), see Figure 5-12.

The production of nitric oxide during lightning discharges in cumulonimbus storms was calculated theoretically by Tuck (1976), Griffing (1977) and Chameides *et al.* (1977): a recent review is given by Borucki and Chameides (1984). Measurements of NO<sub>2</sub> production by Noxon (1976) confirmed this process, and he suggested that some of it could enter the stratosphere. Tuck (1976) calculated that there could be a flux of order 10<sup>34</sup> NO<sub>x</sub> molecules per year into the lower tropical stratosphere from cumulonimbi, which is of the same order as the stratospheric photochemical production from O(<sup>1</sup>D) + N<sub>2</sub>O → 2 NO.

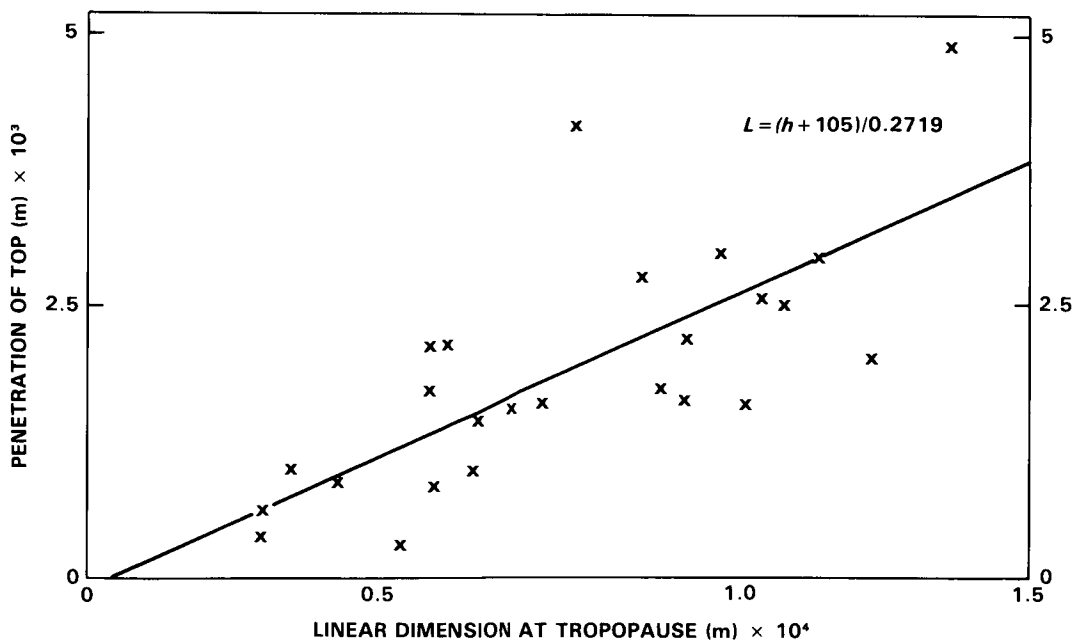
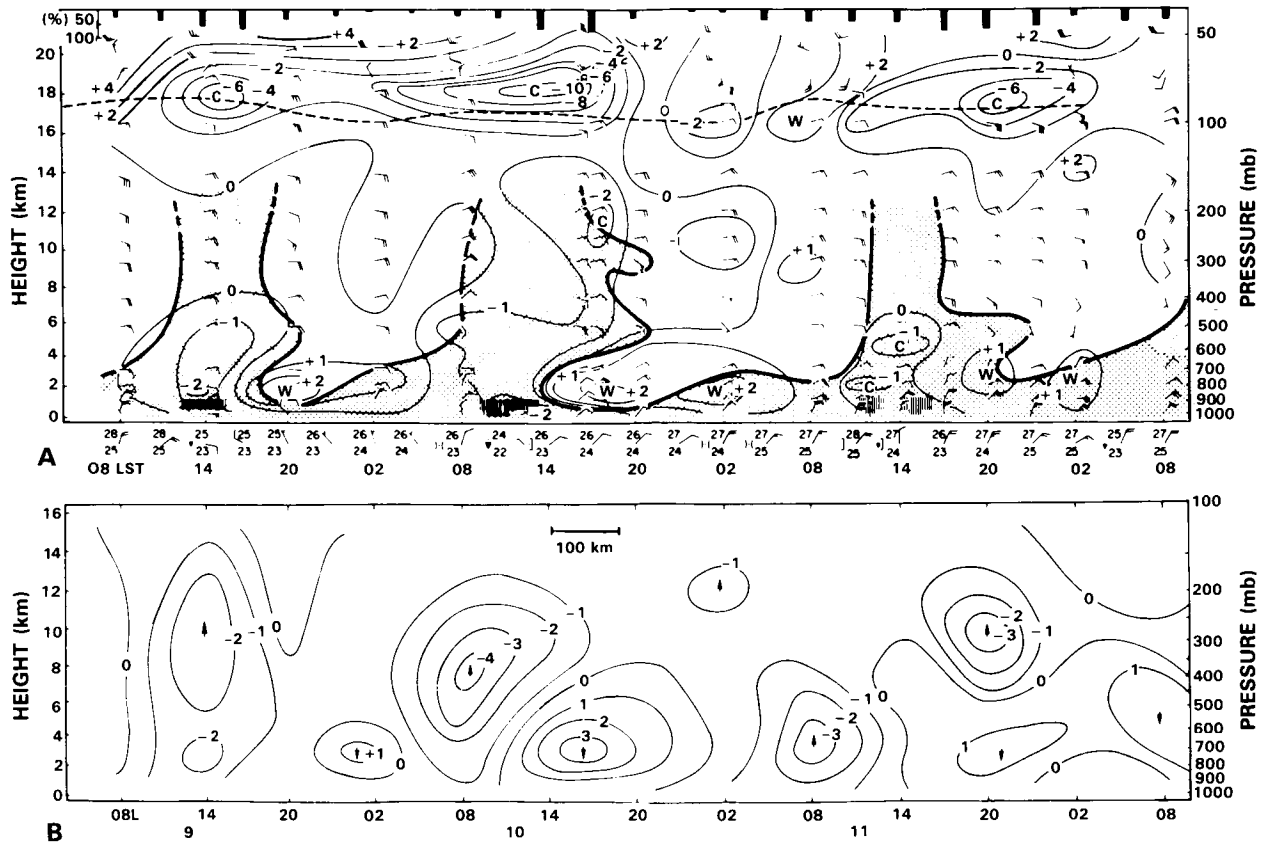


Figure 5-11. A diagram of the height of cumulonimbus tops above the tropopause versus horizontal dimension, from Mattingly (1977) using data from NE India obtained by Cornford and Spavins (1973).

## STRAT-TROP EXCHANGE



**Figure 5-12.** (a) Rawinsonde time series during winter MONEX for 9-11 December 1978. Stippling denotes regions of greater than 80% relative humidity. Solid contours are temperature deviations (K) from the 6-28 December mean. Wind speeds are in m/s (full barb - 5 m/s). Dashed line marks the tropopause. Bars at top indicate fraction of ship array covered by bright IR satellite cloudiness. (b) Vertical pressure velocity in units of 100 mb/day for the ship array computed by the kinematic method. Distance scale indicated represents advective length scale for 6 m/s motion of the anvil clouds. After Johnson and Kriete, 1982.

However, the degree of overlap between discharge channels and updrafts is unknown, and there is no reliable information on the partitioning of lightning-produced  $\text{NO}_x$  between stratosphere and troposphere.

It is clear from the large scale wind fields in the tropics that any volume of air at or a few km above the tropopause will not be simply transported zonally. Dynamical constraints dictate that there will be meridional components to the flow, consistent with the correlation observed by Reid and Gage (1984) between tropical tropopause height and the angular momentum of the atmosphere. Variations in the intensity of the Hadley Cell also show this (Reed and Vlcek, 1969, Newell *et al.*, 1974, Reiter, 1979); Section 5.2.3 also examines the connection between tropical and mid-latitude circulations.

### 5.1.3 Aircraft Studies near Cumulonimbus Anvils in Panama

In this section, we are concerned with the tracer aspect of water vapour. We show that from measurements of water vapour below and above the tropical tropopause it is possible to demonstrate that

tropopause-penetrating cumulonimbus clouds and subsequent anvil formation inject most, if not all, of the water that is found in the stratosphere above the tropopause.

In 1980, NASA conducted the second of a series of experiments to investigate the exchange of air from troposphere to stratosphere in a tropical region. A U2 aircraft was equipped with a multitude of instruments. Among these was a fast responding  $Ly(\alpha)$  hygrometer (Kley and Stone, 1978). Some initial results obtained from this experiment have been published earlier (Kley *et al.*, 1982). Whereas those results were basically a statistical analysis of height profiles of water vapour mixing ratios, detailed examination of individual profiles of total water mixing ratio (total water means the sum of water in all phases) and atmospheric temperature shows some prominent features.

1. The tropopause is well defined. Height and temperature show little variability.
2. Above tropopause, usually a little more than 2 km higher, there is a secondary temperature minimum. The temperature at the height of this minimum has values very similar to those at the tropopause.
3. Water vapour profiles decline sharply over a small height range to values around 6 ppmv at tropopause. At higher altitudes, this drop continues but the trend reverses soon to give rise to a relative maximum of the mixing ratio at the height of the secondary temperature minimum. Above the height of the relative maximum, there is another decline to an absolute minimum between 18 and 19 km. Finally, consistent on all profiles, the water mixing ratio increases above the height of the absolute minimum.

Figure 5-13 shows these prominent features enhanced. Also, Figure 5-14 was prepared. That figure presents the material of Figure 5-13 in a semi-log plot. The atmospheric temperature profile is drawn on frost point coordinates. Apparent supersaturation is shown as the cross-hatched area. Since total  $H_2O$  was measured, supersaturation of such magnitude implies ice crystals in the air. Plots, like Figure 5-14, were generated for all flights of the Panama Experiment and gave very similar results (Kley *et al.*, 1983). A cirrus deck from the tropopause on down to 12 or 11 km was therefore ubiquitous but never reached across the tropopause. Supersaturation, i.e., hydrometeors above the tropopause, was only observed on two occasions during penetration or "skimming" of active stratospheric anvils (Kley *et al.*, 1982; Knollenberg *et al.*, 1982). However, the observed water mixing ratios at the height of the temperature minimum above tropopause were mostly extremely close to saturation. As Figure 5-14 shows, the water mixing ratio comes within  $\sim 1.5^\circ C$  of being saturated at 16.7 km. Exceptions were encountered for flights 5 and 9 where temperatures were closer to an unperturbed stratospheric profile and the mixing ratios thus were farther away from saturation.

The key to the understanding of the injection mechanism of water into the stratosphere is in the interpretation of Figure 5-13 which serves as our standard case. If the Danielsen (1982) anvil formation hypothesis is accepted then the negative temperature anomalies at 17 km can be explained as being produced by this process. Figure 5-13 then shows that water injection is the result of anvil formation. One might even think of the relative water maximum at 17 km as giving proof of the Danielsen hypothesis. The profiles were all taken during aircraft descent, i.e., while not flying through active anvils. Therefore, the observations show the perturbed conditions that exist *after* the anvils have dissipated. It is not surprising that the water mixing ratio remains high because the layer is subsaturated and mixing ratio will be conserved since mixing will be inefficient due to the horizontal extent of the layer and the short elapsed time since dissipation of the anvil. It is possible to estimate this time if we use  $-83^\circ$  to  $-84^\circ C$  as initial anvil temperatures (Danielsen, 1982) and typical e-folding times for radiative cooling rates of five days for a dry atmosphere

STRAT-TROP EXCHANGE

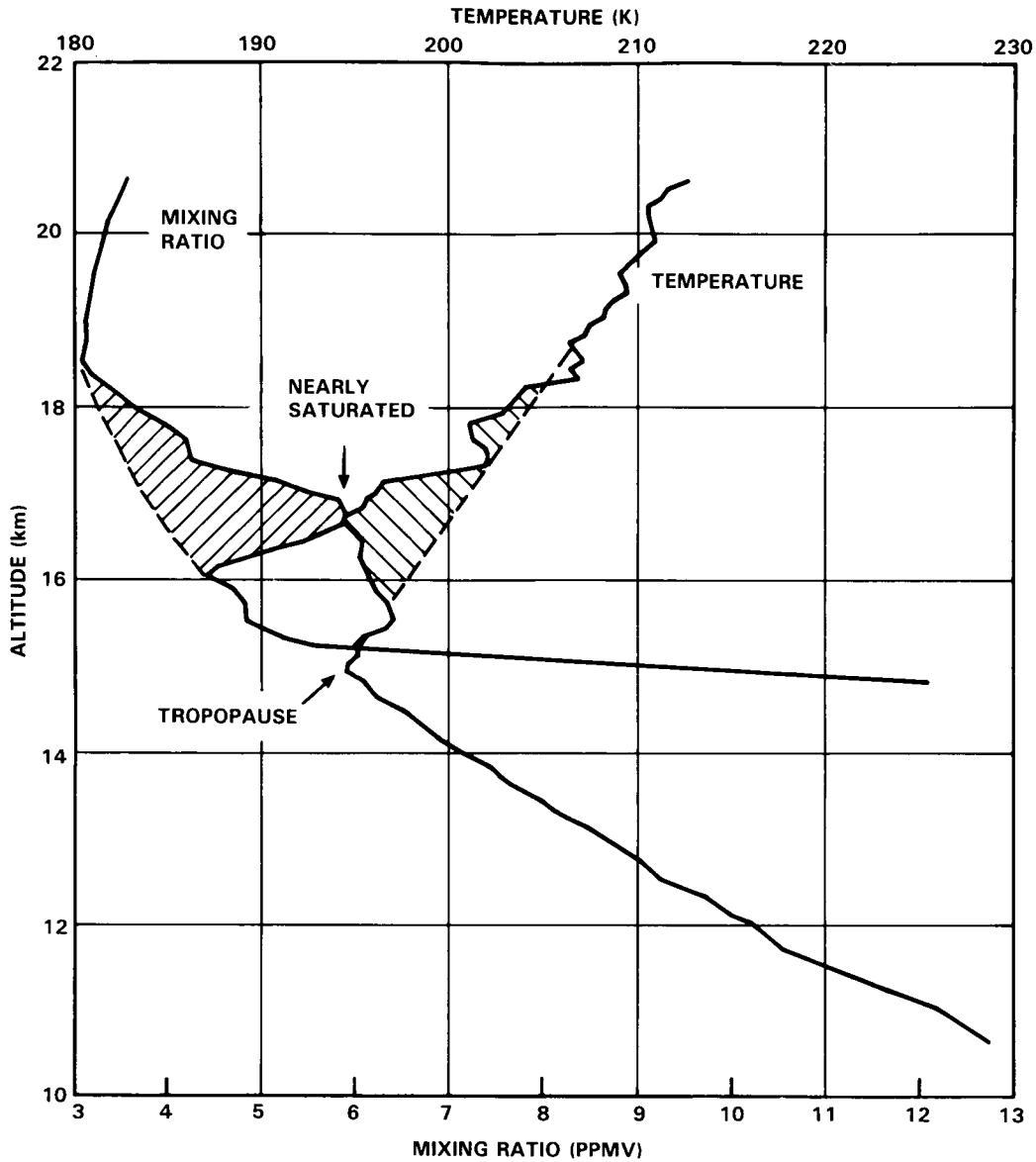
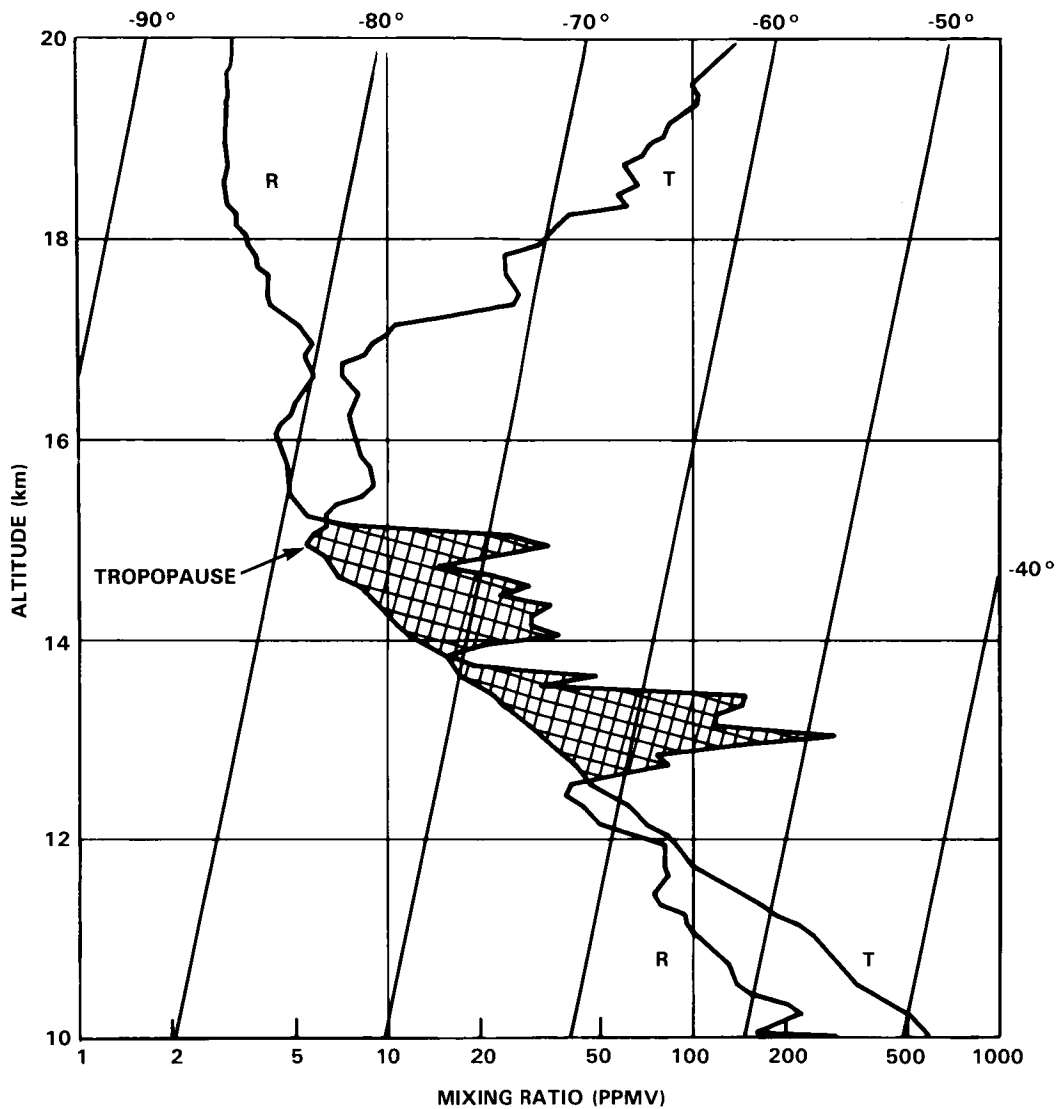


Figure 5-13. Water vapour mixing ratio and temperature, averaged over 100 m intervals, from U2 aircraft instrumentation at descent to Howard AFB on 11th September 1980.

(Fels, private communication). This implies that less than five days have passed since the air was part of an anvil. The enhanced mixing ratio with a maximum at ~17 km cannot have been produced below the layer and then diffused upward since there is a dryer layer between 16 and 15 km, followed by much higher mixing ratios below 15 km. The results typified by Figure 5-13 demonstrate that injection occurs at the altitude around 17 km. We must think of the process as one in which the turret overshoots and transports large amounts of ice into the stratosphere, and that the subsequent anvil formation distributes the ice quasi-horizontally. This process can lead to saturation while the excess ice precipitates out. There has been discussion on the thermodynamics (Danielsen, 1982) and the microphysics (Knollenberg *et al.*,



**Figure 5-14.** Mixing ratio (R) and temperature (T) for the 11th September data in Figure 5-13, on a semi-log plot. Cirrus deck indicated by cross-hatching. Temperature profile plotted on frost point coordinates.

1982) of water injection during cumulonimbus penetration and anvil formation. However, the answer, as far as injection of water into the stratosphere is concerned, is contained in Figure 5-13. These experimental results impose constraints on thermodynamics and microphysics of anvil formation. Whatever the microphysics are, they lead to saturated water conditions. Rather than asking the question whether the microphysical processes lead to hydration or dehydration of stratospheric air, it would perhaps be better to pose the question in a way as to ask what is the atmospheric temperature after anvil dissipation and what is the role of microphysics and radiative processes, modifying the initial anvil temperature after overshoot of the turret and entrainment of stratospheric air has taken place.

## STRAT-TROP EXCHANGE

### 5.1.4 Discussion of Tropical Exchange

We now turn to a discussion of the question whether or not anvils are sources or sinks of stratospheric water vapour above the hygropause level. We limit the discussion to this level, since the hygropause is well defined, both in altitude and water mixing ratio, and Danielsen (1982) has shown that the maximum height that anvils could reach is 19 km over the Eastern Pacific. There is direct experimental evidence of cumulonimbus tops reaching 21 km in May over the Bay of Bengal (Cornford and Spavins, 1973). We make the assumption that all water found in the tropical stratosphere has been anvil-processed or, in other words, there is no transfer of water to regions above the hygropause by diffusion or slow advection through the tropopause. Clearly, the anvils are a source of stratospheric water vapour by imposing boundary conditions of temperature and H<sub>2</sub>O saturation mixing ratio on the air in the anvil. This process can be called dehydration, if the air entrained during anvil formation has a mixing ratio higher than what is imposed as boundary conditions by the microphysical/radiative processes during the lifetime of the anvil. Such a source of water vapour would be methane oxidation. As Figure 5-13 shows, there is a slight increase of the H<sub>2</sub>O mixing ratio with height above the hygropause.

Our point made earlier that no water penetrates into the tropical stratosphere unless associated with overshooting thunderstorms is more than just an assumption. All flights of the Panama Experiment (Figure 5-14 and Figures 30 to 37 of Kley *et al.*, 1983) show saturation at the tropopause with mixing ratios around 6 ppmv, followed by the discussed decrease above the tropopause up to the level of anvil injection. A similar result was obtained during the only other sounding we made in the tropics (Kley *et al.*, 1979). It therefore seems appropriate, in the absence of counter-examples, to associate the physical source of stratospheric water vapour mainly with overshooting deep cumulonimbus convection. An alternative view may also be considered, in which, on some space scale, the low temperatures associated with overshooting Cb's and their anvils provide a source of dryness. Which of these is chosen depends upon the hypothetical reference state chosen for stratospheric humidity; if it is  $\chi_{\text{H}_2\text{O}} = 0$  then Cb's may be viewed as a source, if the reference is taken as the upper troposphere, it is more natural to think of a "source of dryness".

In the remainder of the discussion we will briefly investigate the longitudinal distribution of tropical lower stratospheric water vapour and the hygropause phenomenon. This part is more fragmentary and more observational work needs to be done. All the available information suggests that the water mixing ratio at the hygropause level shows little variability along a latitude circle in the tropics. The mean of the data typified by Figure 5-13 is  $\chi_{\text{HP}} = 3.4 \pm 0.2$  ppmv, where the subscript indicates altitude of the hygropause. Danielsen and Kley (1986, submitted for publication) analyzed a balloon sounding made on 31 January 1979. They show that air at 15 km over Laramie, WY with a mixing ratio of 3.2 ppmv had been isentropically transported on the 405 K potential temperature surface from a tropical sector (120°-140°E). Transport time from the source region to Laramie was only five days, during which time diffusion had not appreciably changed the mixing ratio of the layer. Mastenbrook (1968) reported monthly soundings over Trinidad (11°N, 61°W). His yearly mean at 60 mb was 3.4 ppmv. Remsberg *et al.* (1984) present zonal mean values of  $\sim 2.5$  ppmv at 60-70 mb and note that, due to retrieval uncertainties, these values might be too low by a margin equal to or less than 25%. In the absence of sufficient data it seems appropriate, at present, to adopt a hygropause mixing ratio around 3 ppmv with no justification to argue for a strong longitudinal asymmetry. However, it is not readily apparent that the assumption of little mixing during the 5-day passage to Wyoming is compatible with the implicit assumption of rapid mixing associated with no longitudinal asymmetry in the hygropause in the tropics despite the "source of dryness" being confined to, say, 70°-170°E.

If stratospheric anvils are the major source for stratospheric water vapour, then infrared enhanced satellite photography could be used to map injection areas. Danielsen (1982) shows that the intensity of

overshooting cumulonimbus convection is ultimately related to sea surface temperature and to the amount of latent heat stored in near-surface air. He points out that over the Micronesia area (centered on 150°E), sea surface temperatures are 3 K warmer than over other parts of the Pacific; this can produce 10 K colder temperatures during overshoot to 19 km. This implies that mixing ratios as low as 1.5 ppmv are possible, and could be lower than this (Cornford and Spavins, 1973).

Newell and Gould-Stewart (1981) have proposed a stratospheric fountain to occur during the winter season over Micronesia/Bay of Bengal. If the injection mixing ratio over Panama and other tropical areas with similar sea surface temperatures is 5.5 ppmv and the hygropause mixing ratio is 3 ppmv in the zonal mean, then the mass of air injected with a water mixing ratio of 1.6 ppmv needs to be 64% of the total. However, the area over which these very low mixing ratios at 19 km might occur is mainly located in a certain sector (i.e., Micronesia) and a strong zonal asymmetry of the hygropause mixing ratio would result. The available information does, therefore, not favour this concept. Alternatively, we could think of the process as one in which air that has been anvil processed at injection altitudes below the hygropause to resulting mixing ratios of  $\sim 5.5$  ppmv is entrained during anvil formation of the hygropause level and leaves with a resulting mixing ratio of 3 ppmv. Vertical diffusion times from 17 to 19 km would be about 46 days for  $K_{zz} = 5 \times 10^3 \text{cm}^2 \text{s}^{-1}$ . Adopting a mean zonal flow of 10 m/s it takes 23 days to advect material horizontally by 180° of longitude. Since  $K_{zz}$  could be lower than the value used here (Kida, 1983a, b), it seems justified to assume that freeze drying over the Micronesia/winter Monsoon area can account for the uniform mixing ratio of the hygropause. Anvil temperatures of  $-86.5^\circ\text{C}$  are required at 60 to 70 mb. These low temperatures are not found everywhere in the tropics. However, they do occur. Johnson and Kriete (1982) show temperature profiles over the winter monsoon area that exhibit characteristics of the Danielsen anvil mechanism at the height of the hygropause.

The results from the  $\text{Ly}(\alpha)$  hygrometer during the 1980 Panama Experiment show that water injection to the stratosphere occurs by overshooting cumulonimbus clouds and anvil formation above tropopause. The stratospheric water mixing ratio is determined by the anvil temperature at the time of dissipation, i.e., the transition from supersaturated to saturated conditions. The apparent uniformity of the hygropause represents a problem that needs further experimental and theoretical work. In the meantime, the experimental results are best explained by a cold trap of  $-86.5^\circ\text{C}$ , located at  $\sim 19$  km. The trap is provided by anvil spreading at that altitude from overshooting cumulonimbi. Injection of water vapour into the stratosphere occurs whenever anvils are formed above the tropopause. However, due to fast zonal flow, air with larger mixing ratio from lower altitude injection is entrained again at 19 km and leaves the hygropause with a mixing ratio of  $3 \pm 0.2$  ppmv.

As a consequence of the convective nature of this process, overshooting reverses positive surface temperature deviations of air parcels on the scale of convective events into negative temperature deviations above the tropopause. We like to suggest that an increase of the earth's surface temperature in the mean would, also, due to the increased amount of water in surface-near air, increase the intensity of overshooting. This would lead to a decrease in stratospheric water vapour. However, it must be remembered that it is very difficult to calculate the balance between radiative and convective processes near the tropical tropopause, and behaviour under such a perturbation is not yet predictable.

### 5.1.5 Summary of Tropical Exchange

There is a spatial and temporal correlation between the large scale tropical temperature minima at 100 mb (Figure 5-5) and the locations of the occurrence of the deepest cumulonimbus anvils. Although the lowest tropopause temperatures in the sector from 70°E to 170°E are low enough to account for the

## STRAT-TROP EXCHANGE

lowest water vapour mixing ratios observed in the stratosphere, quasi-uniform slow large scale ascent over this area of the tropical tropopause cannot account for the occurrence of the hygropause (minimum mixing ratios in the vertical water vapour profile) some 2-4 km above the tropopause. Appeal to some other mechanism must be made, and large cumulonimbus storms are the obvious candidate. Much remains to be learnt about the details however; tropical cumulonimbus frequently organise in clusters or on the mesoscale, for example. There may be cooperative interaction between deep local convection and large scale temperature minima at the tropopause, which could produce drier air for overshooting turrets collapsing back to mix with than would otherwise be the case. If a zonally symmetric hygropause is maintained throughout the year (and this is not established), there is a need to understand how the drying mechanism remains balanced with the horizontal mixing at subtropical and middle latitudes, particularly during the June-September period. It may be that both tropical convection depth and poleward motion in the subtropics are stronger in the northern winter, and weaker in the summer as a result of angular momentum conservation, but global scale observations are required.

One critical experiment which needs doing is to determine whether or not there are fine ice crystals (cirrus) near tropopause levels in the sector 70°E to 170°E in the tropics, and the areal extent of their occurrence. It is also necessary to do aircraft studies of the tallest cumulonimbus towers (which apparently occur during May/June over the Bay of Bengal and Ganges delta). If the explanation of the hygropause over Panama is correct (i.e., that it is produced by deeper convection elsewhere), then the hygropause should be coincident in altitude with the tops of the highest anvils. The odd nitrogen content of the stratospheric outflow from cumulonimbus storms needs to be measured.

## 5.2 EXTRATROPICAL EXCHANGE

### 5.2.1 Meteorological Processes

The exchange, or irreversible transfer of mass, trace gases and aerosols between the stratosphere and troposphere varies with latitude, longitude and season. Outflow from the stratosphere is predominantly by tropopause folding in association with large scale wave amplification and the formation of extratropical cyclonic storms. These storms amplify rapidly where the atmosphere has a large latitudinal temperature gradient and small static stability. Both conditions are more probable at low latitudes in the extratropics during late winter and early spring, and at high latitudes in late summer and early fall. The corresponding longitudinal variations are related to small static stability, produced by the passage of cold air over warm oceans or land surfaces. Thus during winter, cyclogenesis is more frequent and vigorous over the warmer oceans while in the spring the optimum conditions shift longitudinally to the high arid plateaus where surface heating is a maximum.

The outflow process was predicted by Reed (1955) and Reed and Danielsen (1959) who used potential vorticity as a quasiconservative tracer to identify air of recent stratospheric origin in the middle and upper troposphere. The process was verified by Briggs and Roach (1963), Danielsen (1964), and Reiter and Mahlman (1965) via aircraft measurements of ozone, water vapour and radioactivity of nuclear bomb test origin. Danielsen (1968) obtained direct correlations with the spatial distributions of potential vorticity. At that time, fast responding ozone and water vapour sensors were not available for aircraft experiments, but during the same spring a special ozone-sonde network was established in North America by Air Force Cambridge Research Laboratory (Hering and Borden, 1964-1966). Some of these sondes permitted indirect comparisons between ozone and radioactivity by relating both to computed distributions of potential vorticity (Danielsen, 1968). As anticipated, the three quantities were positively correlated in the lower stratosphere and in the folded tropopause layers in the middle and upper troposphere. These results are

consistent with the stratospheric sources of the three quantities and with a dominant influence of stratospheric mixing. The latter is required to explain the positive correlations despite the latitudinal and sometimes longitudinal differences in their upper or middle stratospheric sources (Danielsen, *op. cit.*).

Having direct *in situ* measurements of radioactive isotopes was a distinct advantage for identifying air of stratospheric origin and for establishing the relative importance of irreversible mixing. One can argue, as meteorologists and chemists do, about the nonconservation of potential vorticity and ozone and hence their use or misuse as stratospheric tracers. But, when radioactivity is corrected for radioactive decay it is unambiguously conserved. Only mixing processes can change the mixing ratio of a given isotope in an air parcel. By tracing three dimensional trajectories of these parcels and measuring changes in each parcel's mixing ratio one can evaluate the mixing. Furthermore, if the changes in potential vorticity and/or ozone are comparable to those of radioactivity, mixing processes are clearly responsible for the changes.

The mixing referred to here is small scale and irreversible. It is essentially independent of direction and tends to destroy gradients of any quantity including gradients of tracer  $i$ 's mixing ratio  $\chi_i$ . On the other hand, the larger scale motions from which trajectories are computed, in principle, are reversible. They are quasihorizontal and tend to create gradients by deformation, i.e., as illustrated in Figure 5-15, the flow increases the vertical gradient by convergence and spreads the gradient to a larger horizontal area by divergence. Steady state is maintained locally by a balance between flow deformation tending to increase the gradient and small scale mixing tending to decrease it.

In general, the stratosphere differs from the troposphere by having much larger vertical gradients of quasiconservative quantities. This characteristic is a consequence of the larger static stability of the stratosphere which acts to resist vertical motions and prevents large scale overturning, and also of chemical processes that generate vertical gradients. Conversely, in the troposphere, heating at the earth's surface reduces static stability and generates vertical overturning. Also, latent heat released by condensing water vapour in updrafts accelerates the updrafts, producing large cumulonimbus clouds that can traverse the entire depth of the troposphere. The prefix tropo - meaning to turn - implies vertical overturning, small vertical gradients, and a tendency for vertical homogeneity. These conditions are most clearly seen in the boundary layer but they are evident also in the vertical profiles of long-lived trace gases of lower tropospheric origin such as nitrous oxide and methane.

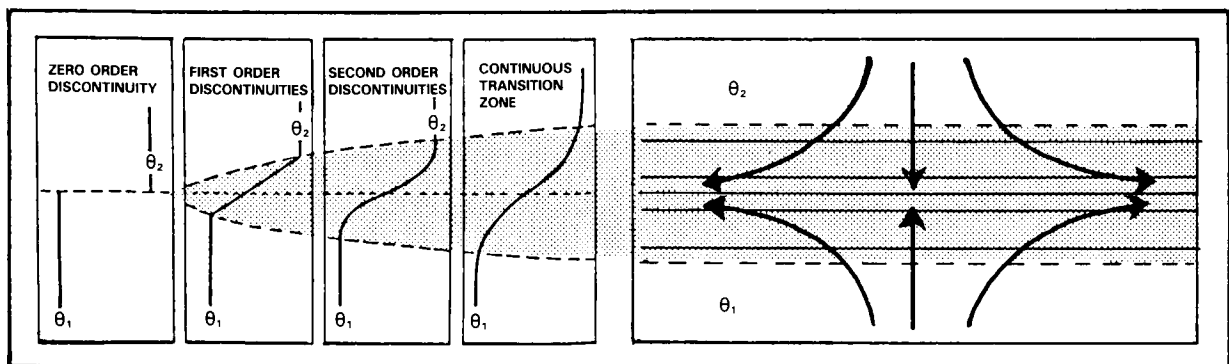


**Figure 5-15.** Continuous gradients of transition zone maintained by opposing actions of velocity deformations and small scale mixing. Discontinuities are physically unrealistic approximations. After Danielsen and Hipskind (1980).

## STRAT-TROP EXCHANGE

Relative to the troposphere, the much larger vertical gradients of the lower stratosphere resemble a transition zone whose lower boundary is the tropopause. When averaged zonally and/or temporally the distributions of stratospheric tracers support this concept. In particular, the surfaces of constant mixing ratio and potential vorticity are parallel to the mean tropopause. As seen in Figure 5-1a and 5-1b they slope downward from the equator to the pole with the maximum negative slopes at the latitude of the mean west wind jet stream, Figure 5-1c. It follows that the mean tropopause can be identified by a constant value of potential vorticity, except near the equator where a large meridional gradient occurs due to a sign reversal in the southern hemisphere.

Figure 5-1b was derived and contoured from the potential temperature and zonal velocity analyses of Figure 5-1c. They, in turn, were computer derived from the observations of temperature, pressure, humidity, zonal and meridional wind velocities provided by the global radiosonde network. The conversion from temperature  $T$  to potential temperature  $\theta$  by

$$\theta = T \left( \frac{1000}{p} \right)^{0.286} \quad (5.1)$$

incorporates the nonconservative effects of compression on  $T$ ;  $\theta$  is conserved in adiabatic parcel motion, whereas temperature is not. In Equation (5.1),  $p$  is expressed in millibars, thus  $\theta$  is the temperature an air parcel would attain if compressed adiabatically to 1000 mb. The specific entropy is proportional to the logarithm of  $\theta$ , so a surface of constant  $\theta$  is often referred to as an isentropic surface. Trajectories computed from the horizontal winds on a constant  $\theta$  surface also are called isentropic trajectories. They follow the three dimensional adiabatic motions of the air and therefore one can obtain reliable estimates of the unmeasurable vertical velocities.

Potential temperature is not conserved when the air is heated by radiation or by conduction. Generally these diabatic heating rates are small because air consists predominantly of diatomic molecules, poor radiators and absorbers in the visible and infrared. Triatomic molecules, aerosols and hydrometeors, the radiatively active entities, are always trace species. Thus, the adiabatic assumption is realistic for cloud free transports, at least on timescales of a few days. When cloud forms in ascending air the release of latent heat by condensing water vapour increases  $\theta$ ; therefore a diabatic heating rate must be incorporated into trajectory computations.

Potential vorticity, the quantity Reed (1955) used as a tracer for stratospheric air, can also be used to detect mixing. It is a quasi-conservative scalar derived from the vector equation of motion, the continuity and energy equations, and is defined by

$$P = \alpha \nabla \theta \cdot (\nabla \times \mathbf{V} + 2\boldsymbol{\Omega}) \quad (5.2)$$

where  $\alpha$  is the specific volume,  $\nabla \theta$  is the three dimensional gradient of potential temperature and the term in parenthesis, the absolute vorticity, is the sum of the curl of the velocity and twice the angular velocity of the earth.

To an excellent approximation equation (5-2) can be reduced to

$$P_{\theta} = -g \frac{\delta \theta}{\delta p} (\zeta_{\theta} + f) \quad (5.3)$$

## STRAT-TROP EXCHANGE

where  $g$  is the acceleration of gravity,  $\delta\theta/\delta p$  is a measure of the stability of a parcel subject to a vertical displacement and  $(\zeta_\theta + f)$  (the sum of the horizontal curl or vorticity measured on a  $\theta$  map and the vertical component,  $f$ , of the earth's vorticity) is a measure of the stability of a parcel subject to a horizontal displacement.  $P_\theta$  combines as a product the two parcel stability criteria, namely hydrostatic stability and inertial stability. If both terms are positive, a displaced parcel is forced back to its equilibrium position. If either is negative, the displacement is amplified and mixing develops.

Reductions of static stability are produced by the horizontal convergence at constant  $\theta$  associated with propagating internal waves. The convergence reduces  $\delta\theta/\delta p$  by vertical stretching and simultaneously increases the vorticity  $(\zeta_\theta + f)$ . Conversely, divergence increases static stability and decreases inertial stability. Therefore, both vertical and horizontal mixing can occur with internal waves of large amplitude and long periods, but only locally where the waves have reduced the appropriate stability.

As shown by Reed (1955) and by Reed and Danielsen (1959), the values of  $P_\theta$  in the stratosphere exceed the tropospheric values by one, two or three orders of magnitude. In the absence of mixing,

$$\frac{dP_\theta}{dt} = -g (\zeta_\theta + f) \frac{\delta}{\delta p} \frac{(d\theta)}{(dt)} \quad (5.4)$$

From this we can easily account for the creation of large stratospheric and low tropospheric values. Heating above and cooling below increases  $P_\theta$ , thus the heating source of the ozone layer generates large values in the stratosphere. Conversely, heating at the earth's surface generates low values and leads to vertical mixing in the troposphere. When cloud or moisture layers extend up to the tropopause the radiative cooling at their top accentuates both trends.

Excluding radiative cooling at cloud tops,  $d\theta/dt$  is a small quantity in the free atmosphere, i.e., above the friction layer and below the ozone production layer. Therefore,  $P_\theta$  tends to be conserved as does  $\theta$ . For short periods both quantities approximate scalar invariants of the fluid and can be used as stationary Lagrangian coordinates.

This property permits one to trace and identify air of stratospheric properties. When the tropopause folds, tropospheric air with small values of  $P_\theta$  folds over an extruded layer of stratospheric air with large values of  $P_\theta$ . Since each parcel conserves its value of  $P_\theta$  during the folding process, the air of stratospheric origin can be readily identified even after it is considered a part of the troposphere.

Returning to Figure 5-1b, we can take advantage of the fact that the mean tropopause coincides with a constant  $P_\theta$  and define both the statistical mean tropopause and the synoptic tropopause by a threshold value of  $P_{\theta,T}$ . This definition, a generalization of the conventional definition avoids the concept of the tropopause as a discontinuity surface and the necessity for breaking such a surface when its slope becomes quasivertical. A discontinuity surface is an absolute barrier to mass exchange but, as discussed above, gradients that characterize the lower stratosphere are finite precisely because of small scale mixing and their associated mass exchange. Furthermore, the deformations maintaining the gradients imply divergence along the tropopause. This divergence demands an increase in area, which the tropopause can achieve only by folding. When the tropopause folds the gradients rotate but are not destroyed because potential vorticity is conserved in the folding process.

We can use  $P_{\theta,T}$  as a reference surface for computing irreversible mass transfers as the synoptic tropopause defined by  $P_\theta^h$  (the superscript denotes a local mean) oscillates relative to it. The displacements

## STRAT-TROP EXCHANGE

producing the oscillations can be reversible if they are stable but will become irreversible if they amplify exponentially with time. This type of irreversibility has been demonstrated by in situ and remote measurements of tropopause folding events described later.

These folds, which transfer air, trace gases and aerosols from the lower stratosphere into the mean troposphere, develop by a steepening of the tropopause at the jet core followed by a downward and southward stretching of the jet. Descending air on the north side of the jet is stratospheric, richer in ozone, potential vorticity and radioactivity but poorer in water vapour, carbon monoxide and aerosols than the descending tropospheric air on the south side of the jet. The atmosphere adjusts to this rapid downward and southward transport of horizontal momentum by forcing warmer air downward on the south side and cold air upward on the north side of the jet. This thermally indirect circulation, shown schematically in Figure 5-16, increases the horizontal pressure gradients in the upper and middle troposphere, balancing the increasing centrifugal accelerations of the developing cyclonic vortex. Thus, clouds and precipitation are generated in the cold air, in the core of the vortex, while clear skies predominate in the fold and in the tropospheric air southwest and south of the fold.

The streamlines in Figure 5-16 are similar to those in Figure 5-15 except for their inclined axes of convergence and divergence. Convergence normal to the fold counteracts diffusion by advecting tropospheric

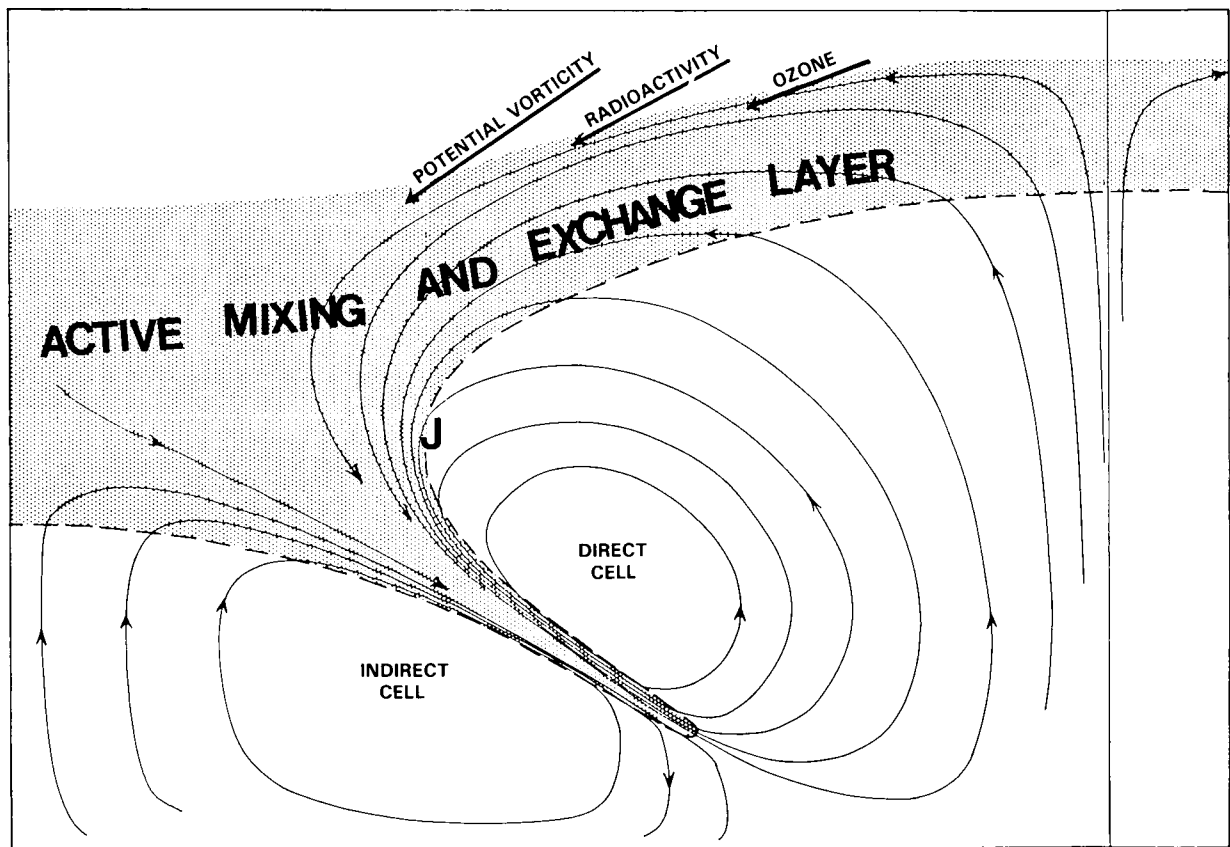


**Figure 5-16.** Thermally indirect and direct circulations which fold the tropopause and lead to irreversible transport from stratosphere to troposphere. Note entrainment of tropospheric air into fold along both boundaries, and that streamlines not trajectories are shown. From Danielsen (1968).

air into the fold. This entrained tropospheric air dilutes the mixing ratios of the stratospheric tracers - the mixture being advected southward and downward towards the surface boundary layer.

As the vortex continues to intensify, warm air to the east and north of the vortex ascends, producing more clouds and precipitation. This air turns anticyclonically (clockwise) away from the vortex, contributing to amplification of the ridge to the north and east of the vortex. The accelerating air resupplies momentum to the downstream jet, compensating for the momentum lost previously by the jet during the initial phase of cyclogenesis, and the amplifying ridge effectively cuts-off the vortex from its potential vorticity reservoir at high latitudes.

The result is an irreversible transfer of stratospheric air from the polar reservoir to lower latitudes and to lower altitudes. The process results in the formation of an isolated vortex at lower latitudes, each amplifying wave producing the same effect to varying degrees.

Less is known about the inflow of tropospheric air into the stratosphere. If there were no bulk transports associated with a large scale folding of the synoptic tropopause, the synoptic gradients of  $P_\theta$ ,  $\chi_{O_3}^1$ , and  $\chi_{Sr}^{1,0}$  in the stratosphere would be smooth and monotonic as are the zonal-annual means in Figures 5-1a and 5-1b. Analyses of  $\chi_\theta$  by Danielsen (1964, 1968) and vertical profiles of  $\chi_{O_3}^1$  from the AFCRL ozonesonde network (Hering and Borden, 1964-1966) demonstrate that such is not the case. There are well defined local maxima and minima in the lower stratosphere. Dobson (1973) postulated that the ozone minima were produced by ozone poor air from the upper subtropical troposphere entering the stratosphere at the conventional tropopause break and travelling northward at essentially constant altitude. The latter was based on statistical evidence of a maximum frequency of ozone partial pressure minima being  $15 \pm 1$  km from  $30^\circ$  to  $80^\circ$ N lat. There was also a similar maximum at higher latitudes at 23 km, for which Dobson could offer no explanation.

However, when the same data are analysed for ozone mixing ratio minima with  $\theta$  rather than  $z$  as the vertical coordinate, Danielsen and Kley (1986) show the maximum frequency occurs at  $\theta$ 's  $> 380$  K, i.e., much warmer than the  $\theta$ 's in the subtropical troposphere at the same height. In fact, the  $\theta$ 's are comparable to those in the lower tropical stratosphere. If the tropospheric air enters the stratosphere in the tropics and descends along constant  $\theta$  surfaces as it moves to the extratropics the adiabatic transport can be fast and effective in generating a sharply defined  $\chi_{O_3}$  minimum. Conversely, if the air enters at the subtropics and travels horizontally in the stratosphere the air must be diabatically heated by radiation to increase its  $\theta$  some 30 to 50 K. Much slower transports are then implied, with the transport times increasing greatly if the air is cloud free. Then one has difficulty explaining the well-defined minima given the evidence for ubiquitous small scale mixing in the stratosphere (but see Chapter 6).

However, an alternative view can also be taken. Figure 5-17 shows cross-sections of potential temperature and  $u$  from the climatology of Heastie and Stephenson (1960), for  $140^\circ$ E and  $75^\circ$ W in January. It is apparent that the isentropic surfaces in the 355-375 K range span the upper tropical troposphere and the middle and high latitude stratosphere, and that air can not only enter just above the core of the subtropical jet stream but can travel isentropically from  $30^\circ$ N to  $80^\circ$ N while maintaining an altitude of  $15 \pm 1$  km. This is consistent with the general circulation model results of Allam and Tuck (1984a, b), and the behaviour of the isentropic surfaces over the annual cycle is consistent with the maximum frequency of occurrence of the ozone-poor layers in late winter and early spring noted by Dobson (1973). Finally, inspection of ozonesonde ascents shows that ozone-poor minima in northern mid-latitudes are common in the range 350-380 K.

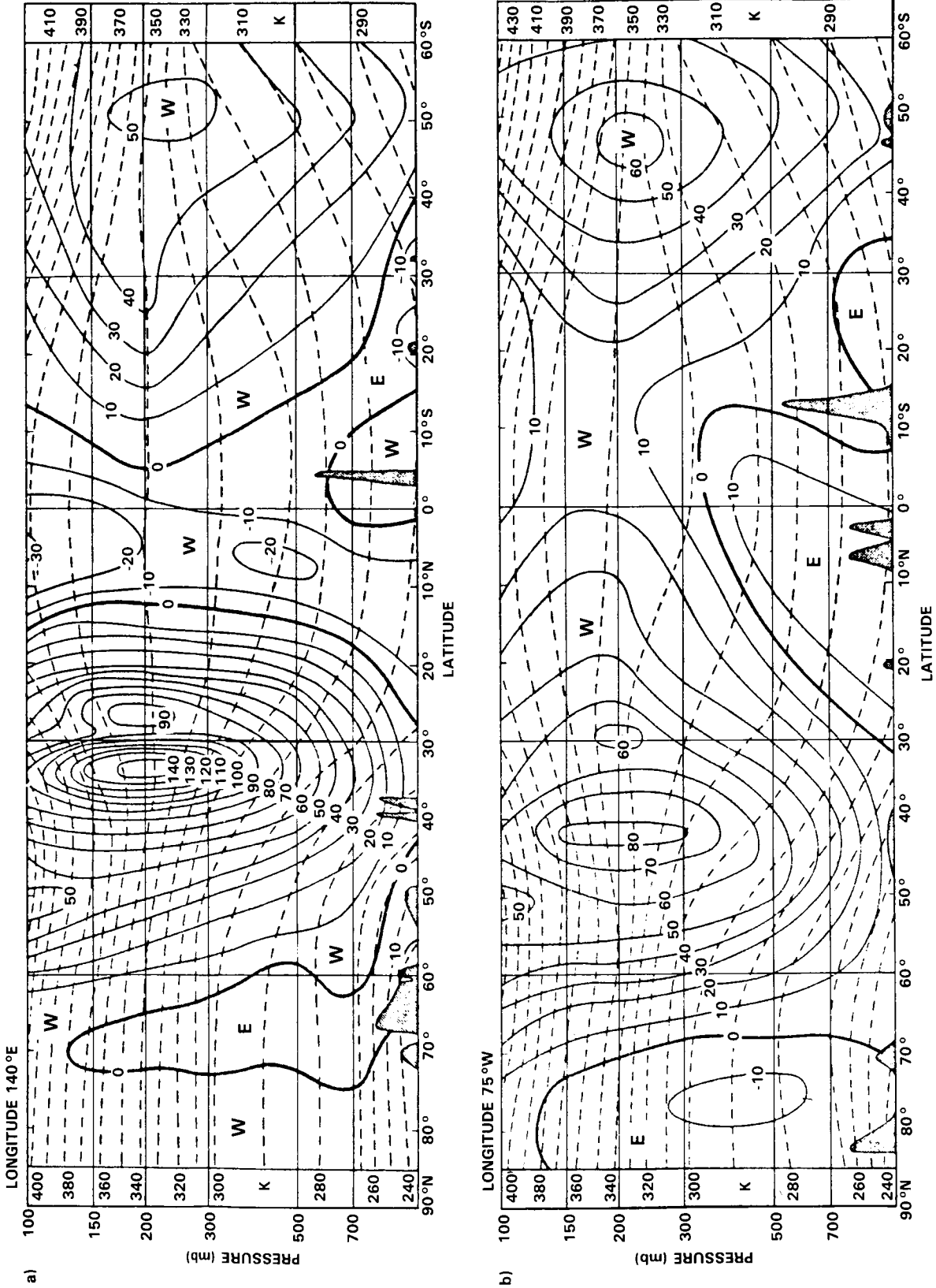


Figure 5-17. Vertical cross-section showing average zonal wind (knots) and potential temperature (K) in January. Isotachs are continuous lines, potential isotherms are dashed. (a) longitude 140°E, (b) longitude 75°W. From Heastie and Stephenson (1960).

In the case studied by Danielsen and Kley (*op. cit.*) the  $\chi_{O_3}$  minimum coincided with a  $\chi_{H_2O}$  minimum, i.e., it was cloud free and extremely dry. Also, their constant  $\theta$  trajectory analyses trace the air back to the tropics in 5 days. Furthermore, *in situ* observations made by the NASA U2 in the Spring 1984 STEP experiments show that the ozone-poor layers are dry and occur at  $\theta$ 's greater than 380 K. If these observations are statistically representative, then the bulk transports from troposphere to stratosphere must occur in the tropics. This however is subject to the counterarguments noted above, and to an absence of case studies near subtropical jet streams.

### 5.2.2 A Theoretical View of Mid-latitude Exchange

The dynamics of extra-tropical stratosphere - troposphere exchange are strongly influenced by two factors. The first is the contrast between the two regions in the very important quantity potential vorticity (PV):

$$\begin{aligned} P &= \frac{1}{\rho} \zeta_{\text{abs}} \cdot \nabla \theta \text{ in height coordinates} \\ &= -g \zeta_{\theta} / \frac{\partial p}{\partial \theta} \text{ in isentropic coordinates,} \end{aligned} \quad (5.5)$$

where  $\zeta_{\theta}$  is the vertical component of absolute vorticity evaluated in an isentropic surface. As discussed in detail in the review by Hoskins et al. (1985), in the absence of diabatic processes,  $P$  is conserved following the atmospheric motion. Further, the three dimensional isentropic potential vorticity (IPV) distribution plus the boundary temperature distribution at a particular time is sufficient to uniquely determine the atmospheric flow at that time provided only that the total mass between isentropic surfaces is known and the flow is in some sort of balance (e.g., quasi-geostrophic). A region of anomalously high IPV is generally associated with cyclonic vorticity in an extended region as well as compensating static stability changes (see Kleinschmidt, 1957 and refs). In the troposphere the PV has values below 1.5 units, where 1 PV unit equals  $10^{-6} \text{ K m}^2 \text{ s}^{-1} \text{ kg}^{-1}$ . The tropopause marks an abrupt transition to values of greater than 1.5 units and the magnitude increases rapidly with height in the lower stratosphere.

The second important factor is that there is significant potential temperature variation along the tropopause, which is therefore a sloping internal boundary when viewed in isentropic, as well as pressure and height, coordinates. Thus individual isentropic surfaces can sample both the stratospheric and tropospheric regions, and adiabatic flow on the surface can involve both regions. The lower stratosphere on such surfaces tends to move in association with synoptic disturbances that occur in the tropospheric region and it can indeed play a crucial role in the development of such disturbances.

#### 5.2.2.1 Deductions from Two-dimensional Models

Consideration of the stability of a 2-D flow  $v(x,z)$  in thermal wind balance with a temperature field  $\theta(x,z)$  to disturbances also independent of  $y$  yields (Ooyama 1966; Hoskins, 1974) an equation for the perturbation streamfunction in the  $x, z$  plane of the form

$$\frac{\partial}{\partial t^2} \left( \frac{\partial^2 \psi}{\partial x^2} + \frac{\partial^2 \psi}{\partial z^2} \right) = L(\psi) \quad (5.6)$$

## STRAT-TROP EXCHANGE

where  $L$  is an elliptic operator if  $P$  is positive. Analysis shows that the least stable direction is approximately along the isentropes and oscillations in this direction have a frequency

$$\sigma_{\min} = (f\xi_{\theta})^{1/2} \quad (5.7)$$

The most stable direction is approximately perpendicular to isentropic surfaces and their oscillation frequency  $\sigma_{\max}$  is such that

$$\sigma_{\max} \sigma_{\min} \propto P^{1/2} \quad (5.8)$$

Thus the large PV of the stratosphere implies markedly increased stability to motions perpendicular to isentropic surfaces, but no more resistance than the troposphere to motions along these surfaces.

In almost 2-D situations scaling arguments suggest that the flow  $v$  into the  $xz$  section should remain in geostrophic balance even for relative vorticities many times the Coriolis parameter. In this case the streamfunction for the ageostrophic flow ( $U_{ag,w}$ ) must be such as to maintain  $v$  in thermal wind balance with the temperature field, and consequently (Sawyer, 1956; Eliassen, 1962) must satisfy the equation

$$L(\psi) = 2Q_1. \quad (5.9)$$

Here  $L$  is the same elliptic operator as in Equation (5.6) and  $Q_1$  is a purely geostrophic term, being the tendency of the geostrophic wind to increase the  $x$ -temperature gradient. Synoptic disturbances in the troposphere will lead to non-zero values of  $Q_1$  and ageostrophic circulations. If the stratosphere was a high PV region with no isentropic gradient along the tropopause, it would act as a slightly flexible lid on the tropospheric circulation. However, since the isentropic gradient does exist and the stability of the stratosphere to motions along isentropes is not enhanced, the stratosphere tends to respond to tropospheric geostrophic forcing by ageostrophic motion along isentropes.

An example of a simple frontogenesis model in which this process occurs is shown in Figure 5-18. A temperature distribution which is independent of  $y$  contracts under the action of a geostrophic convergence  $u = -\alpha x$ .

Without any ageostrophic motions the tropopause slope would be gentle at this time. The tendency for the stratosphere to react to the forcing in the troposphere by moving along isentropic surfaces is marked. Equally marked is the tendency for the descent of stratospheric air to occur in a shallow tongue (as viewed in physical though not isentropic space), in contrast to the broad region of ascent of tropospheric air. This is in agreement with the scale analysis that suggests that the vertical scale of the response varies as  $P^{-1/2}$ . A further point of interest is that the Richardson number at the base of the tongue in Figure 5-18 has values as low as  $1/4$ , suggesting a high probability of mixing which would involve tropospheric and stratospheric air.

It is of interest to consider the applicability of quasi-geostrophic theory to the features discussed above. One of the basic assumptions of the theory is that static stability differences from those of a standard atmosphere, which is a function of the vertical coordinate only, are small. Thus it is not strictly applicable in the region of a sloping tropopause and, in particular, it would not give the development shown in Figure 5-18. In terms of Equation (5.6), the elliptic operator would be poorly approximated, but the geostrophic forcing  $Q_1$  would be correctly represented.

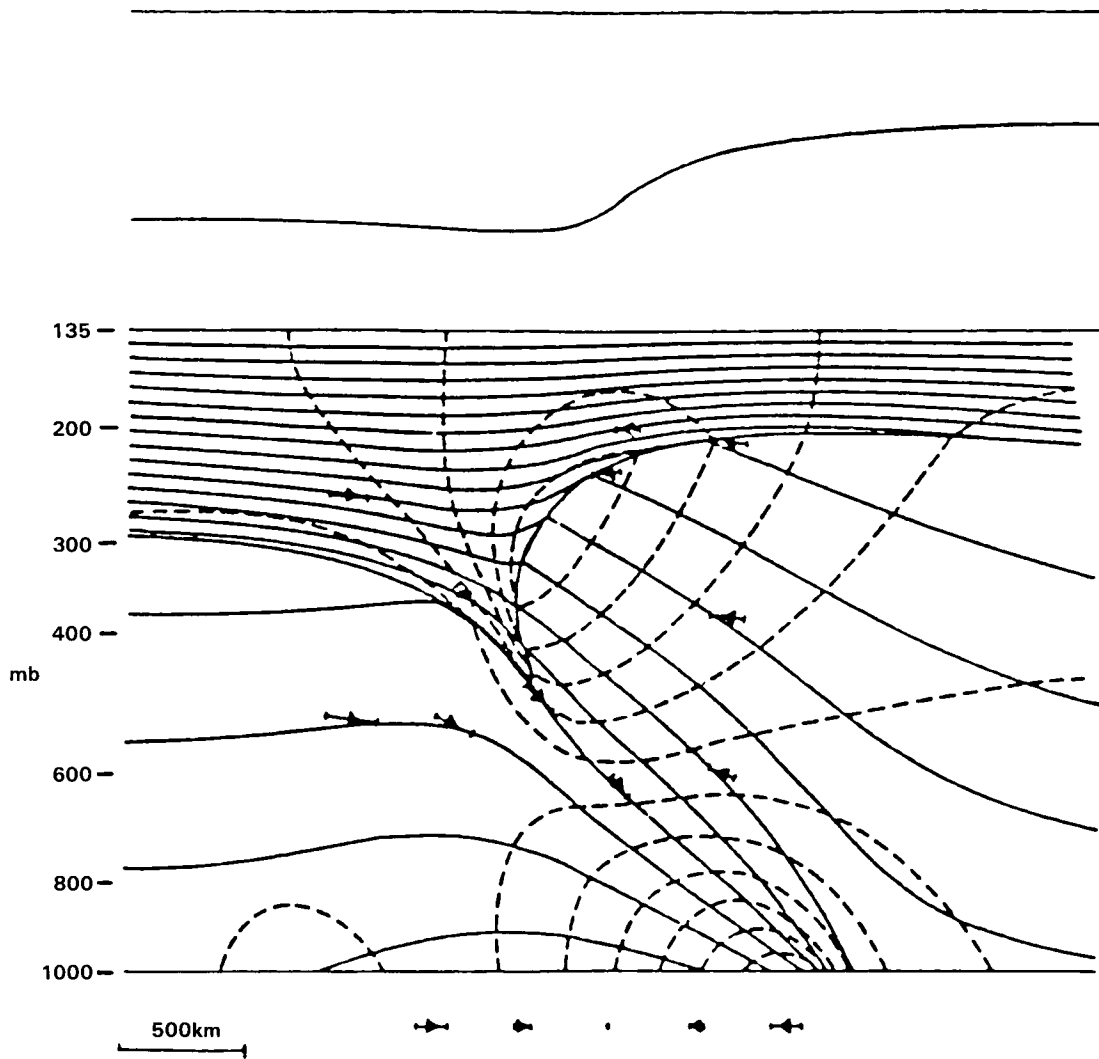


**Figure 5-18.** A simple frontogenesis model in which the basic deformation field shown below the lower axis acts on a 2-D situation with a tropopause which in the absence of any other motions would look as shown above. The actual tropopause position (heavy line), isentropes every 7.8 K (continuous lines), isolines of velocity into the section every  $10.5 \text{ ms}^{-1}$  (dashed contours) and particle motions (arrows) are shown in the centre. (After Hoskins, 1972).

### 5.2.2.2 Deductions from Three-dimensional Models

In three dimensions there are quasi-geostrophic (Hoskins *et al.*, 1978) and semi-geostrophic (Hoskins and Draghici, 1977) extensions of Equation (5.6), both describing the forcing of vertical circulations associated with a vector  $Q$  which is the tendency of the geostrophic wind to increase the vector temperature gradient on a fluid particle moving with the geostrophic wind. It is possible to find situations in the atmosphere (Shapiro, 1981) and understand them in these terms (Hoskins and Heckley, 1982) in which very strong descent of stratospheric air along isentropic surfaces is forced locally.

## STRAT-TROP EXCHANGE

As in two dimensions, quasi-geostrophic theory is wrong in its detailed prediction of tropopause movement. The semi-geostrophic equations (Hoskins, 1975) should be valid for motions whose Lagrangian time scale (time scale for change in  $v$  following a fluid particle) is much larger than  $f^{-1} \sim 3$  hours. Again they should be able to correctly treat movement of the tropopause because they do include a full vertical advection of PV. They have been used to model the growth to finite amplitude of a baroclinic wave or a basic zonal flow including a simple stratosphere as in the frontal example discussed above. As the wave grows, stratospheric air descends during its movement from the ridge towards the trough so that a vertical section across the trough shows the PV distribution given in Figure 5-19. The indication is that with more resolution in the numerical calculation it would become apparent that a standard synoptic development would exhibit marked tongues of stratospheric air descending along isentropes in upper air frontal structures. The model illustrated suffers from the numerical difficulty of accurately describing the advection of PV with its almost discontinuous structure at the tropopause.

The primitive equations have also been used to describe the growth of baroclinic waves to finite amplitude in situations with no diabatic heat sources. Shapiro (1975) used a 20-level isentropic coordinate model and showed the production in a strong synoptic development of very significant tongues of stratospheric air pushing into the troposphere. Another view of the probably irreversible mixing of stratospheric air into the troposphere in a baroclinic wave development is provided by the isentropic potential vorticity (IPV) and relative flow shown in Figure 5-20. The darkened region indicates the approximate location of the tropopause. As discussed in Hoskins and McIntyre (1985, paper in preparation), this picture is typical of the onset of decay in most, but not all simple baroclinic wave simulations. Sometimes the development is more similar to that in a cut-off low (Hoskins, *et al.*, 1985) in which, as viewed on an isentropic surface, a quasi-circular distribution of PV is separated from a near polar stratospheric vortex.

### 5.2.2.3 Diabatic Processes

The change of the IPV distribution in the presence of diabatic heating is approximately given by

$$\left( \frac{\partial}{\partial t} + \mathbf{v} \cdot \nabla_{\theta} \right) P = P^2 \frac{\partial}{\partial \theta} (\dot{\theta} P^{-1}) \quad (5.10)$$

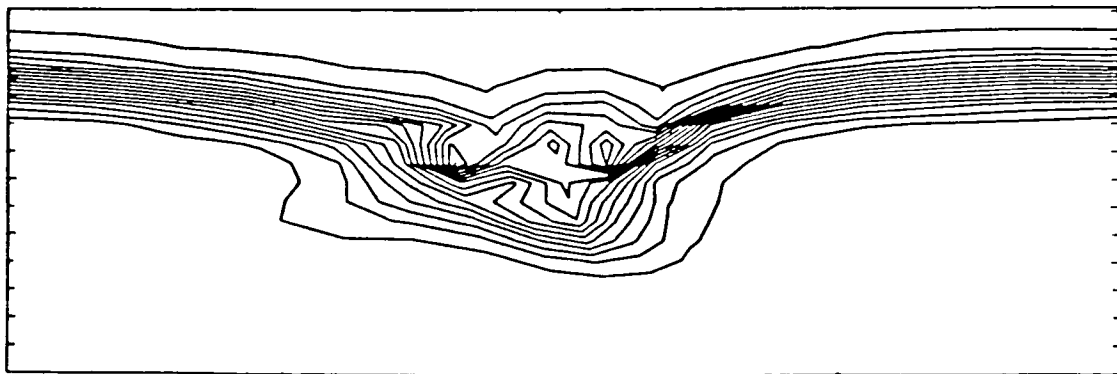


**Figure 5-19.** A vertical-zonal section across the trough of a non-linear baroclinic wave produced in a semi-geostrophic integration. The contours are those of potential vorticity defined for a Boussinesq fluid. The baroclinic wave had grown on a basic state with a narrow but finite transition from tropospheric to stratospheric values of potential vorticity. (After Hoskins and Heckley, 1982).

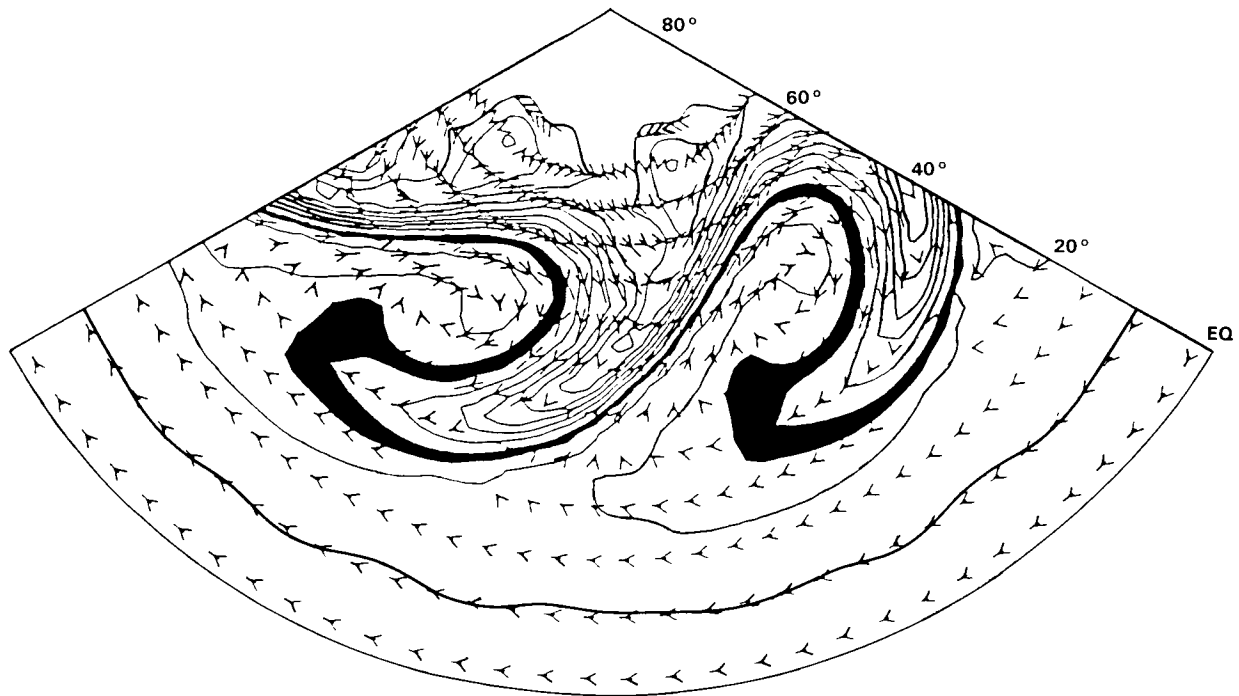


**Figure 5-20.** The day 8 350 K IPV map for a basic zonal wavenumber 6 baroclinic wave life-cycle experiment. The contour interval is  $0.8 \times 10^{-6} \text{ m}^2 \text{ s}^{-1} \text{ K kg}^{-1}$ . Also shown by arrows is the wind field on this isentropic surface in a frame of reference moving with the waves. The arrows nearest the equator represent a speed of  $16 \text{ ms}^{-1}$  (After Hoskins, *et al.*, 1985).

In the lower stratospheric polar vortex the radiative timescale determines the rate of change of  $P$  and indeed the maintenance of the vortex. However a descent of stratospheric PV along isentropes, as indicated above, induces cyclonic vorticity and reduced static stability in the underlying troposphere to an extent dependent on the surface temperature. If the anomalous IPV is moving relative to the low-level air, it also induces upward motion on its leading side. It thus leads to a region of much enhanced likelihood of moist convection, the extent of which depends on the low-level supply of moisture. The latent heating associated with this convection causes a change in the IPV distribution above it which occurs at a rate which may be deduced from Equation (5.10) as being sufficient to reduce the PV of the lower stratospheric air to tropospheric values in a matter of days. The descending stratospheric air therefore efficiently induces a process which usually absorbs it into the troposphere in a few days.

As in the 2-D models, one may also expect a 'lowered' tropopause to be a region of enhanced turbulent mixing. Shapiro (1976, 1978, 1980) produced evidence of such behaviour. However, as discussed by Shapiro (1978) and Gidel and Shapiro (1979), the result of this turbulence may not necessarily be a reduction in the PV contrast between air of stratospheric and tropospheric origin.

Upward motion of the middle latitude tropopause, on the other hand, is associated with anticyclonic vorticity and increased static stability in the troposphere. The chances of diabatic processes occurring on anything but the radiative timescale are reduced, and so it is not envisaged that these relatively broad regions will be favourable for major exchanges of tropospheric and stratospheric air. A blocking high, according

## STRAT-TROP EXCHANGE

to Hoskins *et al.* (1985), is the dynamical twin of the cut-off low, having such a raised tropopause associated with the poleward advection along isentropic surfaces of sub-tropical air. However as far as diabatic processes are concerned the nature of the two phenomena is very different, the blocking high tending to decay slowly on an advective or radiative timescale as opposed to the usually convection dominated, fast decay of the cut-off low.

Nevertheless, detailed studies of the relative rates of radiative lowering of the tropopause and advective decay in cut-off anticyclones have not been made, so exchange induced by radiative effects in such systems cannot be excluded.

### 5.2.3 A View Based on Isentropic FGGE Analyses

In this section a global scale view of the general circulation is developed, using isentropic analyses of the FGGE year (1979), as a context in which to see stratosphere-troposphere exchange, and to derive some constraints on the scales and location of exchange. The approach is to examine the scale of the mass circulation in the framework of the scale of the differential heating (taken to include radiation and latent heat release), by using Helmholtz's theorem to decompose the flow into irrotational ( $\nabla \times \mathbf{V} = 0$ ) and rotational ( $\nabla \cdot \mathbf{V} = 0$ ) components. Accordingly, the quasi-horizontal mass transport in an isentropic layer may be written as

$$\overline{\rho \mathbf{J} \mathbf{U}} = \nabla_{\theta} \bar{\chi} + (\mathbf{k} \times \nabla_{\theta} \bar{\psi}) \quad (5.11)$$

where  $\rho$  = density,  $\mathbf{J}$  is the Jacobian for transformation of vertical coordinate to potential temperature  $\theta (= | \delta z / \delta \theta | )$ ,  $\mathbf{U}$  is horizontal velocity,  $\chi$  = transport potential function,  $\psi$  = transport stream function and the overbars are time averages.

Then

$$(\overline{\rho \mathbf{J} \mathbf{U}})_{\chi} = \nabla_{\theta} \bar{\chi} \quad (5.12)$$

is the irrotational component of the flow, and

$$(\overline{\rho \mathbf{J} \mathbf{U}})_{\psi} = \mathbf{k} \times \nabla_{\theta} \bar{\psi} \quad (5.13)$$

is the rotational component.

The Poisson equations used to determine  $\chi$  and  $\psi$  are

$$\nabla_{\theta}^2 \bar{\chi} = \nabla_{\theta} \cdot (\overline{\rho \mathbf{J} \mathbf{U}}) = \delta \quad (5.14)$$

$$\nabla_{\theta}^2 \bar{\psi} = \mathbf{k} \cdot \nabla_{\theta} \times (\overline{\rho \mathbf{J} \mathbf{U}}) = \zeta \quad (5.15)$$

where  $\delta$  = divergence and  $\zeta$  = vorticity.

The approach is to calculate the divergence and curl of the mass transport from the NMC FGGE Level IIIa analysis.

By considering the time-averaged isentropic mass continuity equation (Johnson, Townsend and Wei, 1985) it is possible to show that, relative to isentropic surfaces, horizontal mass convergence (divergence) is balanced by an increase (decrease) of the upward mass flux in regions of heating, or a decrease (increase) of the downward mass flux in regions of cooling. It is thus possible to isolate thermodynamically coupled planetary circulations that connect regions of heat sources and heat sinks. It turns out that there is a component of such a circulation which is involved in stratosphere-troposphere exchange.

Considerable evidence exists regarding the extrusion of stratospheric air into the troposphere during cyclogenesis through circulations attending jet streams. Reed (1955), Briggs and Roach (1963), Danielsen (1964, 1967, 1968), Mahlman (1965), Reiter (1969, 1971 and 1972), Shapiro (1980), as well as others, clearly establish that stratospheric extrusions into the troposphere are maximized during cyclogenesis (see following section in this report). Return transport of tropospheric air into the stratosphere is required for the stratospheric balance of mass. Smith (1968), Reiter, Glasser and Mahlman (1969) and others have pointed out that quasi-horizontal transport processes serve to return tropospheric air to the stratosphere. Note however that Mahlman (1973) diagnosed transverse circulation in a steady (non-cyclogenetic) polar front jet stream which could produce exchange. Others have emphasized the importance of rising motion across the tropical tropopause (Brewer, 1949; Dobson, 1956) in conjunction with a "cold trap", tropical convection, and dehydration (Danielsen, 1982; Holton, 1984b). Details of the return of tropospheric air into the stratosphere however, are uncertain (Reiter, 1972; Ellsaesser, 1979; Holton, 1984b). The purpose of this discussion is to draw attention to physical processes associated with baroclinic phenomena and geostrophic motion in middle latitudes which provide for systematic stratospheric-tropospheric exchange (Johnson, 1979). While the importance of geostrophic modes of transport of properties has been established for decades, the systematic planetary nature of geostrophic mass transport, stratospheric-tropospheric exchange and differential heating within secondary and primary scales of atmospheric circulation has not been fully recognized.

In a recent study of the transport of water vapour within a stratospheric-tropospheric general circulation model, Allam and Tuck (1984a and b) concluded "that most of the water enters the stratosphere near the tropopause breaks by quasi-horizontal advection from the upper tropical troposphere into the lower extratropical stratosphere, although an appreciable amount moves vertically in the same region and at rather higher latitudes. This advection occurs chiefly through the action of eddies." They stated "that the simulated transport of water vapour by eddies in the stratosphere is greater in the northern than in the southern hemisphere" and that "the transport is greater during winter than during summer." Allam and Tuck (1984b) also noted from a trajectory analysis of general circulation model data that through quasi-horizontal transport, motions induced in regions of high shear and vorticity resulted in dry air from the upper tropical troposphere being mixed into the stratosphere. The evidence from these simulations substantiates suggestions that intrusion of tropospheric air into the stratosphere is associated with quasi-horizontal transport processes embedded within baroclinic waves and the meandering of polar and subtropical jet streams as well as with deep vertical convection in the tropics, a view emphasized by Reiter (1972).

From a dynamical point of view, this behaviour is to be expected. Within latitudinal regimes where rotation is important (i.e., scales large enough for the Coriolis force to largely balance the pressure gradient force), quasi-horizontal exchange processes through geostrophic motion are dominant. The important role that quasi-horizontal exchange within baroclinic waves plays in forcing meridional circulations in the troposphere is firmly established (Lorenz, 1967). The condition that quasi-horizontal exchange processes play an important role in the stratosphere is also established; however, the relative importance of quasi-horizontal exchange of trace constituents as opposed to exchange by mean meridional circulations is not well established, although a framework for providing a mechanistic means of doing this has been

## STRAT-TROP EXCHANGE

suggested recently (Mahlman *et al.*, 1984). Much of the uncertainty stems from lack of observations; however conceptual awkwardness also stems from averaging within coordinate systems that fail to permit degrees of freedom to isolate mass and energy transport processes within the atmosphere which are directly linked to the differential heating (Johnson, 1980, 1984b).

Within isentropic coordinates, the scale of the time-averaged mean mass circulation corresponds with the scale of the mean energy transport by differential heating. "Direct" planetary scale mass circulations exist in the sense that a branch of the circulation transports mass and energy from heat source to heat sink in upper isentropic layers and from heat sink to heat source in lower layers. Satisfaction of global energy balance requires that such mass circulations and transport processes exist apart from the distributions of atmosphere trace constituents. However, if within isentropic layers a correlation exists between a branch of a mass circulation and a trace constituent, it is likely that the isentropic mass circulation will be a key element in determining the scale and intensity of the quasi-horizontal transport of the trace constituent.

Before setting forth a simple model of stratospheric-tropospheric exchange, it is important to emphasize underlying reasons for systematic isentropic mass circulations in the atmosphere that serve to transport trace constituents. Concepts basic to the isolation of systematic isentropic mass circulations at the planetary scale were set forth by Shaw (1942). He noted that heating forced motion upward through isentropic surfaces while cooling forced motion downward, and that such motion constituted upward and downward branches of a mass circulation embedded within a stratified atmosphere. Horizontal branches linking heat sources and sinks through irrotational modes of mass transport are implied from the isentropic equation of continuity. The same mass circulations transport more dry static energy from heat source to sink in the upper layers than is returned in lower layers. Thus, net energy is transported from the heat source to the heat sink even though the net mass transport vanishes (Johnson and Townsend, 1981; Johnson, 1984a; Johnson, Townsend and Wei, 1985). As such, these global circulations are monsoonal in nature and will be at their maximum intensity in the winter season (Johnson, 1984a and b). These constraints, which require that within time-averaged circulations the scale of mass and energy transport corresponds with the scale of differential heating, permit no compromise, at least within hydrostatic atmospheres. While complexities are introduced by baroclinic, symmetric and convective instabilities, a fundamental premise for the development of monsoonal planetary circulation is that the transport processes during such instabilities should satisfy the basic requirement of net energy transport from heat source to heat sink, in the time-averaged sense.

### 5.2.3.1 Systematic Meridional Exchange by Geostrophic Modes of Isentropic Mass Transport

In their numerical simulation, Allam and Tuck (1984a,b) established that poleward and upward transport of water vapour from the troposphere into the stratosphere of each hemisphere occurred through eddies. These eddy circulations in their analyses are finite amplitude baroclinic features of middle latitudes. Johnson (1979) emphasized that systematic meridional mass exchange in finite amplitude baroclinic waves provided for intrusion of tropospheric air into the stratosphere by quasi-horizontal exchange and that this intrusion of tropospheric air would occur within an isentropic mass circulation that spanned the hemisphere. The combination of Allam and Tuck's results and the systematic nature of geostrophic transport processes point out the importance of isolating isentropic mass circulations embedded within baroclinic phenomena.

Recently Townsend and Johnson (1981, 1985) and Johnson (1984a) contrasted isobaric and isentropic zonally averaged meridional circulations; Figure 5-21 portrays isobaric and isentropic stream functions of the zonally averaged mass transport. Within the isentropic mass circulation the upward branch in tropical latitudes is associated with net heating while the downward branch in polar latitudes is associated with

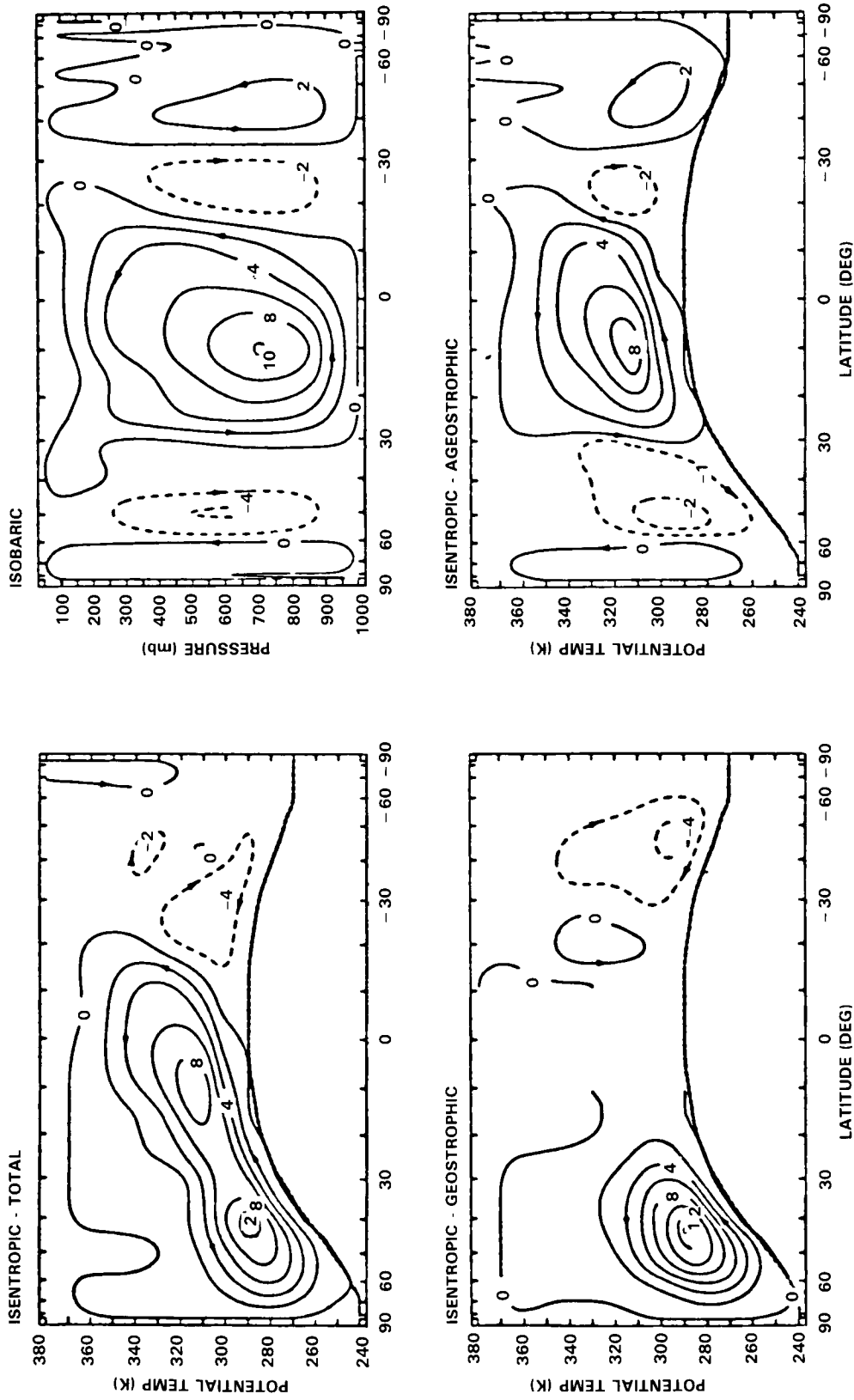


Figure 5-21. Mass stream function for the isobaric and isentropic mean meridional circulations for January (1979) (units,  $10^{10} \text{ kg s}^{-1}$ ). Arrows indicate the direction of the circulation. Note that a branch of the circulation spans the upper tropical troposphere and the lower stratosphere of middle and high latitudes.

## STRAT-TROP EXCHANGE

net cooling. As noted earlier, quasi-horizontal branches are required by mass continuity. These isentropic results verify Shaw's (1942) argument that the scale of the isentropic mass circulation corresponds with the scale of the differential heating.

While reasons for the differences between the scale of the meridional circulations in isobaric and isentropic coordinates involve several factors, one of the key factors is the degree of freedom for geostrophic mass transport in isentropic coordinates. Note in Figure 5-21 that the isentropic mass circulation can be partitioned into geostrophic and ageostrophic components. The scales of isentropic, ageostrophic meridional exchange are identical with the scales of meridional exchange in isobaric coordinates. Within low latitudes the mass transport within the isentropic Hadley circulation is through the ageostrophic mode while in extratropical latitudes it is through the geostrophic mode. Mean meridional velocities within this geostrophic circulation are of the order of a few meters per second and are of the same magnitude as the meridional velocities within the ageostrophic Hadley circulation. Isentropic mass circulations entail a handover between the ageostrophic and geostrophic modes of transport which does not require a change in the scale of horizontal transport within an isentropic layer (Johnson and Downey, 1975). This degree of freedom allows the establishment of a direct link between the global scale of differential heating and the scale of the atmospheric response, in the context of a temporally or zonally averaged mass circulation. The implication of this for stratosphere-troposphere exchange is that a portion of the meridional mass transport in upper isentropic layers begins in tropospheric regions of the tropics and subtropics and ends in the stratospheric regions of the extratropics and polar latitudes. One should note that within polar latitudes, the downward diabatic mass flux with respect to the isentropic stratification also provides for a systematic transfer of air from the polar stratosphere into the polar troposphere (Figure 5-21).

### 5.2.3.2 Geostrophic Modes of Mass Transport and Quasi-horizontal Stratospheric-Tropospheric Exchange Within Middle Latitudes

With regard to extratropical cyclones, jet streams, and baroclinic waves the quasi-horizontal stratospheric-tropospheric exchange will have characteristic features which are different within each of the phenomena and, as such, each of these phenomena deserves attention in order to understand their specific role. In summarizing atmospheric transport processes, Reiter (1972) reviews in detail the work of Reed, Danielsen, Staley, Reiter, Mahlman and others, and discusses exchange within each of these phenomena. Major emphasis has been placed on exchange processes attending jet streams. Viewed within a larger scale context however, none of these phenomena are independent since, within the structure of a large scale amplifying baroclinic wave in the westerlies (Newton and Palmen, 1963), all of these phenomena will be present. As a consequence all of the phenomena may be considered to be components of baroclinic instability or "sloping convection" (Hide and Mason, 1975) as it is realized in the actual atmosphere. Large scale meridional energy exchange within the amplifying baroclinic waves is accompanied by cyclo- and fronto-genesis in the lower troposphere in conjunction with jet stream circulations in the upper troposphere. In the following discussion the primary focus will be on physical processes within amplifying large scale baroclinic waves which provide for systematic stratospheric-tropospheric exchange through geostrophic modes of mass transport (Johnson, 1979).

Some physical insight into mean meridional motion within mid-latitude baroclinic waves is provided from the structure of a steady and an amplifying baroclinic wave (Charney, 1947; Eady, 1949). In the schematic (Johnson, 1979; Townsend and Johnson, 1985) showing the horizontal distribution of pressure and potential temperature of the steady baroclinic wave, the pressure and temperature are assumed to be in phase

(Figure 5-22). Within the zonal vertical cross-section of a layer extending from a lower isentropic surface  $\theta_1$  to an upper isentropic surface  $\theta_u$ , a midvalue isentropic surface  $\theta_m$  divides the hypothetical atmosphere into two regions. Ideally an isentropic surface  $\theta_m$  equal to 315 K would for the most part separate polar and subtropical air masses in the troposphere. In the cross-section, the dotted vertical lines designate trough and ridge positions that separate regions of poleward and equatorward geostrophic motion. The increase of wind with height reflects the thermal wind contribution from the baroclinic temperature distribution.

With a vertical scale linear in pressure, the relative position of the isentropes shows the greater mass ( $g^{-1}(\delta p/\delta\theta)d\theta$ ) in the layer between  $\theta_1$  and  $\theta_m$  to be positioned in the trough and lesser mass to be located in the ridge. The reverse mass distribution occurs in the layer above  $\theta_m$ . With the in-phase relation of the potential temperature and pressure fields, the intensity of the isentropic mass transport  $\rho Jv$  is symmetric about the trough line within each layer ( $J$  is the Jacobian of transformation,  $|\delta z/\delta\theta|$ ). The poleward mass transport forward of the trough is exactly balanced by equatorward transport to the rear of the trough. Thus, the mean meridional motion vanishes within each layer.

In the model of the amplifying baroclinic wave, the potential temperature is assumed to lag the surface pressure wave by a phase angle of  $90^\circ$  (see Figure 5-23). In the zonal cross-section, this lag of potential temperature introduces a westward tilt of the baroclinic wave in conjunction with the displacement of the coldest air to the inflection point of the surface pressure wave. A systematic structure results which provides for net poleward geostrophic mass transport above 315 K and an equatorward mass transport below 315 K. Ahead of the trough, poleward mass transport above 315 K located within a deeper layer of mass is greater than in the rear of the trough with its equatorward motion. Beneath 315 K the reverse

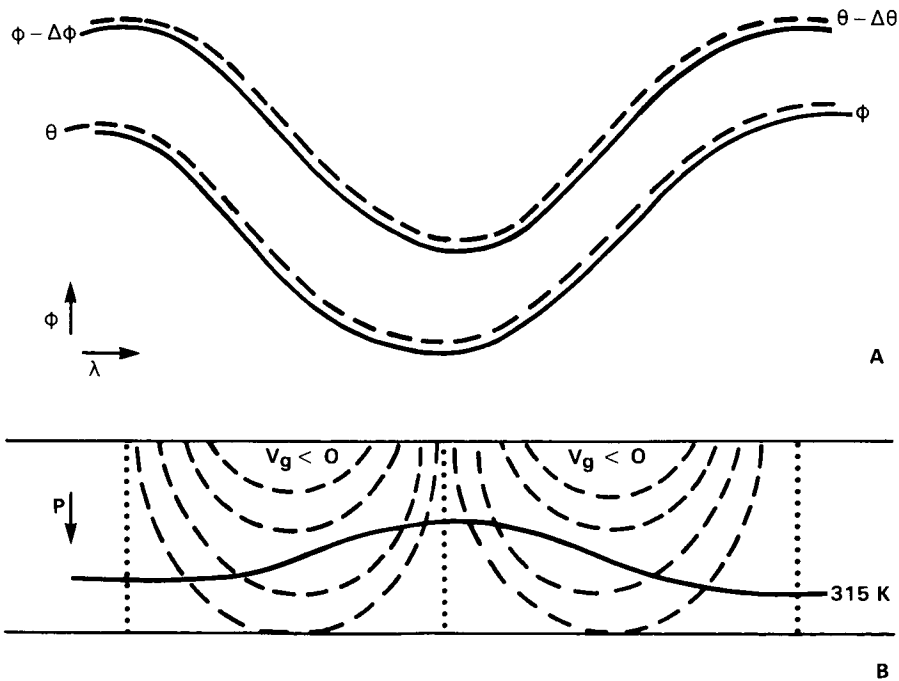


**Figure 5-22.** Schematics of horizontal ( $\lambda, \theta$ ) and vertical ( $\lambda, p$ ) distributions of geopotential and potential temperature within a steady baroclinic wave. In the zonal, vertical cross-section the dashed lines designate trough and ridge positions which separate regions of poleward and equatorward geostrophic motion within two isentropic layers. The layer in part (b) extends from a lower isentrope  $\theta_1$  to an intermediate isentrope  $\theta_m$  to an upper isentrope  $\theta_u$ . From Johnson (1979).

## STRAT-TROP EXCHANGE

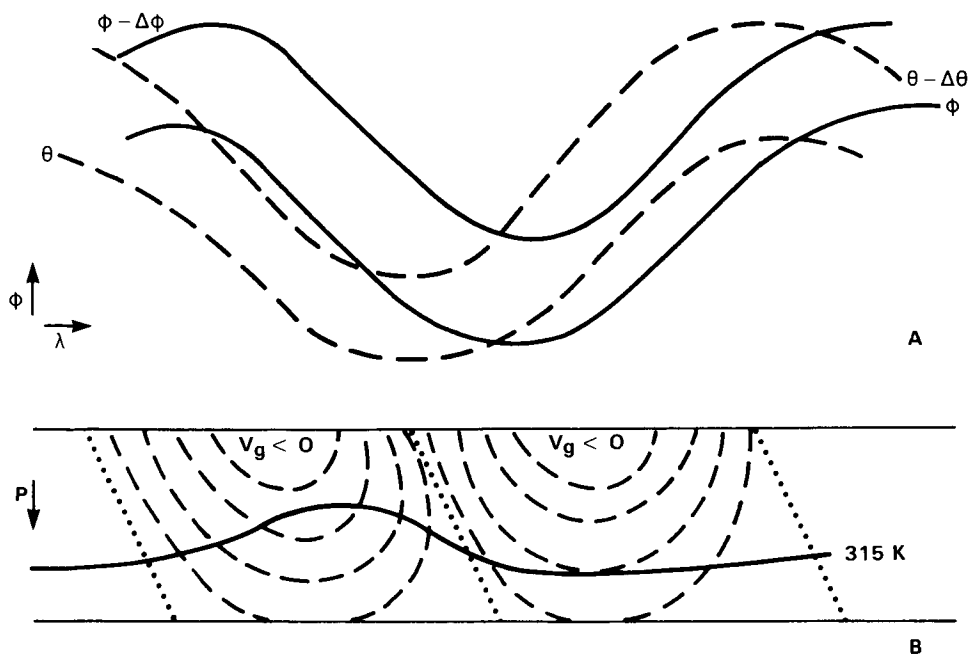


**Figure 5-23.** Schematic of amplifying baroclinic wave. See legend of Figure 5-22 for structural details.

occurs with more mass moving equatorward in the rear of the trough than ahead of the trough. As a consequence, the mean meridional mass transport within active baroclinic waves for this two-layered structure is poleward above 315 K and equatorward below 315 K.

The isentropic structure illustrated in Figure 5-24 transects a large amplitude wave that was studied extensively by Newton and Palmen (1963). This vertical cross-section is orientated nearly east-west along a line from Tucson to Bermuda. Newton and Palmen's analyses have been modified by rescaling the vertical coordinate. The layer extending from the earth's surface to 320 K contains more mass in regions of equatorward motion than in regions of poleward motion and reflects the strong equatorward movement of the polar air mass. Within the shaded area from 320 K to 335 K, more mass is located in the region of poleward motion (which is also more intense) than in the region of equatorward motion, reflecting the mean poleward movement of the subtropical air mass. The slope of the zero isotach indicates a westward tilt of the pressure wave with height in conjunction with the colder air to the rear of the surface pressure trough, the configuration of an intensifying baroclinic wave. Thus a mean meridional exchange occurring within this wave is similar to the exchange in the schematic of the amplifying wave. Since meridionally this layer spans the subtropical troposphere and the polar stratosphere, the structure indicates that the mean poleward motion is a mode of intrusion of tropospheric air into the polar stratosphere. It is interesting to compare Figure 5-24 with the cut off low described in Bamber *et al.* (1984), see also Section 5.2.6, where trace species profiles showed evidence of mixing over a considerable depth in the upper troposphere/lower stratosphere. This type of exchange would be suppressed in steady baroclinic waves. A similar structure of isentropic mass transport within an amplifying baroclinic wave is even more pronounced in Danielsen's cross-section through a baroclinic wave over the western United States for 1200 GMT, 13 April 1972 (see Danielsen's Figures 1 and 2, 1974). Geostrophic modes of mass transport exist within extratropical cyclones (Johnson and Downey, 1975), jet streams (Uccellini and Johnson, 1979) and baroclinic waves (Johnson, 1979, Townsend, 1980).

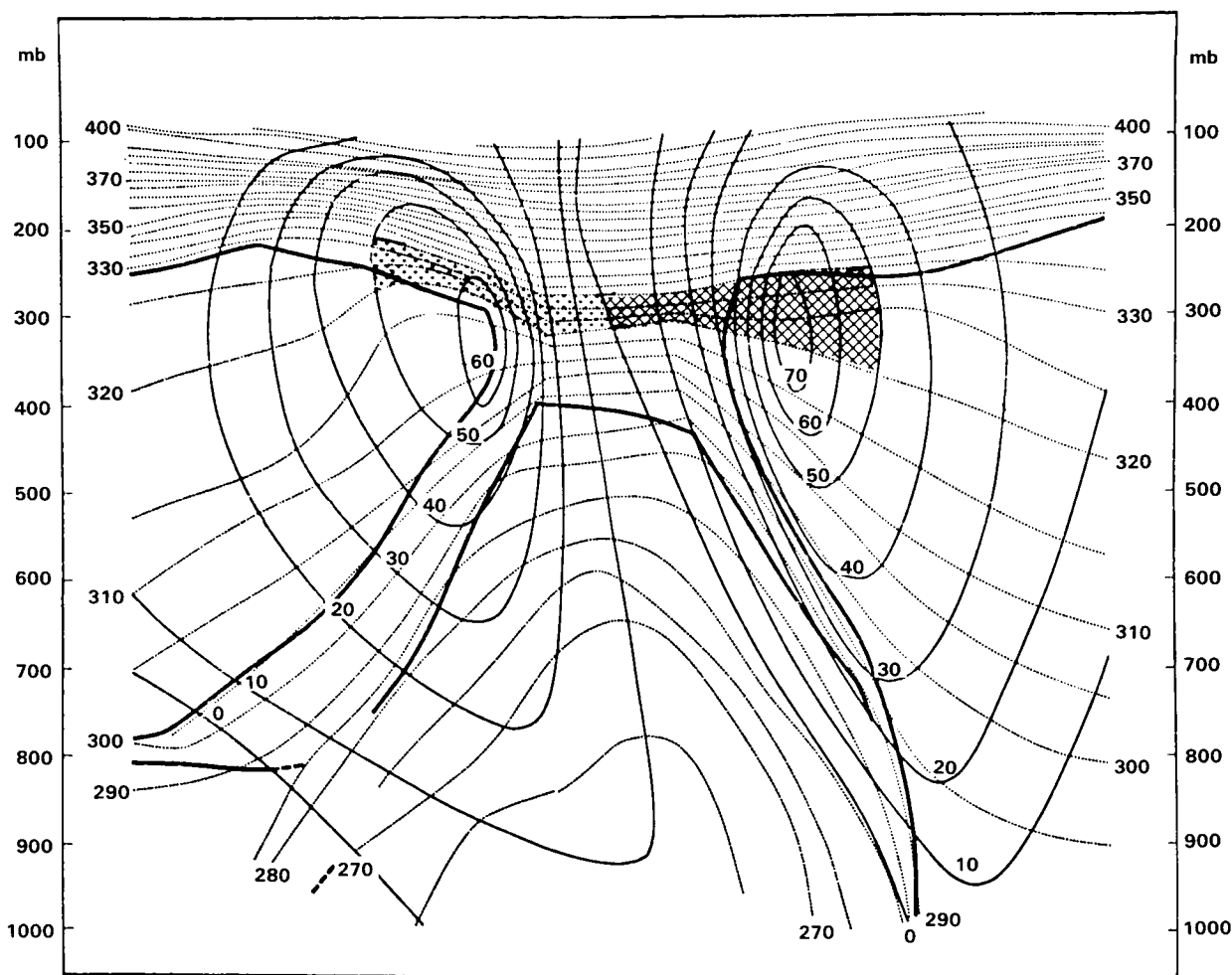


**Figure 5-24.** Vertical cross-section from Tucson to Bermuda through a large amplitude wave studied by Newton and Palmen (1963). Dotted lines are isentropes, solid lines are isotachs of the meridional wind while heavy lines are frontal boundaries and tropopause. Shaded regions show layer of positive covariance of mass and meridional motion embedded in wave structure.

In his study of the isobaric and isentropic circulation Townsend (1980) determined the isentropically time averaged mass transport along  $50^{\circ}\text{N}$  for the FGGE year (1979). Figure 5-25 shows results for the FGGE winter season from Townsend (1980). Note the systematic westward tilt of the zero isopleths of meridional velocity and the baroclinic structure that is indicative of the baroclinic instability process and a systematic geostrophic mode of mass transport. The tilt of the baroclinic disturbances extends upwards through the 360 K isentropic surface indicating that systematic stratospheric-tropospheric exchange is also present.

In interpreting the structure of the zonal cross-section of the isentropic meridional mass transport, one should realize the time averaged transport statistics are determined primarily by the isentropic geostrophic

## STRAT-TROP EXCHANGE

mass transport within all quasi-horizontal baroclinic circulations. As such, the isentropic statistics represent the average exchange occurring in what are commonly regarded to be both stationary and transient eddies in isobaric coordinates. Comparison with similar analyses in isobaric coordinates for 50°N would direct attention to transient components. For example, the embedded isentropic mass circulation in higher latitudes during the wintertime in Figure 5-21 is linked with propagating baroclinic disturbances which develop over the warm ocean currents off the east coasts of Asia and North America as cold polar air streams eastward and acquires latent and sensible energies from oceanic sources. The net meridional mass transport within the zonal cross-section (Figure 5-25) associated with such disturbances is located between 90°E and 90°W. Note that the equatorward mass transport in the low troposphere, which is part of the cold Asiatic winter monsoonal flow, is found between 90°E and 160°E while the poleward mass transport of warmer air is located between 160°E and 150°W.

The relatively large scale of the baroclinic feature from 90°E through 150°W and the depth also suggests that this feature is associated with a systematic poleward transport of tropical tropospheric air from the Philippine-Indonesia tropical convection zone within the Indonesian tropical belt. See Johnson and Townsend (1981, also Johnson, Townsend and Wei, 1985) for the mass and energy transport associated with these features at the planetary scale which within the three-dimensional structure provide for systematic intrusion of tropospheric air from the tropics into the stratosphere of higher latitudes.

### 5.2.3.3 Some Additional Aspects of Stratospheric-Tropospheric Exchange in Mid-latitudes

In studies of stratospheric-tropospheric exchange by quasi-horizontal transport processes, major emphasis has been devoted to the injection of ozone, radioactive debris and potential vorticity into the troposphere during cyclogenetic activity. With the higher concentration of these constituents in stratospheric air, these properties become excellent tracers of extrusions of stratospheric air into the troposphere. The condition that the concentration of ozone and radioactive debris in the troposphere is maximized during early spring has been associated with intense jet stream activity and deep convection during this season. Although these dynamic features partially explain the spring maximum of ozone concentration near the earth's surface in middle latitudes of the Northern Hemisphere, some aspects of this problem are related to seasonal variations of the isentropic structure of the stratosphere. During the winter an annual maximum of ozone develops in the polar stratosphere (Hering and Borden, 1965). With the energy deficit of the winter hemisphere and the development of an intense circumpolar vortex that extends from the troposphere upward into the stratosphere, isentropic layers climatologically located in the low polar stratosphere and the high troposphere of middle latitudes become entirely displaced into the stratosphere, though the effect of infrared cooling and consequent sinking of the isentropes and tropopause in regions where the mid-latitude upper tropospheric westerlies have moved equatorward. In the depth of winter such layers would not engage in stratospheric-tropospheric exchange in mid-latitudes. The lesser winter time extrusion of stratospheric air is also likely from the increased stratification which suppresses convective and symmetric modes of instability within or near hyperbaroclinic zones of jet streams. In spring, the troposphere of mid-latitudes rapidly warms, particularly over low-albedo land areas between 30° and 40°N, while the troposphere poleward of 50°N warms less rapidly. The result is that isentropic layers of the low stratosphere in winter become a part of the tropospheric circulation of the mid-latitudes during this season while within the troposphere the static and symmetric (inertial) stability of the atmosphere is decreased, in the sense that the horizontal wind shear on the anticyclonic side of the jet streams is increased. Active baroclinic waves in association with cyclogenesis and intensification of jet streams can now more actively tap the stratospheric reservoir of ozone through quasi-horizontal exchange processes which through increased inclination of isentropic surfaces transport ozone from the polar stratosphere into the lower troposphere of extratropical latitudes.

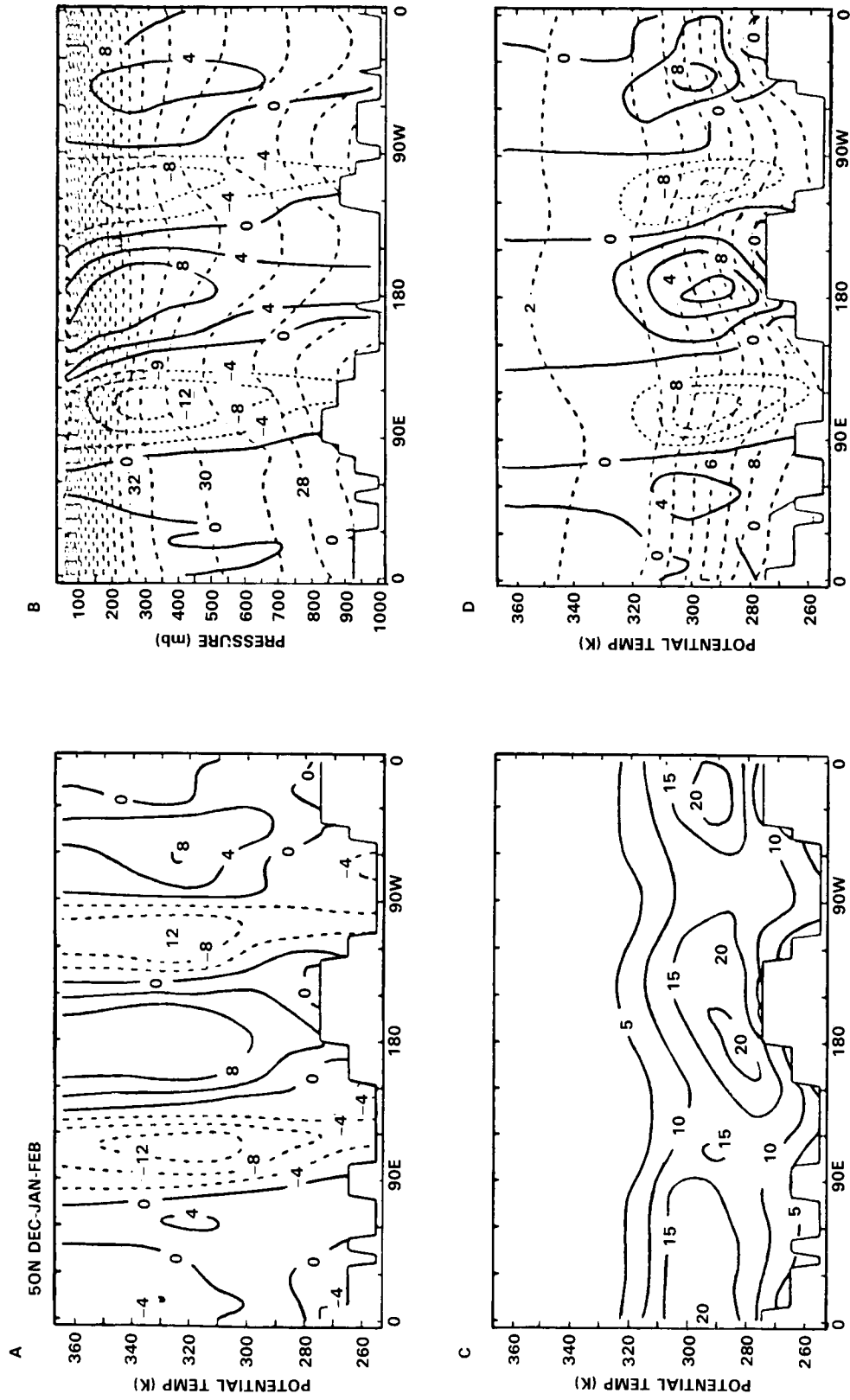


**Figure 5-25.** Zonal cross-sections along 50°N of the following: (a) Mass-weighted time-averaged meridional velocity,  $\langle v \rangle^t$  (units,  $m s^{-1}$ ), in isentropic coordinates; (b) Time-averaged potential temperature,  $\bar{\theta}^t$  (units, 10 K), and meridional velocity,  $V^t$  (units,  $ms^{-1}$ ) in isobaric coordinates; (c) Time-averaged mass distribution,  $\overline{eJ_\theta^t}$  (units,  $10 kg m^{-2} K^{-1}$ ), in isentropic coordinates; (d) Time-averaged pressure,  $p^t$  (units,  $10^2 mb$ ), and meridional mass transport,  $eJ_\theta^t v^t$  (units,  $10 kg m^{-1} K^{-1} s^{-1}$ ), in isentropic coordinates.

## STRAT-TROP EXCHANGE

The occurrence of the springtime maximum of injection of ozone into the troposphere which is associated with jet streams seems at first glance inconsistent with Allam and Tuck's (1984a and b) results that the maximum for the injection of water vapour into the stratosphere occurred in winter. The wintertime maximum of injection of water vapour into the stratosphere, however, is in accord with the wintertime maximum intensity of the isentropic Hadley mass circulation. The distribution of ozone with respect to the structure of isentropic mass transport depends on several factors. Thus, one should not expect that the maximum intensity of the extrusion of stratospheric ozone into the troposphere will occur at the same time as the maximum for the intrusion of tropospheric water vapour into the stratosphere.

In a recent study of the minor atmospheric constituents within a stationary low pressure circulation over the northeast Atlantic, Bamber *et al.* (1984) found substantial evidence for air of stratospheric origin in the upper troposphere of a cut-off, cold core polar low (i.e., one in which the upper troposphere has closed contours of geopotential height). On subsequent days moist convection within the troposphere of the cut-off low led to mixing of stratospheric and tropospheric air. Bamber *et al.* (1984) concluded that such circulations contribute to exchange of air between the stratosphere and troposphere; their case study is further described in Section 5.2.5.

An extratropical cyclone becomes a cut-off low through the process of occlusion. A cyclone occludes through developing a cold core vortex throughout its troposphere and a warm core vortex within the lower stratosphere. The development of the warm core vortex within the lower stratosphere entails isentropic mass convergence superimposed over isentropic mass divergence in the upper troposphere. Through the isentropic mass convergence within the lower stratosphere, stratospheric ozone-rich air descends into the climatological troposphere. Relative to other mechanisms the degree to which mixing within cut-off lows leads to irreversible transformation of stratospheric air into tropospheric air and a subsequent transfer of ozone into the troposphere remains to be determined. Finally, it is noted that the lapse rate of water vapour from the middle and high latitude tropopause to the hygropause, covering a factor of 30 decrease in mixing ratio, is good evidence of some return flow into the stratosphere (see Foot, 1984).

### 5.2.3.4 Summary of Isentropic Analyses

Stratospheric-tropospheric exchange within mid-latitudes, while occurring within baroclinic phenomena, extratropical cyclones, jet streams, and waves, involves planetary scale transport processes as well as deep convection. This exchange within mid-latitudes which primarily occurs through quasi-horizontal transport processes is in part determined by isentropic mass circulations which develop to transport energy from heat source to heat sink.

A primary objective of this discussion has been to relate large-scale quasi-horizontal transport within active baroclinic waves with systematic mass circulations which are forced by differential heating. Balance requirements inferred from zonally-averaged isentropic coordinates and results from FGGE dictate that the mass and energy transport within isentropic layers linking the polar stratosphere with the troposphere of the lower latitudes must be poleward. In lower isentropic layers the meridional mass transport and its geostrophic mode are equatorward. This net meridional mass transport in the isentropic zonally-averaged circulation structure occurs through a systematic covariance between the mass and meridional velocity within amplifying baroclinic waves. An analogy between concepts of sloping convection in a rotating fluid (Hide and Mason, 1975) and isentropic mass circulation occurring through geostrophic modes has been suggested by Johnson (1983, 1984a). The differing contexts provided by this large scale, averaged view and the detailed dynamical studies of exchange near mid-latitude jet streams will be discussed in Section 5.4.1.

#### 5.2.4 Review of Past Work on Exchange in Mid-Latitudes

Case studies of stratosphere-troposphere exchange have mostly consisted of aircraft flights near the polar front jet stream. By constructing wind and potential temperature cross-sections of jet streams from radiosonde data, Reed (1955) and Reed and Danielsen (1959) predicted on the basis of potential vorticity analyses that baroclinic zones beneath jet cores contain stratospheric air, and are therefore regions of active stratosphere-troposphere exchange. Most subsequent aircraft studies of jet streams were aimed at augmenting and lending detail to such cross-sections, making measurements by flying straight legs at constant pressure perpendicular to the maximum wind direction. Specially instrumented meteorological research aircraft have enabled a wide range of atmospheric parameters to be measured, with data from different flight levels combined by assuming no change in the jet stream structure during the mission (lasting about 6 hours).

Briggs and Roach (1963) reported 22 such flights in different regions of jet streams at various stages in their development. With measurements both of humidity and ozone concentration they could identify tracers for both tropospheric and stratospheric air. On all flights, a sharp gradient in tracer concentration was seen on the cyclonic side of the jet core, but only on a few flights did they observe a tongue of dry, ozone-rich air extending into the baroclinic zone beneath the core. This feature was most prominent in the entrance to middle regions of strong jet streams with straight or cyclonically curved contours. Frequently, the decrease in specific humidity within a baroclinic zone greatly exceeded the corresponding increase in ozone over background tropospheric concentrations, dry tongues being observed occasionally with no enhancement in ozone. Such results concur with more recent observations, where high values of potential vorticity were found to coincide with tropospheric concentrations of ozone (Shapiro, 1980; Vaughan and Tuck, 1985).

A systematic aircraft study of the extrusion of stratospheric air into the troposphere beneath jet entrances was coordinated by Danielsen (1964) in the early 1960s as a response to concern about anomalously severe episodes of radioactive fallout. Staley (1960, 1962) also analysed radioactivity data in this context. Mahlman (1965) examined the correlation between radioactivity deposition in the troposphere and a cyclogenesis index. Large atmospheric nuclear explosions prior to 1959 had deposited radioactive isotopes in the stratosphere. Effective mixing processes therein, combined with the moratorium on large nuclear tests after 1958, ensured that  $\text{Sr}^{90}$ , in particular, was by 1960 a reliable tracer for stratospheric air. By using several aircraft to collect filter samples of  $\text{Sr}^{90}$  around the same jet stream system Danielsen was able to investigate thoroughly the distribution of stratospheric air and the correlation between radioactivity and potential vorticity. An example of a cross-section showing both polar front and sub-tropical jet streams, taken from Danielsen (1968), is shown in Figure 5-26. Enhanced  $\text{Sr}^{90}$  concentrations occur beneath each jet stream, with some evidence of mixing also beneath the polar front jet core on its anticyclonic side. The distribution of potential vorticity calculated by hand from the cross-section displays a close correlation with radioactivity, verifying its use as a stratospheric tracer.

Danielsen uses the term 'tropopause fold' to describe the extrusion of stratospheric air beneath a jet stream. Such folds develop as part of the upper level frontogenetic process associated with an intensifying mid-latitude cyclone, and are initiated west of the upper-level trough behind a deepening surface vortex. Occurring thus beneath the entrance region of a strong cyclonically curved jet stream, the folds correspond to the conditions Briggs and Roach (1963) reported as favourable for the existence of dry, ozone-rich air beneath the jet core. The motion of air drawn into such folds was investigated by Danielsen using large-scale analyses of potential vorticity on isentropic surfaces drawn from radiosonde data, coupled with isentropic trajectory calculations. Maxima in potential vorticity, corresponding to tropopause folds, were

STRAT-TROP EXCHANGE

ORIGINAL PAGE IS  
OF POOR QUALITY

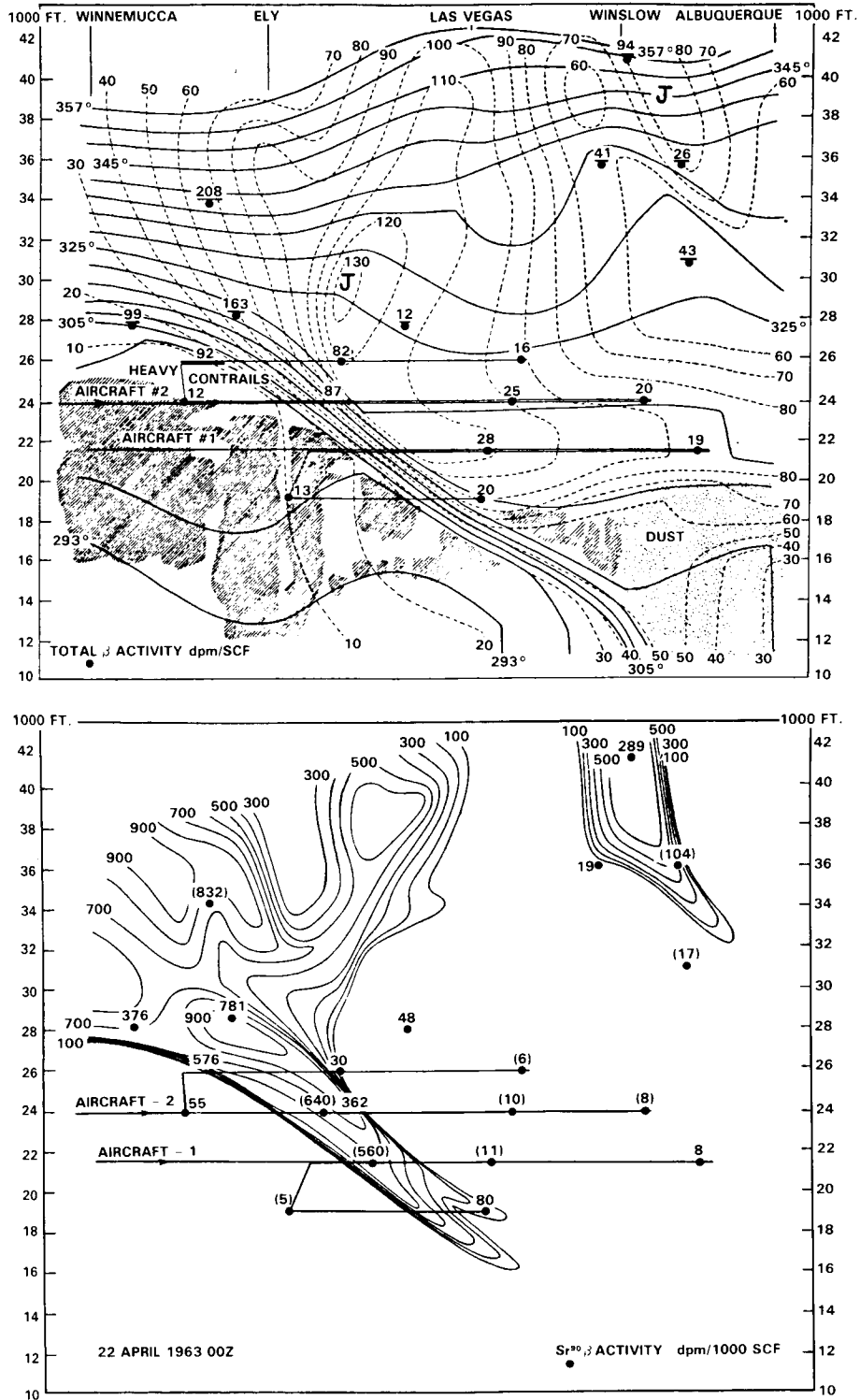
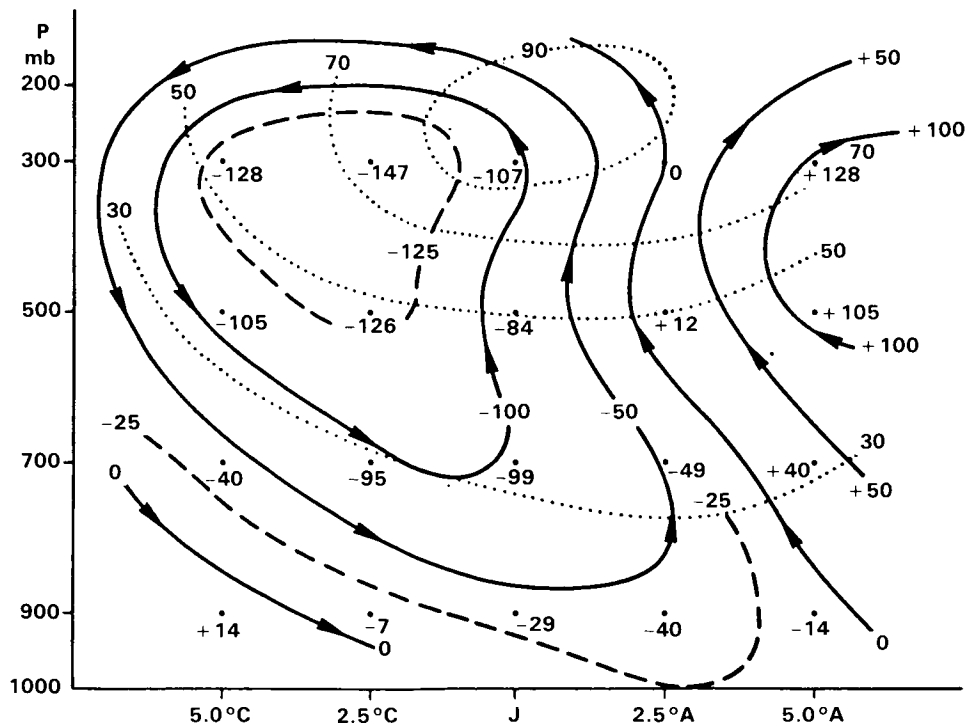


Figure 5-26. (a) Vertical cross-section of potential temperature (solid lines), wind speed in knots (dashed lines), clouds (slant lines) and dust (dots) for 0000 GMT 22 April 1963. Values at sampling locations are total  $\beta$  activity in dpm/SCF. From Danielsen (1968). (b) Potential vorticity, contoured at intervals of  $100 \times 10^{10} \text{ cm}^2 \text{ s}^{-1} \text{ K g}^{-1}$ , and  $\beta$  activity of  $\text{Sr}^{90}$  in dpm/1000 SCF, for 0000 GMT 22 April 1963.

found to maintain their coherence in the tropospheric flow south of the jet stream system for a period of one or two days. Air from the fold depicted in Figure 5-26 was twice intercepted by aircraft as it traversed the United States. Radioactivity measurements demonstrated that the ratio of potential vorticity to  $Sr^{90}$  remained constant to within the accuracy of the observations. It was therefore concluded that potential vorticity and radioactivity could be used as tracers in the troposphere, with layers of high concentration gradually being eroded by small-scale mixing with ambient air. Cumulus and cumulonimbus entrainment on the cold side of the layer were identified as major agents in the mixing process, with mixing on the warm side being considered negligible by comparison. To compensate for the loss of air from the stratosphere in the folding process, Danielsen (1968) proposed a small mean inflow across the tropopause, which would also maintain the sharpness of the tropopause against the diffusive action of small-scale turbulence. A summary of his model of air flow during frontogenetic conditions, again taken from the 1968 paper, is shown in Figure 5-16. The analysis shown in Figure 5-27, due to Mahlman (1973) shows transverse mass transport diagnosed in a steady jet stream, and is consistent with Danielsen's idealized transverse circulation. Note that the region of ascent in this example includes the jet core. Its essential conclusions are supported by Reiter and Nania (1963) reporting several aircraft missions in the late 1950s to investigate clear air turbulence (CAT) near jet streams. Without tracer measurements, these flights can only illuminate the exchange problem indirectly but they do emphasise the role of the strong backing of wind direction with height beneath the jet core, observed in cyclogenetic troughs, in both the extrusion of stratospheric air and generation of CAT. CAT provides an additional process to mix the fold with tropospheric air, this time along the warm boundary where the wind shear is greatest.



**Figure 5-27.** Mean mass transport stream function computed from vertical velocities in a steady polar front jet stream. Note vertical transport between 200 and 300 mb at and equatorward of the jet core. Units are  $mb\ m\ s^{-1}$ , the C and A labels on the abscissa refer to cyclonic and anticyclonic sides of the jet core, J. The averaging was performed relative to the flow, not fixed geographical coordinates. Mahlman (1973).

## STRAT-TROP EXCHANGE

With the instrumentation available in the 1960s, even aircraft-based investigations of jet streams were limited in their horizontal resolution, especially in the case of tracers - Briggs and Roach's ozone measurements, for instance, were 3-7 minutes apart, while Danielsen's radioactivity samples were taken every 20 minutes (although a cumulative count of  $\beta$  activity was recorded on his flights). The advent of inertial navigation systems and gust probes in the early 1970s allowed direct investigations of turbulence parameters, while the development of fast-response chemical sensors permitted a much more detailed delineation of tracer flow. Ozone, in particular, can now be measured reliably using chemiluminescent or ultraviolet absorption techniques with a time resolution of ten seconds or less, which corresponds to a horizontal resolution of a kilometre or better. Humidity, condensation nuclei and carbon monoxide concentrations have all been used as tracers of tropospheric air in recent studies. Good, fast-response measurements may be achieved of condensation nuclei and water vapour, especially by using a Lyman- $\alpha$  hygrometer for the latter (Kley *et al.*, 1979).

A comparison of ozone, radioactivity and potential vorticity on one jet stream cross-section flight was shown by Danielsen *et al.* (1970). Although broad agreement was claimed in the distribution of the three tracers, considerable structure was evident in both ozone and radioactivity above and on the cyclonic side of the jet core. This emphasises the difficulties encountered when investigating small-scale structure in potential vorticity with an aircraft. Although the absolute vorticity field may be resolved with confidence by flying across the mean flow, the stability must be estimated by interpolation between successive flight legs, with some guidance from nearby radiosonde ascents. Consequently, a derived potential vorticity field is both poorly resolved and subjective in nature. Objective local measurements of potential vorticity must await the development of aircraft-borne instruments to measure the local stability directly.

Further doubt of the suitability of potential vorticity as a tracer for stratospheric air was expressed by Shapiro and colleagues after a series of jet stream encounters with research aircraft in the 1970s. Shapiro (1974) found a close correlation between potential vorticity and ozone in both baroclinic zones beneath a double jet stream system, but deduced very high values of the former in the strong cyclonic shear zone on the stratospheric side of the maximum wind level. Four more research flights described by Shapiro (1976, 1978) also revealed a mesoscale region (about 100 km wide) of very strong cyclonic wind shear at the level of the jet core, leading him to deduce anomalously high values of potential vorticity there. As shown in Figure 5-28 (from Shapiro 1978), these do not correspond to anomalously high values of ozone. It must be emphasised that later, fast-response measurements of ozone ( $\tau < 10$ s) have revealed enormous variations in its concentration both in the fold region (Danielsen and Mohnen, 1977; Shapiro, 1980) and on the cyclonic side of the core (Vaughan and Tuck, 1985), which are presumably present also in the detailed potential vorticity field.

Reference has already been made to studies of the small-scale variations in ozone in cyclonic shear zones and tropopause folds. These, together with analyses of the turbulence parameters (Kennedy and Shapiro, 1975, 1980; Shapiro, 1980) have revealed a predominance of structures with length scales transverse to the wind direction of 10-20km (length scales along the wind direction are not known). This corresponds to about two minutes of flying time, and is much longer in horizontal scale than CAT. Turbulent fluxes may be calculated from gust probe and other fast-response instruments by the covariance method on the assumption that the motion is not ordered on the length scale chosen to calculate mean values (50-100km). Fluxes deduced in this way are completely dominated by components of the order of 10-20km in length. Shapiro (1980) suggests that these motions are wavelike phenomena with crests parallel to the jet stream axis, but further research is clearly necessary to determine both their nature and their net contribution to the turbulent transfer of heat and tracers.

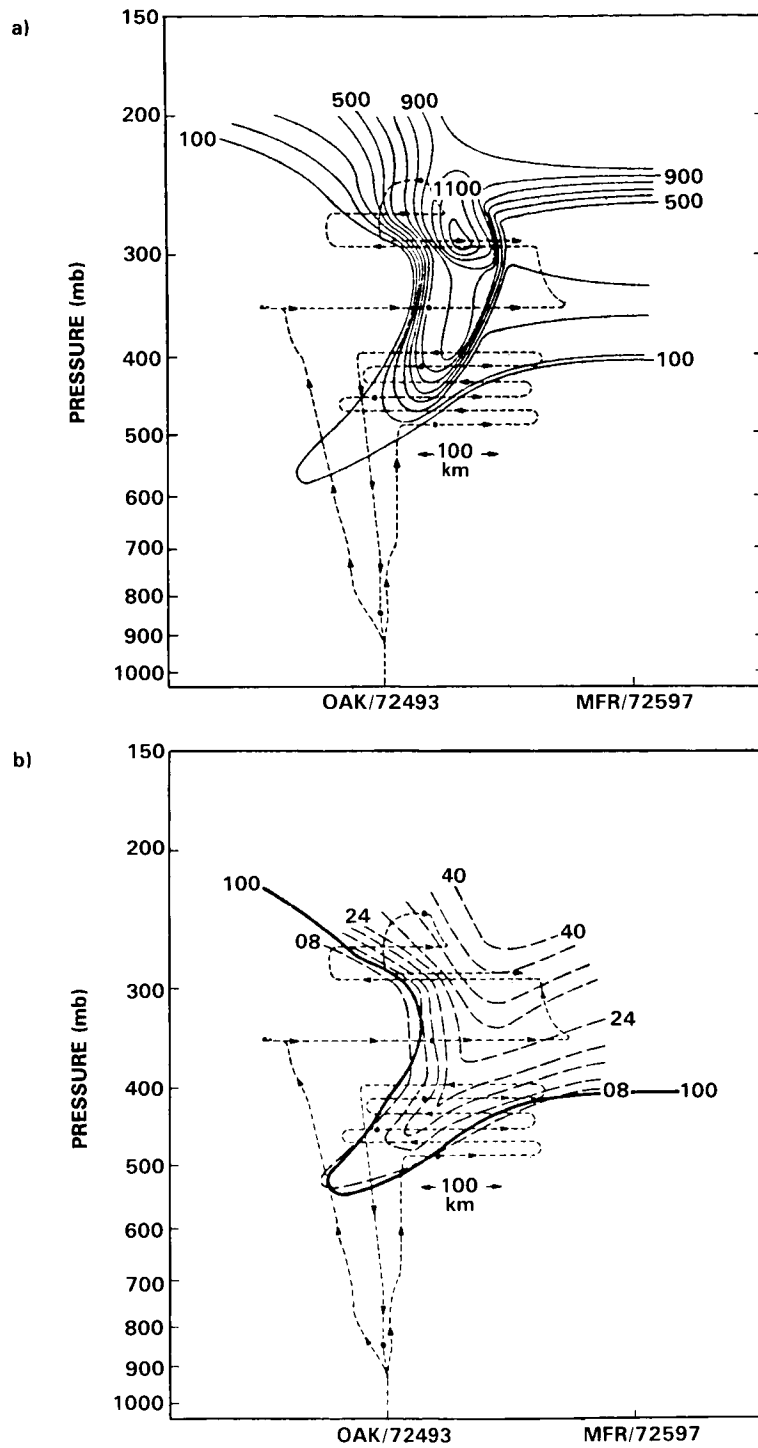


Figure 5-28. (a) Potential vorticity,  $10^7 \text{ K s}^{-1} \text{ mb}^{-1}$ , for 0000 GMT 16 April 1976. From Shapiro (1978).

(b) Ozone,  $10^{-8}$ , vmr, dashed lines;  $100 \times 10^{-7} \text{ K s}^{-1} \text{ mb}^{-1}$  isopleth of potential vorticity, solid line, same case as (a). Note that the region of high  $P_\theta$  gradient on the right of the intrusion is not accompanied by a similar anomaly of ozone. From Shapiro (1978).

## STRAT-TROP EXCHANGE

Observations with fast-response instrumentation revealed tropopause folds to be rather less homogeneous than previously believed. Incomplete correlation between ozone and potential vorticity and planetary boundary layer concentrations of condensation nuclei (Shapiro, 1980) as well as large horizontal variations in the ozone mixing ratio (Danielsen and Mohnen, 1977) suggest that these baroclinic zones can be regions of very active mixing. Direct flux calculations support Danielsen's (1968) view that most of the mixing occurs on the cold side of the fold.

Few estimates exist of the total mass of stratospheric air transferred into the troposphere in a folding event, and assume that air entering a tropopause fold in the cyclogenetic conditions described earlier is irreversibly removed from the stratosphere. The possibility that some of this air may be returned to the stratosphere at the jet exit (together with some entrained tropospheric air) has not been specifically investigated by aircraft flights, although humidity measurements in the lower stratosphere reported by Foot (1984) occasionally reveal very moist air - humidity mixing ratios greater than 15 ppm at 160 mb - well above the tropopause near the British Isles. Without isentropic trajectory analyses the source of this air could not be identified, although it did not appear to have originated near the polar front jet stream.

Measurements of reactive chemical species in regions of stratosphere - troposphere exchange can elucidate both the mixing of air and the chemical processes taking place as a consequence. Bamber *et al.* (1984) report hydrocarbon and ozone concentrations taken in a cut-off low with a cold core remaining in mid-latitudes after an intense period of meridional flow. Air between 7 and 10km was found to have chemical characteristics intermediate between those of the troposphere and stratosphere. The mixing of moist air from the former with ozone-rich air from the latter appears to have accelerated the removal rate of hydrocarbons, presumably by an enhancement of OH radical concentrations. Vigorous convective activity eventually eroded the intermediate layer, establishing a higher tropopause appropriate to its new latitude. More information is required on the extent of stratosphere-troposphere exchange in and around cut-off cold pools before a definitive estimate of their contribution to the total exchange can be made.

### 5.2.5 Recent Aircraft Studies near the British Isles

During April 1983, the C130 W Mk 2 aircraft of the Meteorological Research Flight was used to make 3 flights in a cut-off low (Figure 5-29) near the British Isles. Analysis of ozone traces and grab samples taken by the aircraft on the first two flights, on April 22 and 23, have shown this system to have two stratosphere-troposphere exchange events associated with it, which were found to have accelerated hydrocarbon oxidation, putatively by increasing [OH] (Bamber *et al.*, 1984). The vertical scale of the region of exchange at the centre of the low was 3-4 km (Figure 5-30), considerably deeper than the conventional picture of folds associated with jet streams. A third exchange event occurred in the cut-off low on April 23, as shown by a radiosonde ascent from weather ship C7R and the Total Ozone Mapping Spectrometer (TOMS) on board the Nimbus 7 satellite. Figure 5-31 shows the radiosonde ascents made on April 23 by C7R and the C130 aircraft, while Figure 5-32 shows a sequence of 6 days data from TOMS. Isentropic trajectories started at the point of origin of the large increases in O<sub>3</sub> column density track this feature in the TOMS data for 72 hours as it moves into the centre of the cut-off low (Figure 5-33). The aircraft flight on April 26 shows that the ozone mixing ratio below 5 km has increased, probably as a result of the earlier exchange events, and in the upper troposphere O<sub>3</sub> is almost identical with what it was on April 23 at the centre of the low. However, whereas on 23rd the air in this height range (6-9 km) was not clearly either stratospheric or tropospheric, by the 26th it was clearly beneath the tropopause, as shown by profiles of both temperature and CF<sub>2</sub>Cl<sub>2</sub> (Figures 5-34 and 5-35). By 26th, cumulonimbus clouds at the core of the low were reaching the tropopause, and presumably the updrafts and downdrafts

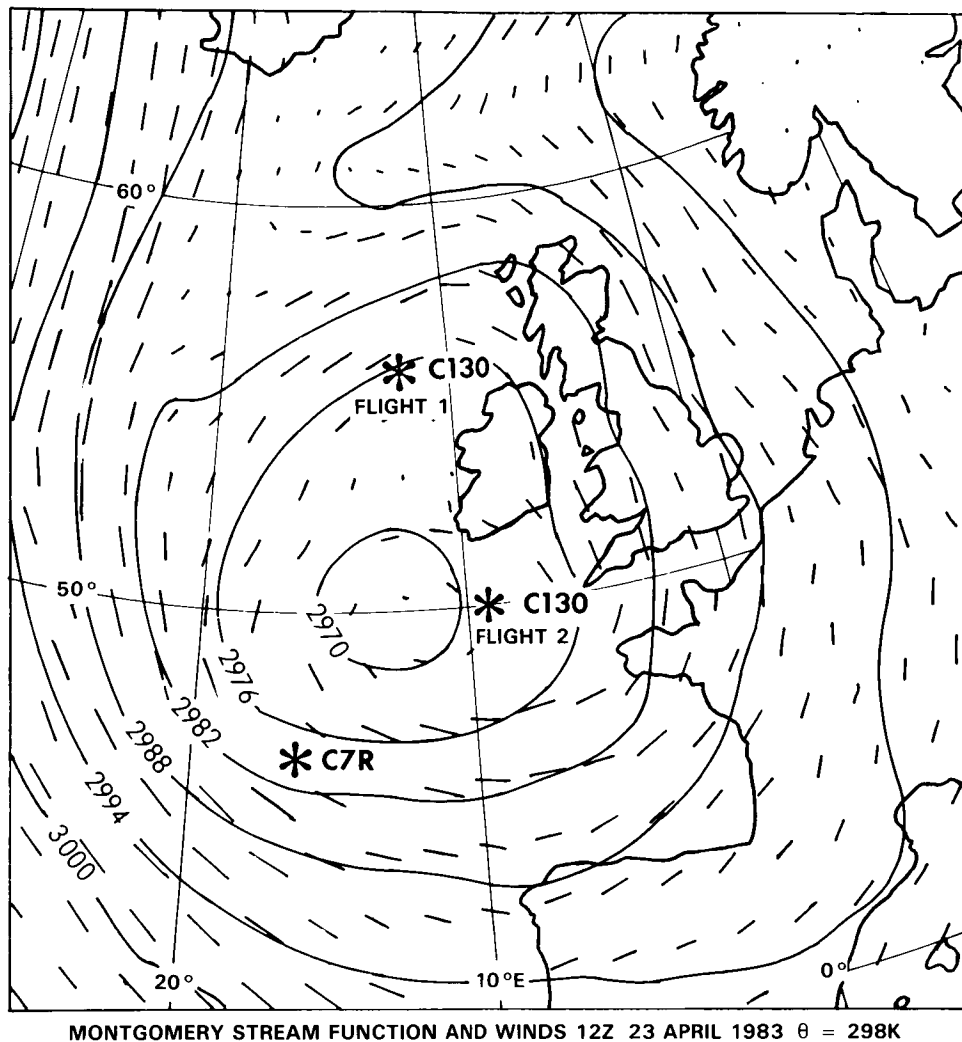


**Figure 5-29.** The cut-off low studied April 22-26. Montgomery stream function  $10^2 \text{ m}^2 \text{ s}^{-2}$  and winds ( $1 \cdot 1 \text{ cm} = 50 \text{ m s}^{-1}$ ) on the  $\theta = 298 \text{ K}$  surface are shown, 12 GMT, 23 April 1983. The feature persisted, with developments, until about 7 May.

involved were responsible for the changes in the  $\text{CF}_2\text{Cl}_2$  profile, which are consistent with the ozone changes in the lower troposphere. The fact that all three of these events are visible in the TOMS data and are supported as producing stratosphere-troposphere exchange by radiosonde profiles is encouraging. Two of the events clearly show evidence for extensive mixing of stratospheric air into the troposphere in the coincident trace gas and ozone data obtained by the aircraft; the third was just missed by the flight track on April 26. The meteorological assimilation field available in 1983 was the coarse mesh ( $1.875^\circ \text{ long} \times 1.5^\circ \text{ lat}$ ); it was used to produce isentropic trajectories at 6-hourly intervals which successfully tracked the enhanced column density feature in the TOMS data. By 1985, when further flights were attempted, in a NNW'ly jet stream in the Iceland-Scotland sector, the fine mesh ( $0.9375^\circ \text{ long} \times 0.75^\circ \text{ lat}$ ) was available and could resolve tongues of potential vorticity, well correlated and anticorrelated respectively, with the aircraft ozone and water vapour data. Again, note the vertical scale of the event (Figures 5-36 and 5-37). Note also that smaller scale features in the operational analysis potential vorticity field, to the

STRAT-TROP EXCHANGE

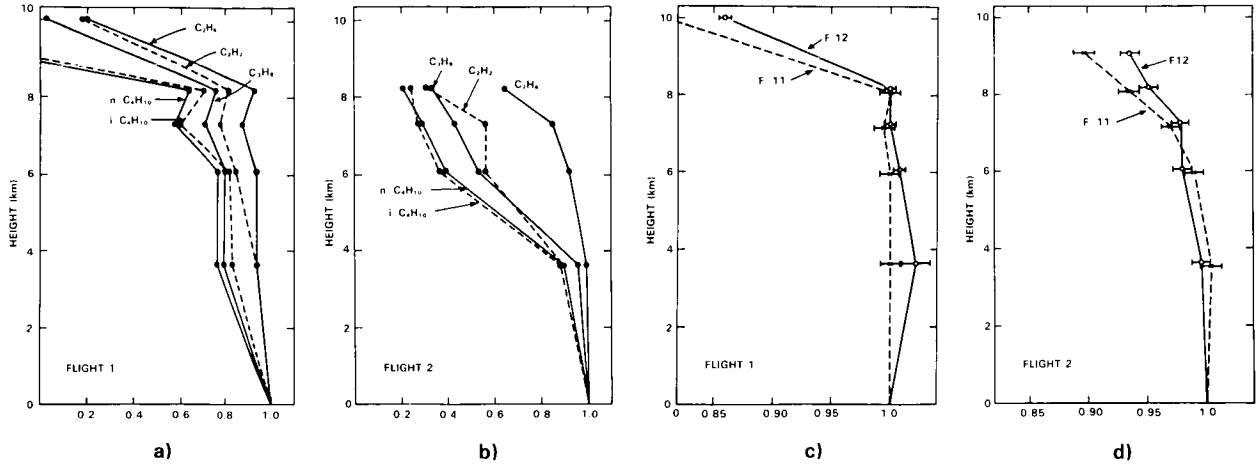


**Figure 5-30.** Flights made in the cut-off low shown in Figure 5-29. (a), (b) Vertical profiles expressed as fractions of the mixing ratios measured at 150 m for some light alkanes and acetylene. The dots represent measurements; lines joining them are included for illustrative purposes only. No butane isomers were detected in the top bottle on the first flight. For the second flight, a leak in the bottle containing air from 9.1 km prevented a hydrocarbon analysis. (c), (d) as (a), (b) but for F-11 ( $\text{CFCl}_3$ ) and F-12 ( $\text{CF}_2\text{Cl}_2$ ). Error bars are standard error estimates.

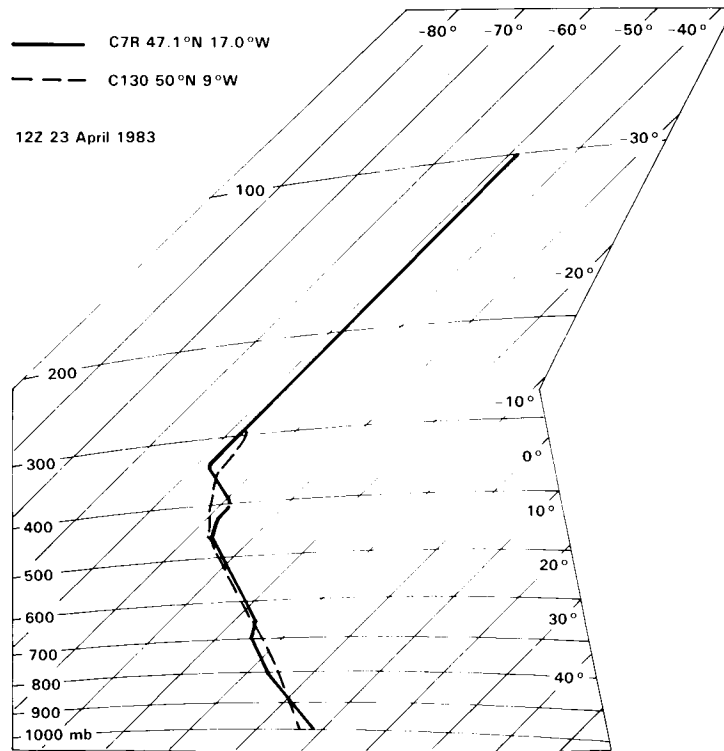
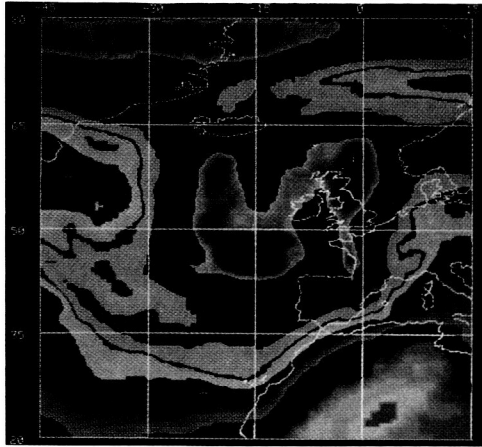


**Figure 5-31.** T- $\phi$  grams from weather ship C7R and the C130 (flight 2) in the cut-off low of Figure 5-29. The temperature curves are shown. Note the stable layer between 400 and 470 mb on the C7R ascent, and the layer between 300 and 500 mb on the C130 ascent with stability intermediate between typical tropospheric and stratospheric values.

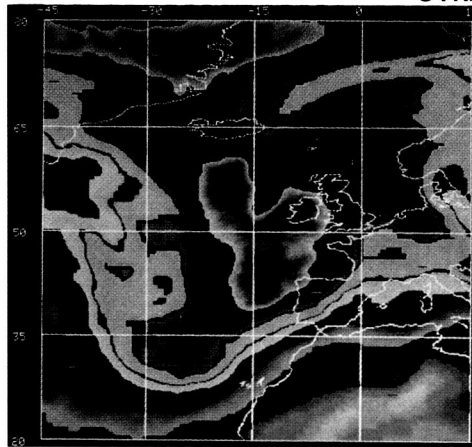
ORIGINAL PAGE  
COLOR PHOTOGRAPH

ORIGINAL PAGE  
COLOR PHOTOGRAPH

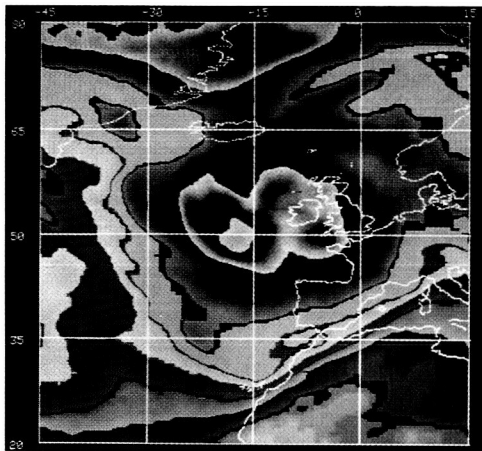
STRAT-TROP EXCHANGE



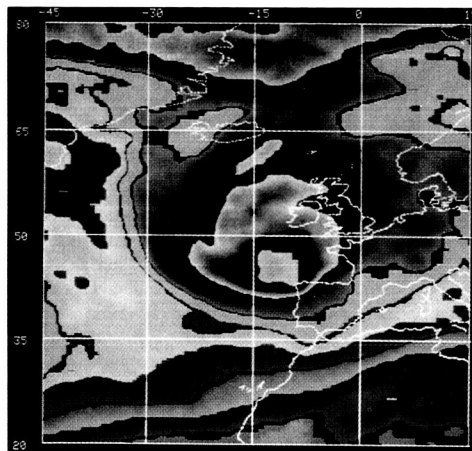
APRIL 21, 1983



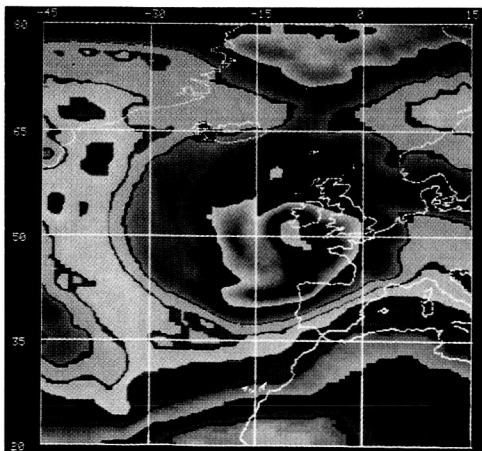
APRIL 22, 1983



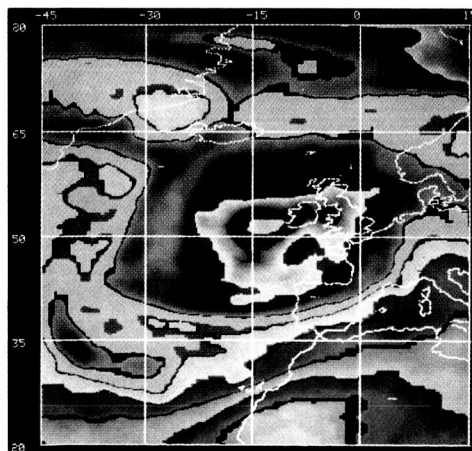
APRIL 23, 1983



APRIL 24, 1983



APRIL 25, 1983



APRIL 26, 1983

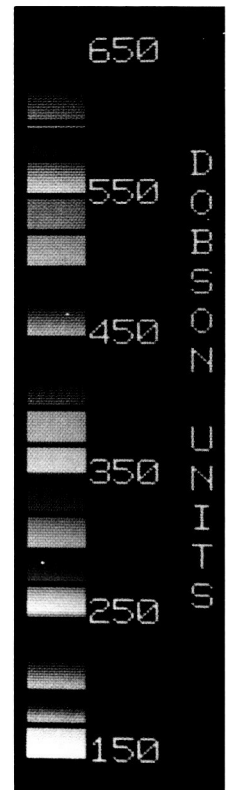
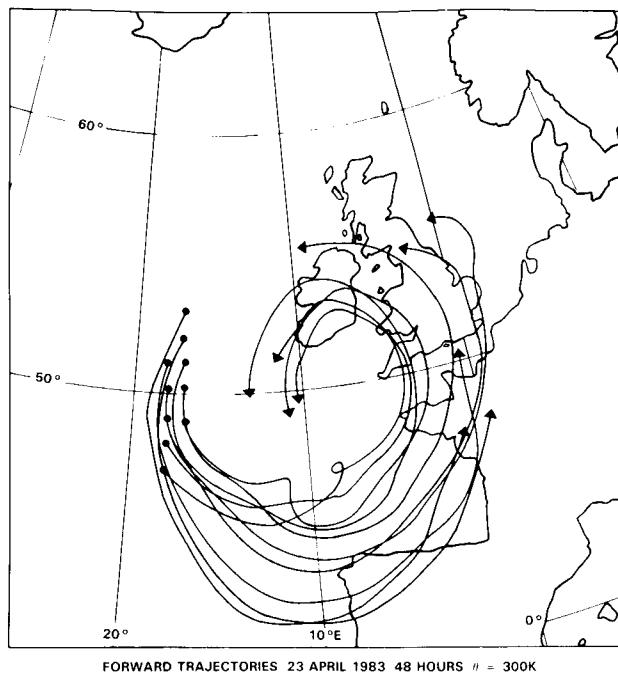
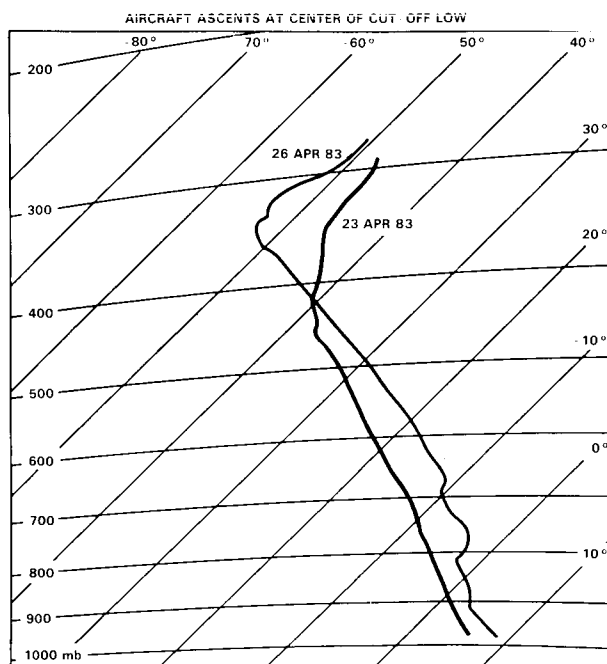


Figure 5-32. TOMS ozone data maps, illustrating cut-off low in the North Atlantic of Figure 5-29 using the color scale as shown. Diagrams are for 21-26 April 1983, in chronological order. By midday 27 April, the 500 DU contour at the center of the cut-off low had disappeared.

## STRAT-TROP EXCHANGE



**Figure 5-33.** Forward trajectories starting 12 GMT 23 April 1983, 48 hours on  $\theta = 300\text{ K}$  surface. Data are from coarse mesh assimilation; cf. Figure 5-32 for the behaviour of the area enclosed by the 500 DU contour.



**Figure 5-34.** C130 aircraft temperature profiles at centre of cut-off low, 23 and 26 April. Back trajectories for 26 April show air through the depth of the troposphere moving round the low centre.

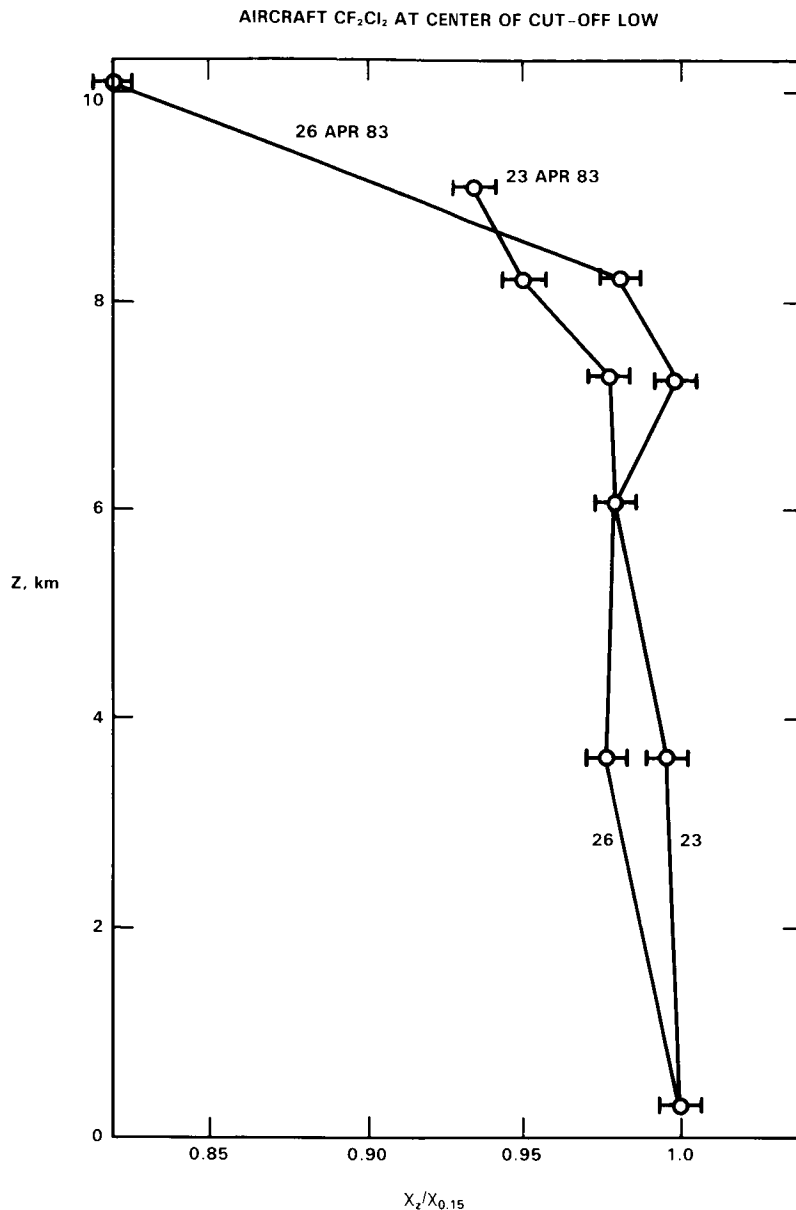


**Figure 5-35.** C130 aircraft  $\text{CF}_2\text{Cl}_2$  profiles at centre of cut-off low, 23 and 26 April; cf. Figure 5-34. The ozone profile changes were consistent with these, showing an ozone increase of 5-10 ppbv below 6 km by the later date (see text).

west and above the jet core in Figure 5-37, are independently corroborated by the aircraft data. This event was also studied by a flight parallel to the jet stream axis in the air bounded by the upper frontal surfaces (tropopause folds), and showed the ozone content to be very variable, but broadly increasing from  $\sim 60$  ppbv beneath the jet exit to  $\sim 180$  ppbv beneath the jet entrance. This development raises the possibility that if and when such resolution is available globally, it may be possible to combine meteorological analyses, TOMS data and aircraft studies to produce more reliable estimates of stratosphere-troposphere exchange on a global scale.

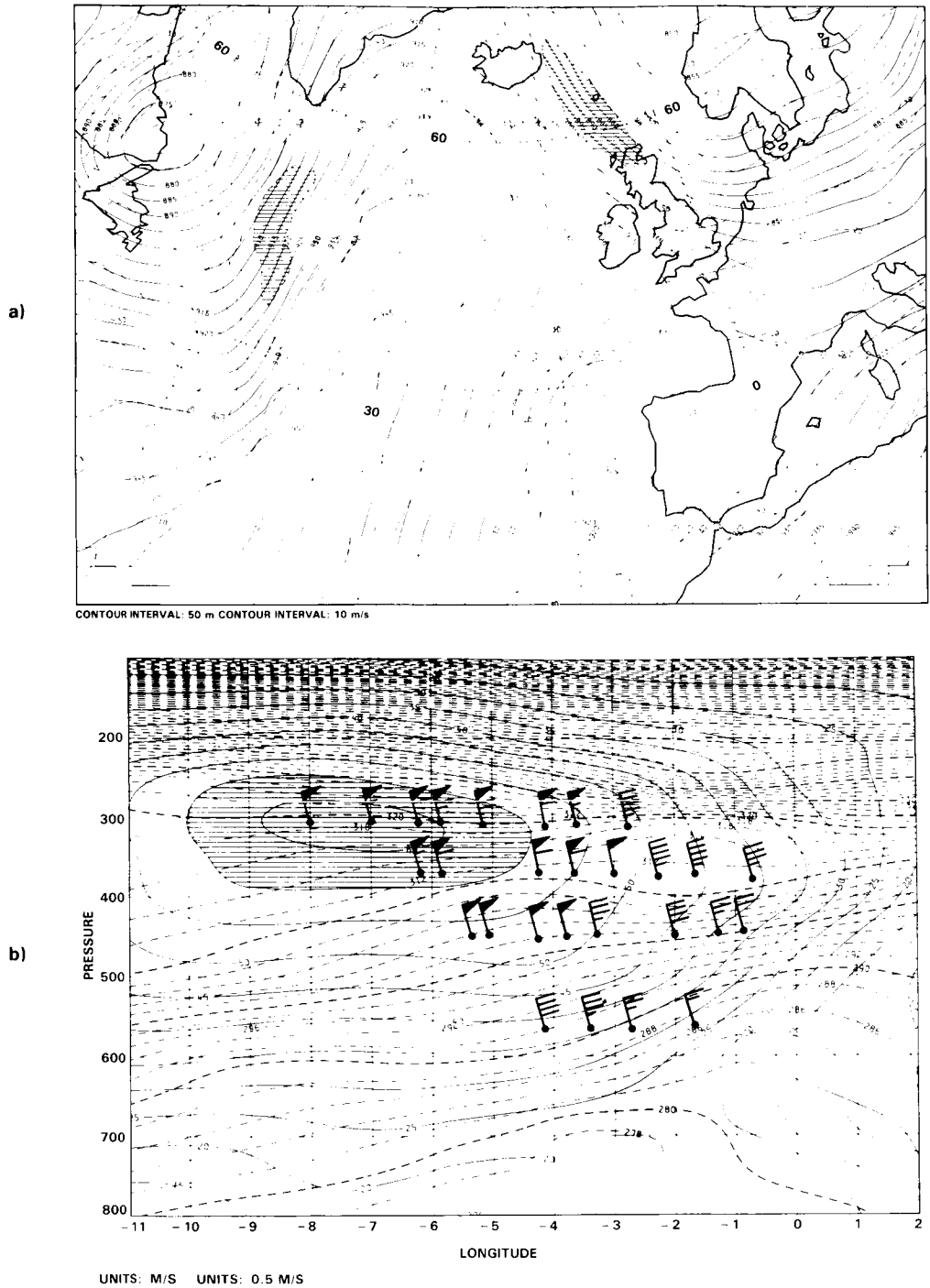


**Figure 5-36.** (a) Fine mesh analysis, 0000Z 27 April 1985, showing jetstream between Iceland and Scotland investigated by C130 aircraft. Dashed lines are isotachs,  $\text{ms}^{-1}$ , with values  $>60 \text{ m s}^{-1}$  shaded. Solid contours are 300 mb geopotential heights, dam. (b) Cross-section of wind speed ( $\text{m s}^{-1}$ , solid contours) and potential temperature (K, dashed contours) corresponding to the analysis in part (a). The section is along the  $60^\circ$  latitude circle; barbed arrows are aircraft winds, with fleches and triangles representing  $10$  and  $50 \text{ m s}^{-1}$ .



## STRAT-TROP EXCHANGE

### 5.2.6 Recent Aircraft Studies over the South Western United States

During late April 1984, two NASA sponsored aircraft-experiments were coordinated to provide an extensive set of *in situ* and LIDAR measurements of tropopause folding events. Convair 990 and Electra aircraft, sponsored by the Global Tropospheric Experiment, GTE, made measurements in the troposphere and lower stratosphere, while a U2 aircraft, sponsored by the Stratospheric-Tropospheric Exchange Project, STEP, extended the stratospheric measurements to 21 km. These aircraft, equipped with fast responding sensors, made meteorological, trace gas and aerosol measurements of exceptional quality. Fast responding sensors are necessary to resolve the large gradients in the stratosphere and in the folds, and to permit cross correlations of all measured variables over a broad range of temporal and spatial scales.

Combining conventional meteorological analyses and numerical prognostic charts with special isentropic and cross-sectional analyses, Danielsen predicted the folding events and designed the aircraft flight paths. The U2 was flown above the jet core in a vertical plane oriented perpendicular to the wind, see Figure 5-38. It traversed this plane at four altitudes, separated by about 10,000 ft, making measurements on both sides of the jet, but skewed towards the cyclonic side. In approximately the same vertical plane the Electra was flown beneath the jet core, skewed towards the anticyclonic side. It traversed the tropopause fold and made essentially continuous vertical profile measurements of ozone and aerosol backscatter by a vertical (downward) pointing LIDAR. The objective here was to determine whether the ozone rich air in the fold descended towards the surface boundary layer and if it did, to measure the ozone dilution caused by the entrainment of tropospheric air at the boundaries of the fold. A much more complicated flight path was assigned to the CV-990, including a horizontal traverse across the jet core towards the center of the large scale cyclonic vortex, a descent into the ascending cold air, a traverse of the folded tropopause layer and then a return flight in the layer.

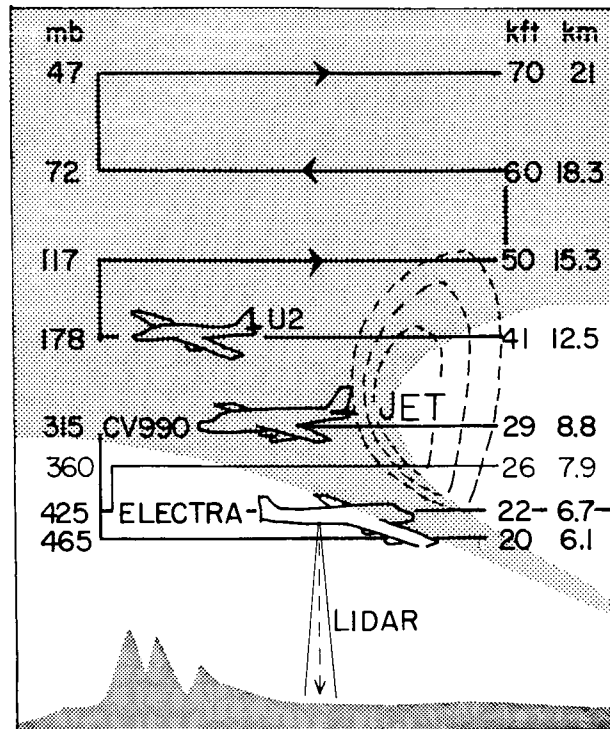


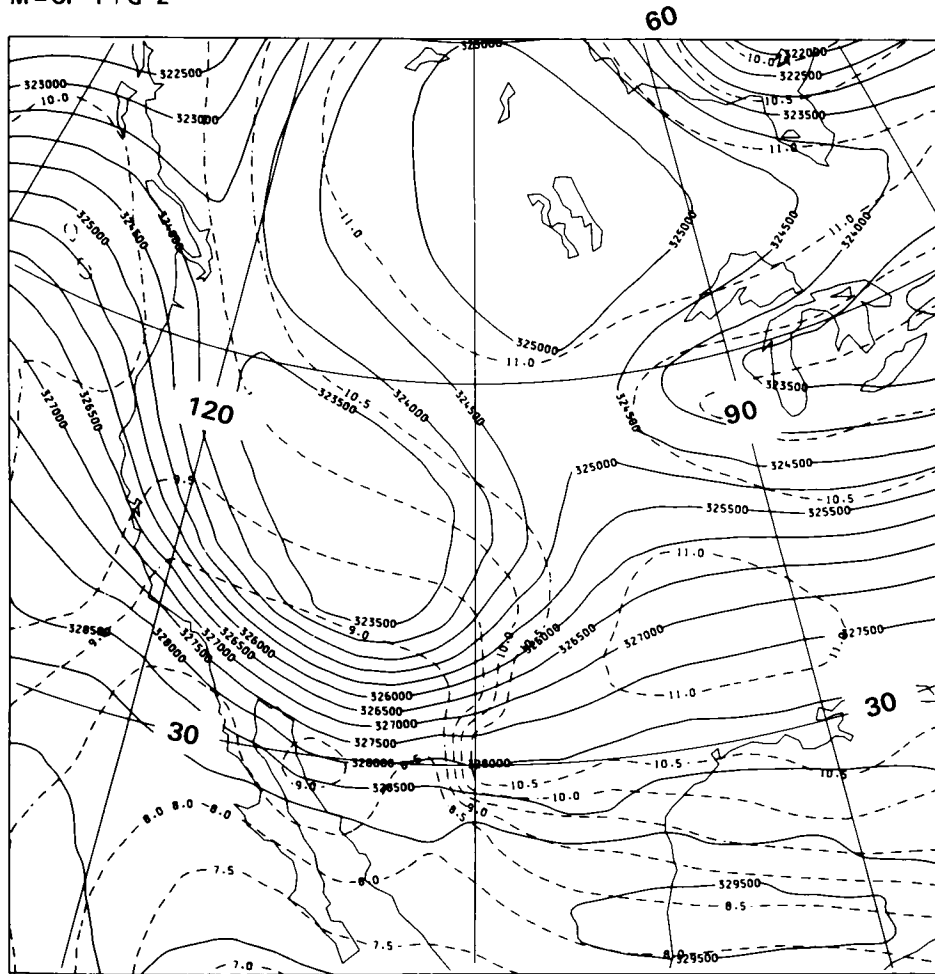
Figure 5-38. Flight paths in vertical plane relative to jet stream axis and tropopause fold.

## STRAT-TROP EXCHANGE

The cyclonic vortex which formed rapidly on April 20, 1984 over the southwestern United States is shown in Figure 5-39. The winds are approximately parallel to the contours of the Montgomery potential,  $\psi_M = c_p T + gz$ . Wind speeds are approximately inversely proportional to the spacing of the  $\psi_M$  contours. In this case, typical of the springtime cyclones, the jet wraps around the south side of the vortex, with speeds in excess of 130 kt. The detailed structure of this vortex is shown in the TOMS map of total ozone (see Figure 5-51).

Horizontal flight paths of the three aircraft are delineated in Figure 5-40. The letters along the CV-990 path identify reference points to be used in comparing trace gas measurements to the computed distribution of potential vorticity.

E.C.M.W.F. DATA FOR WESTERN U.S.A.  
 MONTGOMERY STREAMFUNCTION-THETA = 330.0  
 VALID AT 12Z ON 20/4/84 DAY 111  
 M = CP T + G Z



CONTOUR INTERVAL: 5 mb

**Figure 5-39.** Cyclonic vortex which developed rapidly over south western United States on 20 April 1984. Jet stream on this  $\theta = 330$  K surface is west and south of vortex where contour gradient is maximum. See text for description.

## STRAT-TROP EXCHANGE

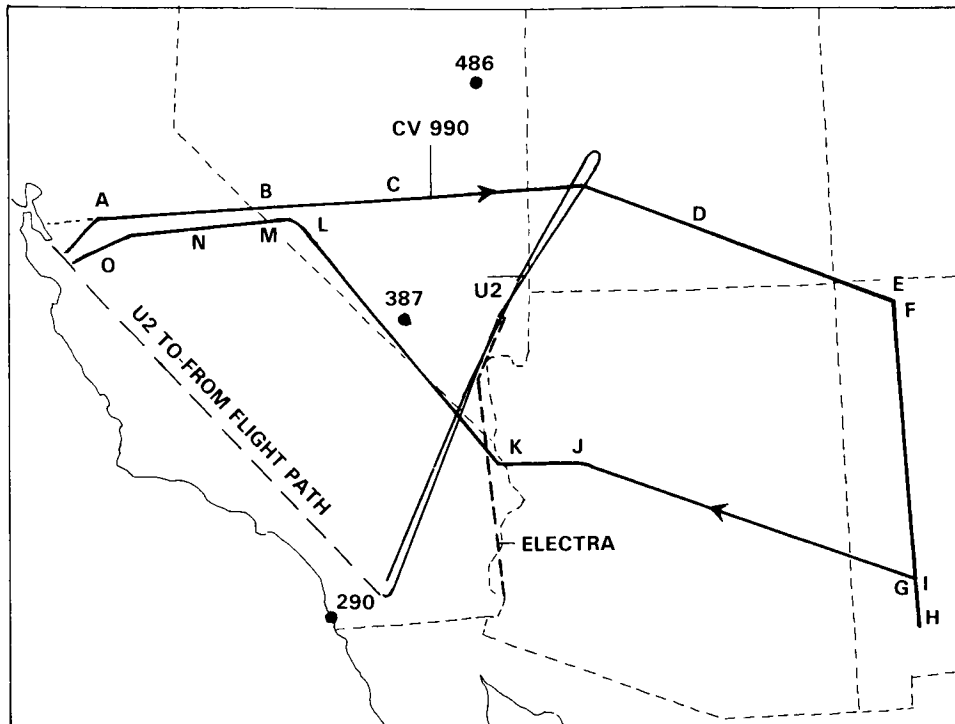


**Figure 5-40.** Flight paths (horizontal) of the three aircraft that made measurements in vortex on 20 April 1984. Letters on 990 path identify relative maxima and minima of tracers. Numbered dots identify 3 of 6 radiosonde stations used in analysing Figure 5-41.

### 5.2.6.1 Analyses and Measurements at and below the Jet

The distributions of potential temperature  $\theta$  in the vertical, from points A to I, and the wind speeds normal to the vertical planes are presented in Figure 5-41. These cross sections were prepared from a set of vertical and horizontal (constant pressure) analyses, mutually adjusted to assure spatial and temporal consistency. A total of nine vertical cross sections were prepared first along lines of radiosonde stations approximately perpendicular to the flow. Thermal and wind speed gradients were then transferred to a set of seven constant pressure charts and analysed. After adjustments were made these analyses were transferred to the vertical planes of the 990's flight path. Finally,  $P_{\theta}^{\dagger}$  was computed and contoured at a grid of points from Figure 5-41a. (The superscript denotes data subjected to a low pass filter). The distribution of  $P_{\theta}^{\dagger}$  (Figure 5-41) plus another 12 hours later were used to derive, by linear interpolation in time, the  $P_{\theta}^{\dagger}$  values for successive positions of the 990.

This labour intensive, time consuming effort was made to determine the diagnostic potentials of radiosonde data. Throughout the analysis only radiosonde observations were used. All flight data were reserved to test the final solutions. Could a three-dimensionally consistent analysis resolve a folded tropopause structure whose horizontal dimensions are less than the separation distance of radiosonde stations? Also, could a representative distribution of potential vorticity be computed from these analyses? The result of one such test is shown in Figure 5-42. The variations of  $P_{\theta}^{\dagger}$  versus time derived from the cross section analyses (continuous bold line) is plotted along with slightly smoothed ozone and carbon monoxide

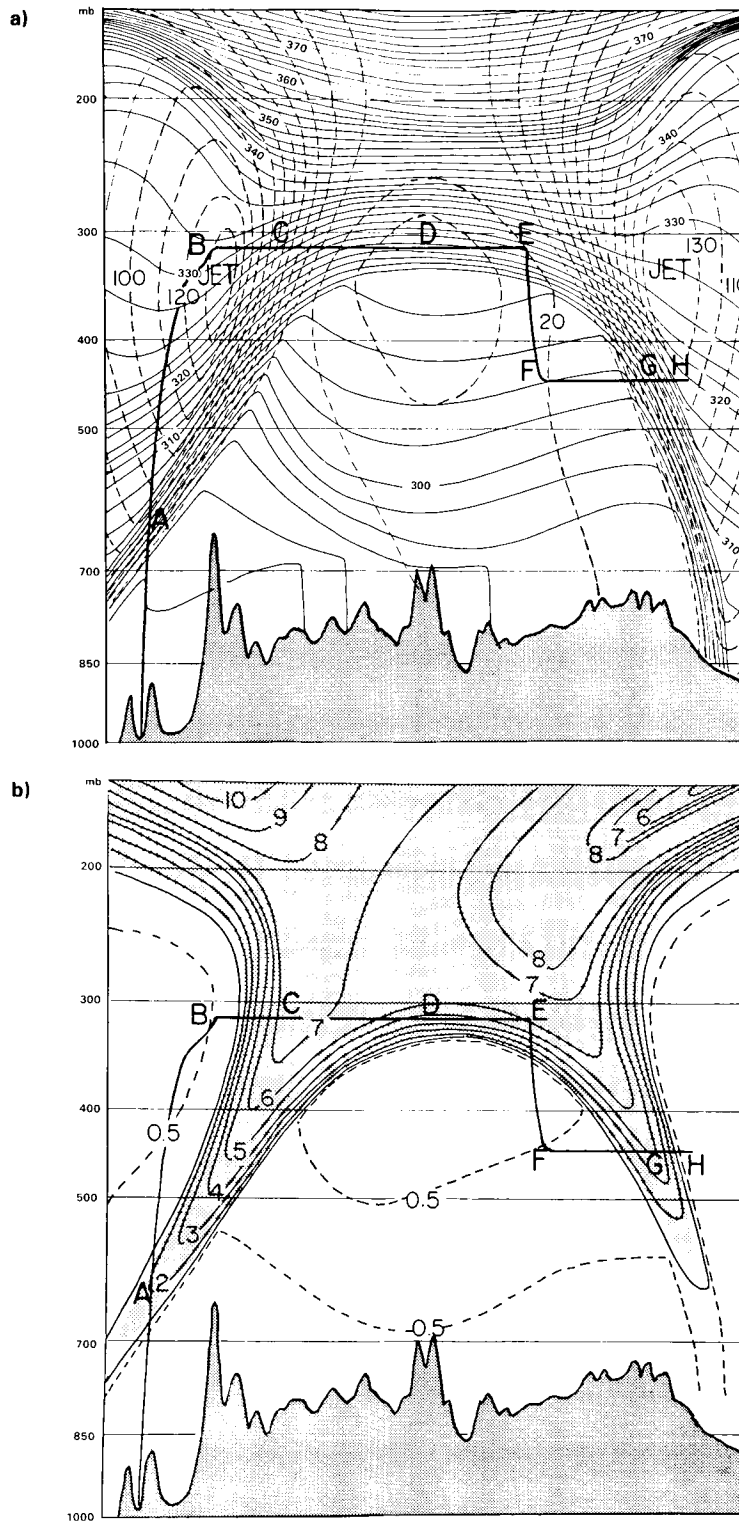


**Figure 5-41.** Vertical cross-sections along 990 flight for 1200 GMT, 20 April, 1984 including: (a) Potential temperature, 2K interval, and wind velocity normal to cross-section (10 knot contour interval). (b) Potential vorticity, along same cross-section, in units of  $10^{-5} \text{ cm}^2 \text{ s}^{-1} \text{ K g}^{-1}$ .

## STRAT-TROP EXCHANGE

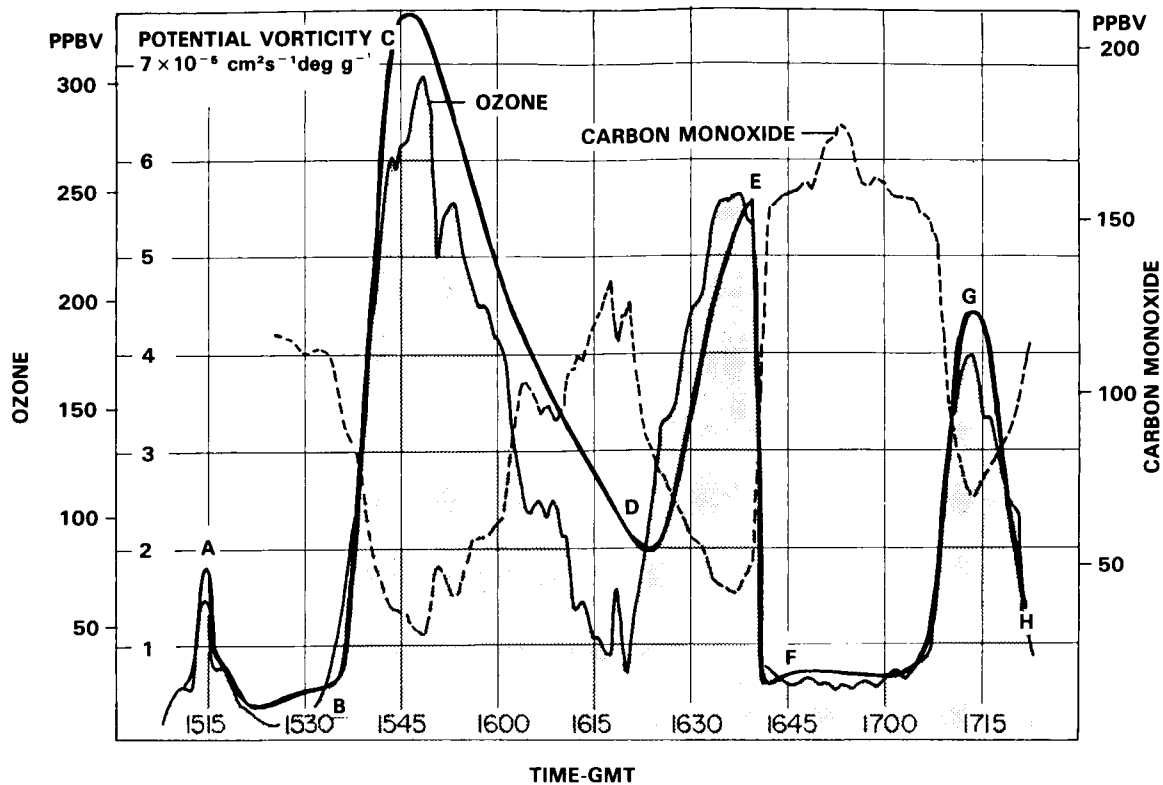


**Figure 5-42.** Potential vorticity  $P_\theta$  (bold line), derived solely from radiosonde data, versus lightly filtered ozone and carbon monoxide data from 990 flight.

measurements from the 990 aircraft. The ozone measurements are by courtesy of G. Gregory of Langley Research Center, the CO by G. Sachse, also of Langley.

Two results are obvious. Except for a small phase error near point D, where the linear interpolation was too crude,  $P_\theta$  and the ozone mixing ratio  $\chi_{O_3}^1$  are positively correlated and proportional to each other. Secondly,  $P_\theta$  and  $\chi_{O_3}^1$  are both negatively correlated with  $\chi_{CO}$ . Therefore  $P_\theta$  and  $\chi_{O_3}^1$  both function as representative stratospheric tracers while  $\chi_{CO}^1$  functions as a tropospheric tracer.

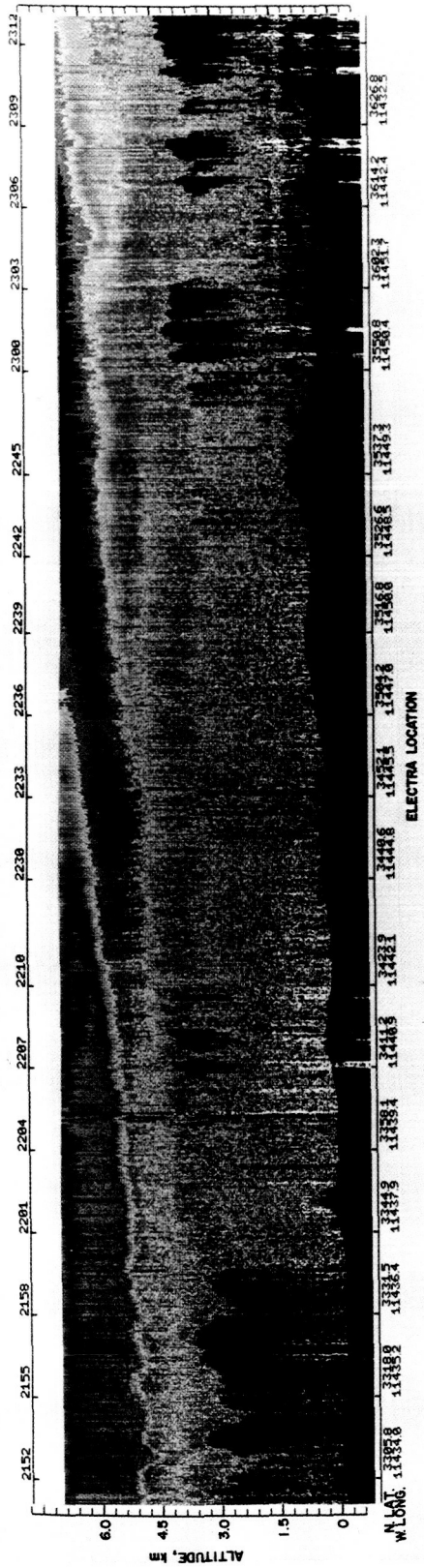
Another conclusion to be drawn from Figures 5-42 and 5-16 is that entrainment of tropospheric air and mixing are responsible for the decrease in  $P_\theta$  and  $\chi_{O_3}^1$  down the axis of the fold and, by implication, mixing is responsible for the gradients in the lower stratosphere. There is no evidence here of a loss of correlation as would be expected if  $P_\theta$  were independently changed by gradients of diabatic heating or if  $\chi_{O_3}$  were significantly changed by photochemistry.

Airborne DIAL measurements (Browell *et al.*, 1983) of aerosol distributions at 600 and 1064 nm were made from 1 km below the aircraft to the ground and ozone profiles were obtained over a 4 km altitude range also starting 1 km below the aircraft. *In situ* measurements of ambient temperature, dew point, ozone, and aerosol number density were made onboard the Electra.

Results of the first airborne DIAL aerosol and ozone measurements across a tropopause fold event are presented in Figure 5-43a and 5-43b. These data were obtained with the Electra flying at an altitude

AIRBORNE DIAL AEROSOL MEASUREMENT OF TROPOPAUSE FOLD EVENT  
APRIL 20, 1984

TIME, GMT



## STRAT-TROP EXCHANGE

of 8.2 km ASL. The violet region at the bottom of Figure 5-43a is the topography along the Electra flight track. The planetary boundary layer (PBL) can be seen to rise to a depth of about 3.0 km above the surface. Convection in the PBL is associated with thermal plumes that originate at the surface and rise to the top of the PBL, where it gives rise to the irregular appearance of the boundary layer top. Several clouds are seen to be present near the top of the PBL, and a few of these clouds are optically thick to the laser beam which produces a shadow below them. The free troposphere typically has a lower aerosol loading than the PBL and this can also be seen in Figure 5-43a. Due to the enhanced aerosol loading from volcanically derived aerosols, the stratospheric air exhibited greater aerosol scattering than did air in the free troposphere. This contrast in scattering permitted the use of aerosols as a tracer of the stratospheric air mass. In Figure 5-43a the stratospheric air can be seen in a layer having a depth of  $\sim 1.5$  km from north of Las Vegas, Nevada, on the right side of the figure to near Yuma, Arizona, on the left. For the first time, the stratospheric air mass resulting from a tropopause fold was continuously traced down to the top of the PBL. Internal gravity waves were induced in the fold by the action of the PBL. It is expected that in addition to the mixing taking place across the boundaries of the fold in the free troposphere, mixing processes at the top of the PBL would mix the diluted stratospheric air into the PBL.

Calculations of the optical scattering properties of the tropospheric and stratospheric aerosols sampled *in situ* at 6.7 km altitude also show an enhancement of a factor of 2.2 in expected aerosol scattering from the stratospheric aerosols compared to the tropospheric aerosols at a laser wavelength of 1064 nm (Browell *et al.*, 1985). This enhancement in scattering resulted primarily from a factor of 4.3 increase in the total number density of aerosols in the 0.5 to 0.9  $\mu\text{m}$  diameter range and the presence of large aerosols in the 0.9 to 2.2  $\mu\text{m}$  diameter range.

The airborne DIAL system also obtained the distribution of ozone along the same flight track. The DIAL remote measurements of ozone are given in Figure 5-43b with higher ozone mixing ratios represented by the yellow and orange display. The maximum ozone level remotely measured in the stratospheric air was 240 ppbv in the centre of the layer near 2232 GMT. This agreed closely with the maximum value of 225 ppbv measured *in situ* at 6.7 km altitude. The concentration in the layer decreased to the 120 ppbv level in the layer above the PBL near 2152 GMT. The correlation coefficient between the DIAL derived aerosol and ozone distributions were calculated over 5 minute intervals with a vertical resolution of 210 m and a horizontal resolution of 2.1 km (105 shot average). The correlation coefficient between ozone and aerosol for each segment across the entire layer was greater than 0.8. This correlation reflects the high degree of spatial coincidence between the ozone and aerosol concentrations determined by the DIAL system.

Potential vorticity was calculated along a transect through the jet stream for 0000 GMT on 21 April 1984. A trajectory analysis was performed to determine the potential vorticity distribution in the cross section along the Electra flight track (see Figures 5-40, 5-41). A plot of potential vorticity isopleths which corresponds to the DIAL obtained aerosol and ozone cross-sections shown in Figure 5-43a and b is given in Figure 5-44. These results were obtained solely from the analysis of radiosonde data. The location of the boundary layer top corresponds closely to the lidar data in Figure 5-43a. The width and altitude of the potential vorticity levels indicating the location of stratospheric air near the top of the PBL on the left of Figure 5-44 agrees in general with the spatial location of the stratospheric air as determined by the DIAL system. Since the potential vorticity is calculated from widely spaced radiosonde data, the analysis cannot resolve the small scale gravity waves seen in the lidar data. In general, the potential vorticity analysis accurately defines the relative characteristics of the stratospheric intrusion. The depth of the layer as determined from the potential vorticity analysis agrees with the lidar measurements; however, the location of

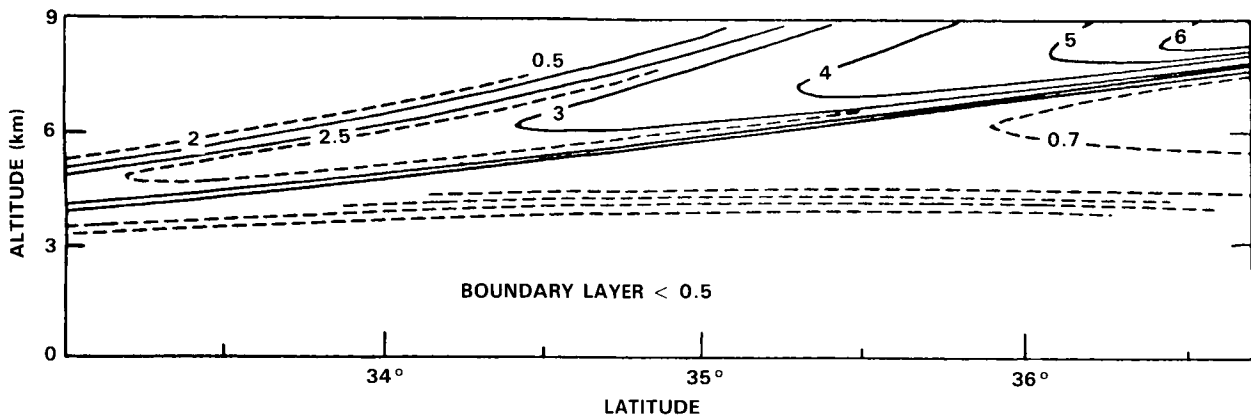


**Figure 5-44.** Isopleths of potential vorticity ( $10^{-5} \text{ cm}^2 \text{ s}^{-1} \text{ K g}^{-1}$ ) along Electra flight track on 20 April 1984. These data were calculated from an isentropic trajectory analysis from radiosonde data.

the warm boundary predicted from the potential vorticity information is higher than its actual location. Incorporation of *in situ* aircraft data into the potential vorticity analysis will improve the agreement with the DIAL data by constraining the location of the tropopause fold at altitudes of 6.7 and 8.2 km.

These results are consistent with the conservation of potential vorticity and ozone mixing ratio as deduced by Danielsen (1968) from simultaneous observations of potential vorticity and radioactive isotopes. They are inconsistent with the deductions by Shapiro (1980) and Gidel and Shapiro (1978). Eddy mixing processes are adiabatic - they redistribute energy, momentum, potential temperature and potential vorticity. When integrated or summed over infinitesimal volumes of a bulk system their effects cancel except at the surface of the bulk system, conversely diabatic heating rates and/or photochemical productions apply to each elemental mass of the bulk system. See Hoskins, McIntyre and Robertson (1985), equation (70b) for a mathematical statement: the mass integrated potential vorticity over a material volume can change only if there are non-zero values of  $d\theta/dt$  or the curl of a frictional force on its boundary. In practice in the atmosphere this means radiation, condensation or interaction with the planetary surface.

A fundamental difference between conservative and nonconservative processes in the atmosphere, is whether the surface integral of the property in question over a material volume is or is not constant in time. It is equally fundamental to our understanding of stratospheric-tropospheric exchange processes. In particular, it affects how we interpret correlations between trace species that we observe along the aircraft flight paths. With few exceptions, the nonconservative processes in the middle and lower stratosphere act slowly and are most effective in determining long term mean distributions. On the other hand, differential advectons by the winds and small scale mixing are most effective in determining instantaneous distributions. If this concept is correct, species whose large scale gradients are positively correlated will remain positively correlated as all internal wave induced velocities displace the larger scale gradients. Similarly, negatively correlated species will remain negatively correlated until small scale mixing becomes important. Then, their correlations will be systematically reduced in magnitude. Correlations computed from the  $\text{O}_3$  and  $\text{CO}$  measurements made on the 990 flight of April 20 confirm this assumption. The measurements were filtered by digital Fourier low-pass and successively higher band pass filters. Correlations approaching  $-1$  for the low pass approach 0 for the highest band pass.

The lowest correlations in the highest frequency band pass were found on the return flight in the folded tropopause zone. Here, tropospheric air is being entrained and mixed with the stratospheric air along both boundaries, as indicated by the streamlines of Figure 5-16.

## STRAT-TROP EXCHANGE

The distribution of ozone mixing ratio and aerosol backscatter obtained from the lidar measurements were presented earlier in this section. Again we see that as a direct result of the small scale mixing and the entrainment of tropospheric air by the velocity deformations that the values of all stratospheric tracers decrease down the fold as it is extended toward the surface boundary layer.

### 5.2.6.2 Analyses and Measurements above the Jet

Several factors conspire to make stratospheric analyses above the jet level much more difficult than those just presented. The time sequence of aircraft (U2) data was filtered, eliminating the short, high frequency waves, and the low pass filtered data combined with the radiosonde data. Analyses of this type based on temporal filtering along each horizontal flight leg will be presented below. However, they still include vertical structures of short vertical wave length associated with long horizontal wave lengths. Their vertical variations were deduced from the U2's ascent and descent profiles which were also incorporated in the analyses. To eliminate these waves, vertical profiles of temperature ( $T^1$ ) and zonal wind speed ( $U^1$ ) were constructed from the analysis at  $1^\circ$  latitude intervals and then these profiles were filtered vertically. The  $\theta$ ,  $U$ , and  $P_\theta$  analyses of Figures 5-45a and b were computed and drawn from the filtered profiles. These heavily filtered fields, denoted by an overbar, are considered representative of the undisturbed mean state. The 1 superscript will refer to the low passed filtered data. Figures 5-45a and b show  $\theta$  isotherms sloping downward to higher latitudes consistent with  $U$  decreasing with height. They also show that the maximum  $U$ , the jet axis, tilts with height toward lower latitudes. The  $P_\theta$  distribution, computed from analyses of Figure 5-45a plus estimated radii of curvature of the mean flow, includes a maximum on the cyclonic side of the jet, a minimum on the anticyclonic side. The horizontal gradient at constant  $\theta$  is largest in the lower stratosphere. It becomes negligibly small at  $\theta$ 's  $>450$  K, indicating that horizontal inhomogeneities produced by differential quasi-horizontal advections would be restricted to  $\theta$ 's  $<450$  K.

Examples of the horizontal inhomogeneities detected by the U2 at 50,000 ft (117 mb) (15.3 km) are presented in Figure 5-46 (a, b, c and d). Flying south-southwestward from the center of the vortex towards the jet,  $\theta$  decreases monotonically with many high frequency oscillations superimposed on the low pass profile. In marked contrast to these trends the  $\chi_{O_3}^1$ ,  $\chi_{H_2O}^1$  and  $\chi_{CN}^1$  oscillate from distinct maxima to minima. We were surprised to find  $\chi_{O_3}^1$  and  $\chi_{H_2O}^1$  positively correlated, and  $\chi_{H_2O}^1$  and  $\chi_{CN}^1$  negatively correlated. However, a comparison of the magnitudes indicates that the flight is in the dry stratosphere, above and to the north of the strong  $\chi_{H_2O}^1$  transition zone whose lower boundary is the tropopause. The flight at 41,000 ft crossed this transition zone and a positive correlation between  $\chi_{H_2O}^1$  and  $\chi_{CN}^1$  was observed where  $\chi_{H_2O}^1$  was large.

The spatial distributions of  $\chi_{O_3}^1$ ,  $\chi_{H_2O}^1$  and  $\chi_{CN}^1$  drawn from the low passed data and ascent-descent profiles are presented in Figures 5-47a, b and c. Here we see correlated relative maxima and minima of all three tracers sloping downward to higher latitude approximately parallel to  $\theta$ 's of Figure 5-45. A comparison of the toned areas reveals that the strong correlations observed at 50,000 ft extend over most of the dry stratosphere. In particular  $\chi_{H_2O}^1$  is positively correlated with  $\chi_{O_3}^1$  at  $\theta$ 's  $> 380$  K. This correlation implies an upper stratospheric source for  $H_2O$ , most probably that due to the oxidation of methane. Conversely the negative correlation at 41,000 ft is due to the surface source for  $H_2O$ .

These distributions combined with the absence of large variations in  $\theta$ , as seen in Figure 5-46a, are consistent with a folding of the  $P_\theta$ ,  $\chi$  etc distributions by a large amplitude, slow frequency, gravity modified inertial wave. In particular perturbation analyses show that waves of short vertical wave length whose wave fronts are parallel to the  $\theta$  surfaces will not disturb the  $\theta$  field but will advect the  $P_\theta$  gradients at

# STRAT-TROP EXCHANGE

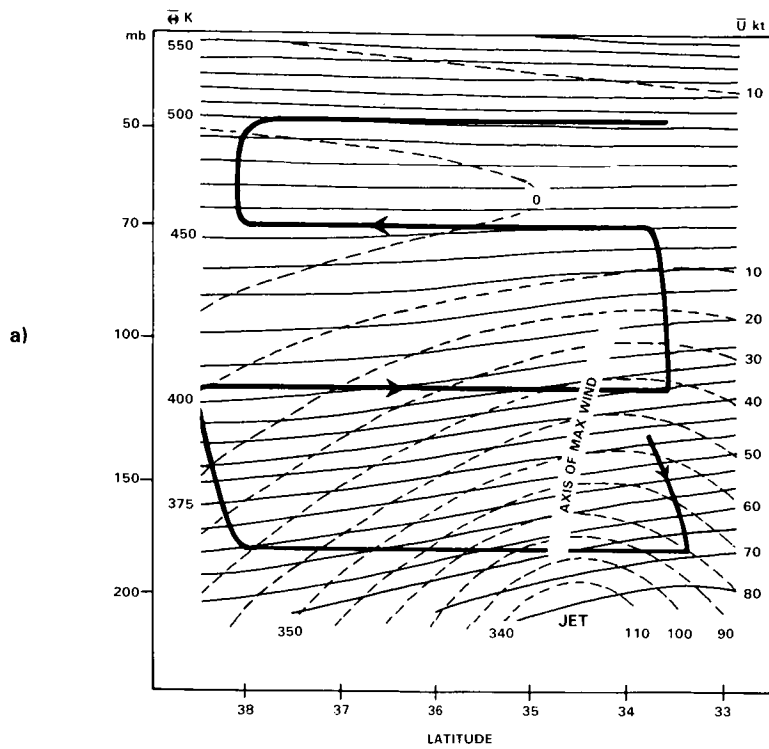


**Figure 5-45.** (a). Vertical cross-sections analysed only from meteorological measurements. See Figure 5-39 for the flow on the 330K surface, and Figure 5-40 for the U2 flight path. Data were heavily filtered to remove oscillations whose vertical wave lengths were  $\leq 3$  km. Note change in  $\theta$  contour interval at 400 K.

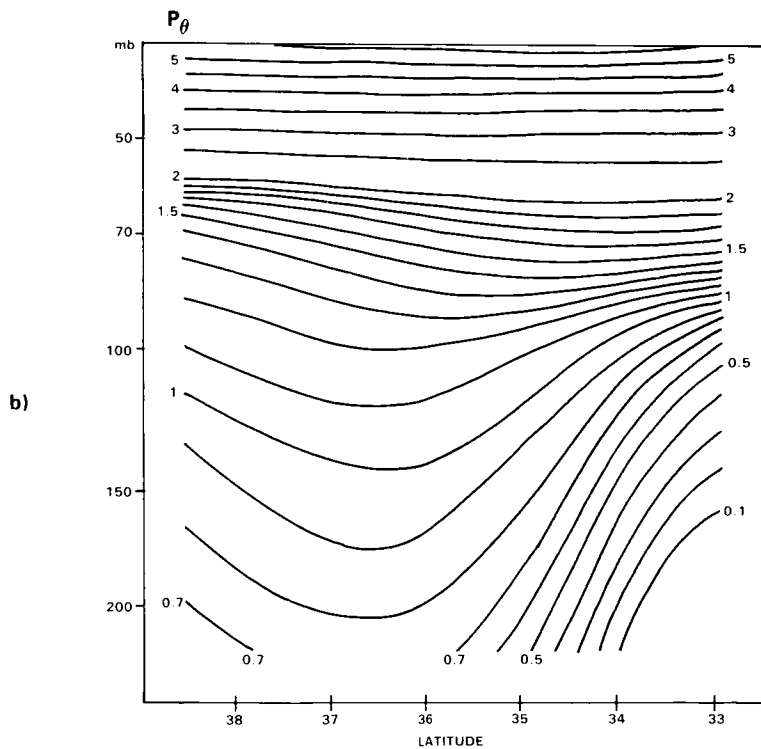
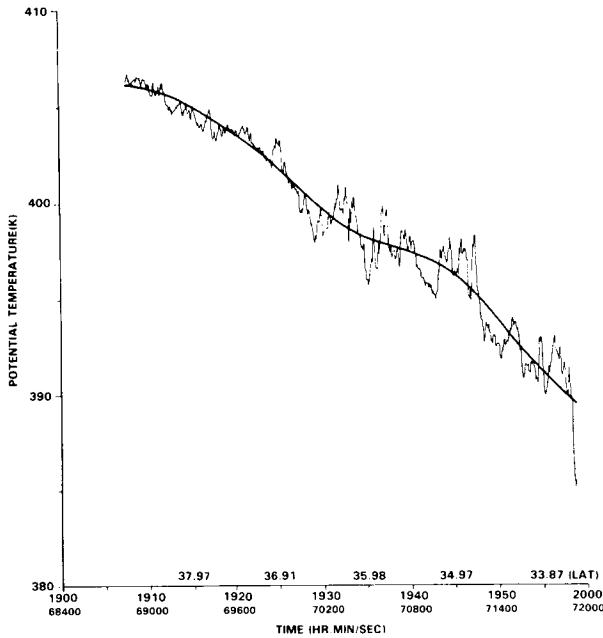
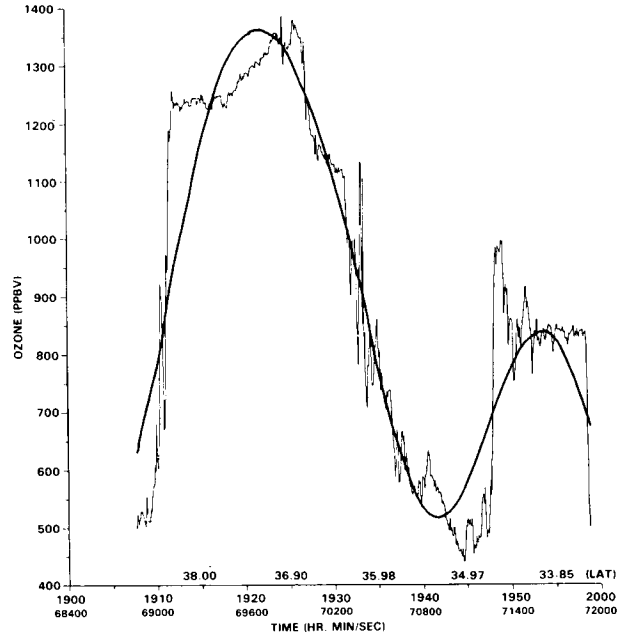


**Figure 5-45.** (b) As in part (a), but for potential vorticity. Note change in contour interval at  $2 \times 10^{-4}$   $\text{cm}^2 \text{s}^{-1} \text{kg}^{-1}$ .

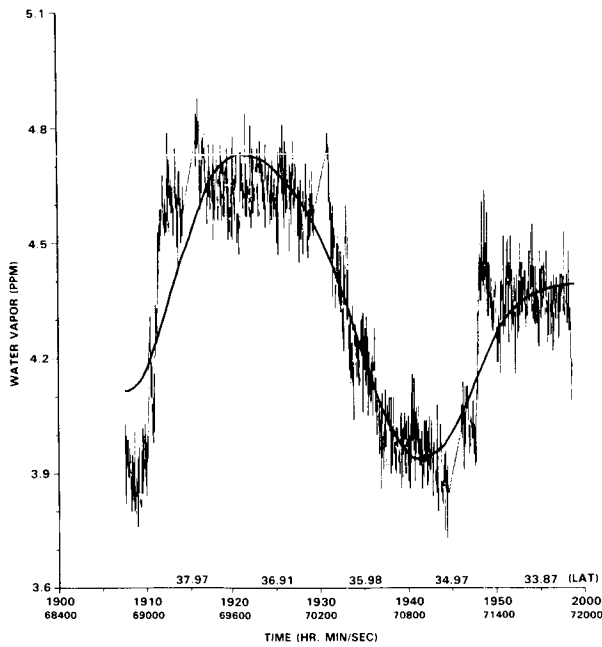
**STRAT-TROP EXCHANGE**



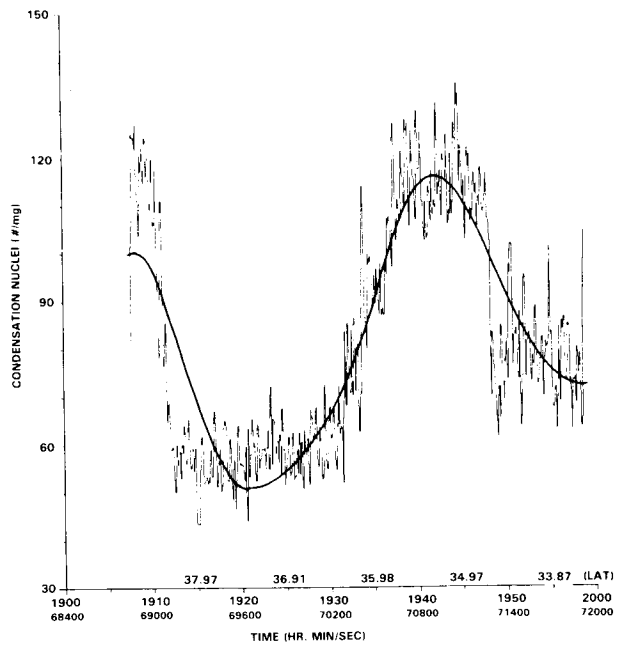
**a, potential temperature;**



**b, ozone mixing ratio;**

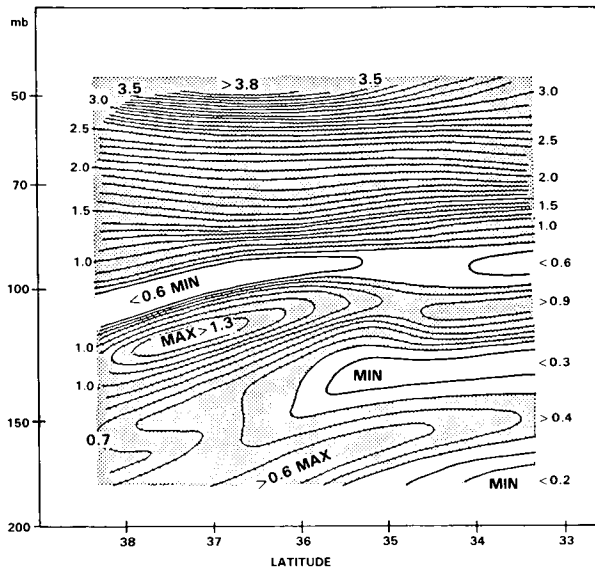


**c, water vapour mixing ratio**

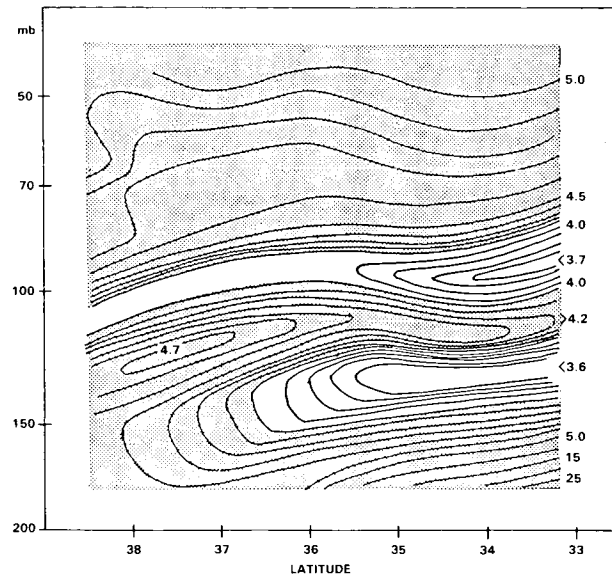


**d, condensation nuclei mixing ratio**

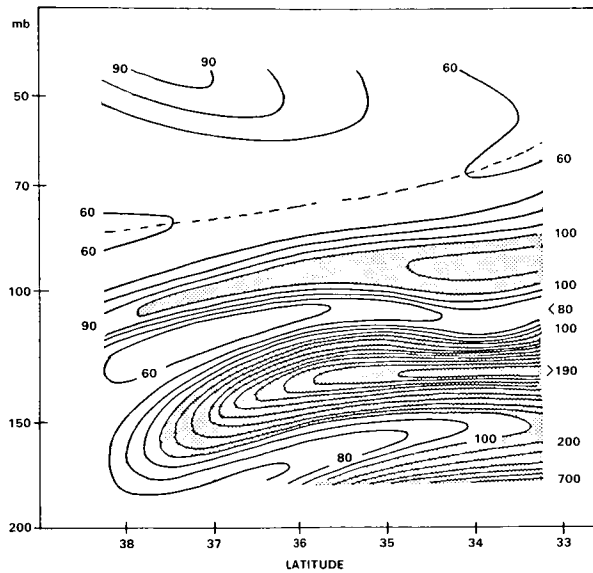
**Figure 5-46.** Temporal variations measured by U2 on 50,000 ft leg, 20 April 1984, including unfiltered and low pass filtered profiles of: (a) potential temperature; (b) ozone mixing ratio; (c) water vapour mixing ratio and (d) condensation nuclei mixing ratio.



a, ozone;



b, water vapour;



c, condensation nuclei mixing ratios

Figure 5-47. Vertical cross-sections analysed from low pass filtered data along flight legs and vertical ascent-descent profiles for: (a) ozone; (b) water vapour; and (c) condensation nuclei mixing ratios.

## STRAT-TROP EXCHANGE

constant  $\theta$ . These waves would be elliptically polarized and the hodographs plotted, during ascent and descent of the U2, from the observed winds confirm this necessary condition. The perturbation vectors,  $7-8 \text{ ms}^{-1}$  in amplitude, rotate anticyclonically with height, producing alternating northward and southward advectons.

These waves could fold and later unfold the distributions of conservative tracers. However, the observed high frequency oscillations indicate that instabilities of the Helmholtz type are generated along the boundaries of the folds. These produce small scale mixing which renders a potentially reversible transfer, irreversible. In this case the folding occurring above the jet is all in the stratosphere. Air from the anticyclonic side of the jet, having tropical (tropospheric) characteristics is folded over and under air from the cyclonic side with polar (upper or middle stratospheric) characteristics.

These high resolution experimental data show that potential vorticity and ozone are both positively correlated and proportional to each other; both are negatively correlated with carbon monoxide, which thus serves as a tropospheric tracer. It is also clear that mixing is an important process in folds.

### 5.2.7 Ground Based Studies over France

New ground based remote sensing instruments such as lidars and scidar have been developed during the last four years allowing a new insight into the relatively small scale phenomena associated with stratosphere-troposphere exchanges. These instruments are presently located in the Northern Hemisphere mid-latitude region and have been mainly used for the study of stratospheric air intrusions occurring primarily in association with the tropopause folding mechanisms taking place at the junction between frontal surfaces and the troposphere and related to the polar jet stream deformations. Their high spatial resolution is particularly well adapted to the vertical scale of such events ( $\sim 1 \text{ km}$ ) and the measurement temporal continuity leads to observations during long time periods compatible with the horizontal scale of a few hundred kilometers characteristic of these events. However the fixed location of the observing stations implies that the description of such an event will be dependent on the position and motion of the front as compared to the observation site and thus only a particular cross-section of the intrusion can be studied in detail. The data interpretation in terms of mixing between stratospheric and tropospheric air requires a synoptic analysis of potential vorticity and potential temperature cross-sections (Reed, 1955; Danielsen, 1968). Nevertheless as shown in the various examples given hereafter such an instrument as the lidar system in use at the Observatoire de Haute Provence Geophysical Station for ozone measurements since 1980 (Pelon and Megie, 1982a) may help to improve our understanding of the small scale processes involved in stratosphere-troposphere exchanges. Two case studies corresponding to different synoptic situations will be analysed hereafter.

The Figure 5-48 shows examples of lidar observations of the ozone vertical distribution taken on December 1 and 2, 1981. During this time period a meridional circulation was established over France due to a developing wave pattern in the jet stream associated with the descent of a low over southern Europe and the presence of an anticyclonic region over the Atlantic. This resulted in a main front located over Southern France at the 500 mb level during the second night of observation (December 2-3). The measurements reported on Figure 5-48b are thus representative of a vertical cross-section through the frontal zone in the southwest part of the low. The observed altitude decrease in the ozone number density maximum corresponds to the displacement of the front during the measurement period. At the lower edge of the front, simultaneous measurements using the star scintillometry technique (Scidar), Azouit and Vernin (1980), gave evidence for the presence of intense turbulent layers, at 5-6 km altitude just below the

# STRAT-TROP EXCHANGE

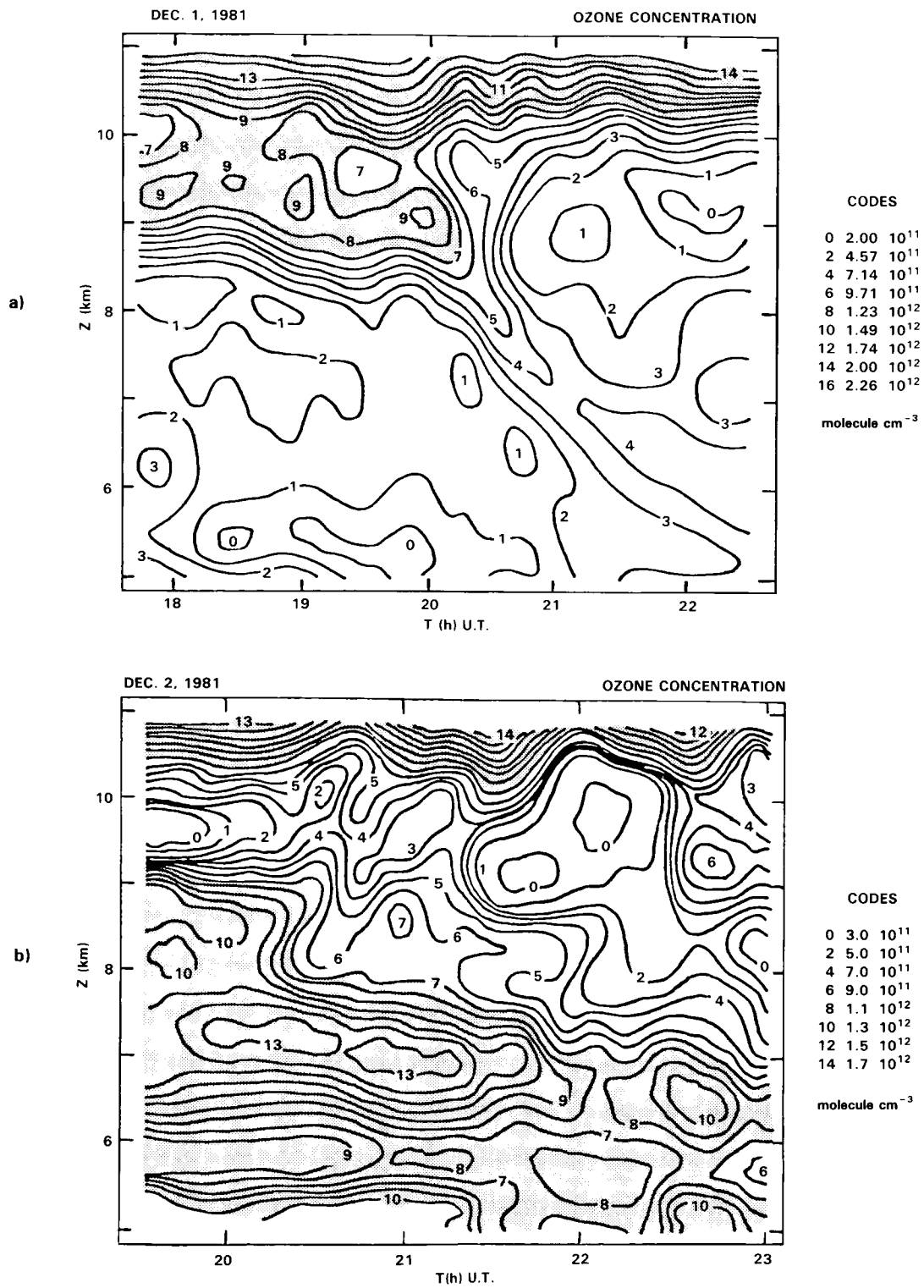


**Figure 5-48.** Ozone number density isocontours as a function of time (horizontal axis) and altitude (vertical axis) for the nights of December 1st and 2nd 1981. The hatched areas correspond to ozone concentrations larger than  $10^{12} \text{ cm}^{-3}$ .

## STRAT-TROP EXCHANGE

peak of the ozone distribution ( $1.5 \times 10^{12}$  mol cm<sup>-3</sup> i.e., 120 ppbv). If for the previous night (December 1-2) the shapes of the ozone isocontours (Figure 5-48a) are similar to the fingered structure observed in tropopause folding events, the observed evolution should not be attributed directly to the influence of the main front: in order to explain the origin of the high ozone content observed at tropospheric levels in both cases and to follow its ensuing evolution, air mass trajectories calculated from radiosonde observations, by the Meteorologie Nationale at the European Center have been used (Figure 5-49). Such trajectories are necessarily crude, especially in the region of frontal surfaces. The trajectories ending at the Observatoire de Haute Provence (OHP) on December 1 (6 pm and midnight UT) at the 300 and 500 mb levels (Figure 5-49a) show that the origin of the air masses four days before (November 28) are quite different. The one observed at 300 mb in the early night originated above Greenland at upper levels (225 mb) in the stratosphere (high ozone content), while those observed six hours later come from tropospheric levels at lower latitude. The synoptic situation on November 28 (0 h UT) corresponds to a very well developed frontal zone stretching from north-west of Southern England to the South of Iceland with a low over northern England and Western Scandinavia and a high over the Azores. The time resolved measurements at the OHP correspond thus to a transverse cross-section through this frontal zone: observed air masses originate at various altitudes with different ozone contents further modified by dispersion and small scale turbulence along the trajectories. Similarly, Figure 5-49b shows the trajectories ending on December 2 (midnight) at two points located at the 500 mb level in the frontal zone. Their origins are in the cyclonic zone above the North Sea four days before at the 400 mb level (points 5 and 6). The ozone rich air masses coming from this region have thus turned around the low in the associated frontal zone before reaching southern France (Figure 5-48b).

Considering the air mass trajectories calculated for the days following the observations, evidence is given that the air coming from points 2 and 3 on Figure 5-49a (December 1) is going back to higher latitudes (49°N and 57°N) and upper levels for point 2, whereas air originated from point 3 remains at the 500 mb level. On the second night (December 2-3), the trajectories originating at points (5 and 6) on Figure 5-49b are quite different: the air masses coming from point 5 continue to travel down to lower latitude (37°N) and higher pressure levels (630 mb). On the contrary air masses originating from point 6 reach a latitude of 68°N on December 7 at the 450 mb level. Such a behaviour illustrates the complexity of synoptic stratosphere-troposphere exchange processes: the air masses observed in the frontal zone can either be definitely transferred into the troposphere at mid-latitudes, or return to the stratosphere at higher latitudes in association with the polar jet stream. This latter conclusion must be tentative in view of the nature of the trajectory calculation. It is however an interesting possible behaviour.

Another example of the influence of cyclogenesis on ozone transfer can be given from observations performed on July 9, 1980 when large ozone concentrations were observed at the 300 mb level associated with a frontal zone located over Southern France and corresponding to a similar jet stream wave pattern as the one described above. The lidar measured ozone profiles give evidence for concentrations as high as  $3.5 \times 10^{12}$  mol cm<sup>-3</sup> (380 ppbv) at 9 km altitude, and  $2.5 \times 10^{12}$  mol cm<sup>-3</sup> (200 ppbv) at 7 km altitude, in the upper part of the frontal zone (Figure 5-50a). Considering the total ozone maps obtained from the TOMS experiment on board the Nimbus 7 satellite, the low observed over France corresponds to ozone total content up to 400 DU, the frontal zone being delimited by the 360 DU contours. Trajectories, calculated as before for the 300 and 500 mb levels, show that the air masses considered originated on July 6 from latitudes west of Ireland, close to 50°N (Figure 5-50b) and thus from the same cyclonic zone before it developed over Southern France. Related to the development of this low, the anticyclonic zone previously settled over the Northern Atlantic region is cut in two parts with a blocking high at 70°N latitude carrying low ozone content in the lower stratosphere as observed by TOMS. No direct correlation can then be

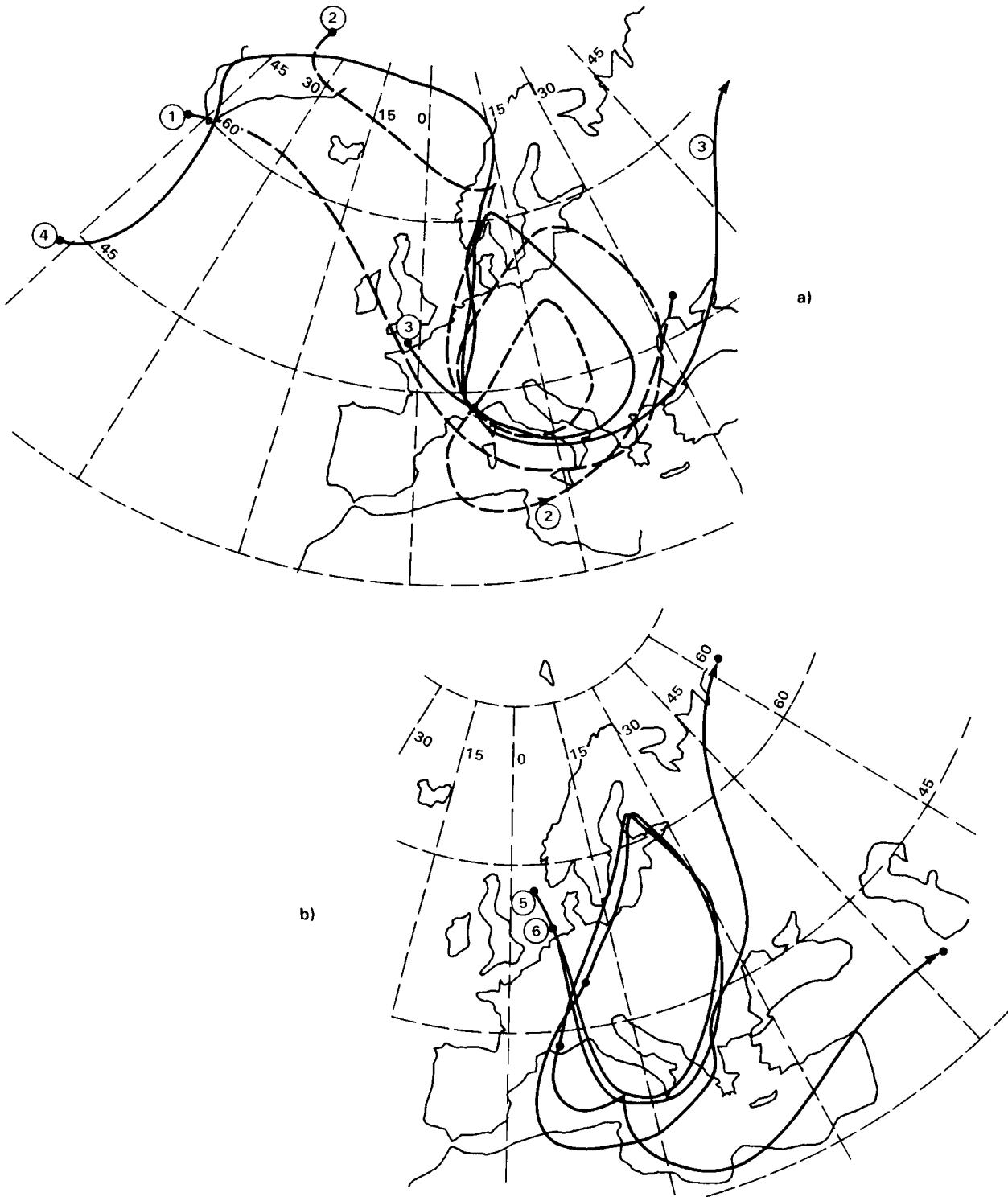


**Figure 5-49.** a) Air mass trajectories ending at the Observatoire de Haute Provence on December 1st, 6 pm ((1) 500 mb pressure level; (2) 300 mb and midnight; (3) 500 mb; (4) 300 mb). b) Air mass trajectories in the frontal zone at the 500 mb level originating at points 5 and 6 and ending at 49°N, 10°E and at the OHP (44°N, 5°E) on December 2nd (midnight) and their ensuing evolution.

# STRAT-TROP EXCHANGE

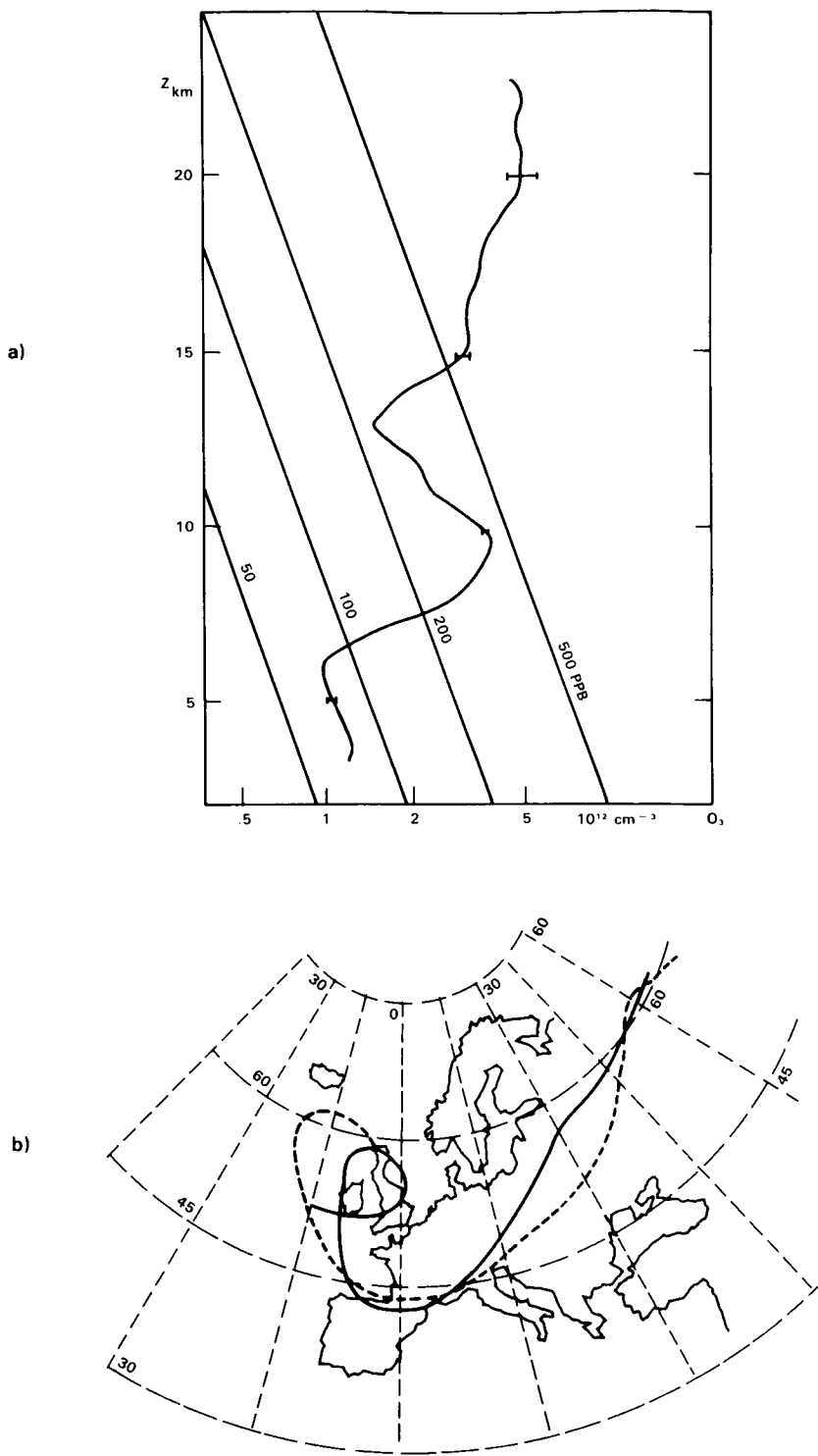


**Figure 5-50.** a) Ozone vertical distribution on July 9, 1980 at midnight as observed by lidar sounding at the OHP. b) Air mass trajectories ending at the OHP on July 9, 1980 (midnight) and their ensuing evolution: full line (500 mb), dotted line (300 mb).

further established between the location of the frontal zone and the ozone vertical distribution. It should also be pointed out that air masses, originating from this low, entered the associated frontal zone where it stayed on the following days, slowly ascending before reaching at higher latitudes on July 14 a cyclonic zone over Siberia (60°N, 70°E), returning thus to the polar stratosphere (Figure 5-50b). Again, the coarseness of these trajectories, together with an absence of measurements which would permit estimation of the rate of mixing, makes this an uncertain interpretation.

These two examples show the difficulty in quantifying the ozone transfer related to mid-latitude stratosphere-troposphere exchange processes. They did not give evidence for a large direct ozone transfer at 45°N from the stratosphere to the troposphere but rather indicated that such transfer occurred at higher latitude. The larger part of the transported ozone remains in the frontal zone for several days with a likely possibility for part of it to return to the polar stratosphere. Evaluation of the magnitude of the ozone transfer is also complicated by turbulent exchange processes in the frontal zone which are more intense than in the free troposphere. Further investigations are needed especially at the synoptic scale (using airborne lidar systems) to provide evaluation of ozone transfer within frontal zone, cutoff lows or blocking highs.

### 5.2.8 Global Coverage: TOMS Ozone Column Measurements

The total ozone column is a particularly sensitive indicator of vertical motions of air due to the peculiar vertical mixing ratio distribution of ozone. In the troposphere, the mixing ratio is small ( $\sim 0.04$  ppm) and nearly constant. Immediately above the tropopause the mixing ratio increases steeply ( $\sim 0.50$  ppm/km) with height in the stratosphere to a maximum near 35 km. Any vertical displacement produces a change in the total ozone due to convergence or divergence. Reed (1950) calculated that a well-developed upper tropospheric trough should contain 24 Dobsons of total ozone greater than the average of 300 Dobsons. An adjacent ridge will be depleted by a similar amount and 15% variations in total ozone should be found. Variations of this magnitude are observed with the Nimbus 7 TOMS in large scale planetary waves (Schoeberl and Krueger, 1983). Much larger changes (greater than 30%) are found in smaller scale troughs (Krueger, *et al.*, 1981). Information about the vertical structure of ozone would aid in diagnosis of exchange events, however, none of the current satellite-borne ozone profile sounding instruments is likely to provide any routine diagnostic coverage of exchange processes due to the lack of horizontal coverage and of vertical resolution.

The TOMS maps global total ozone each day with 50 km spatial resolution at nadir from a local noon orbit. The wavelengths of the instrument are selected for maximum penetration of the ozone region, with the Rayleigh scattering contribution functions peaking low in the troposphere. The precision of measurement, tested by comparison with coincident Dobson Spectrophotometer data (Bhartia, *et al.*, 1984a) is better than the average 2% rms difference and appears to be close to 1%. This figure is of the order of residual cloud biases and radiance measurements errors. Thus, total ozone differences of 3-5 Dobsons are at the limit of detection in individual samples but, by use of spatial coherence on mesoscale or synoptic dimensions, the limit of detection is less. Thus, measurement errors are generally trivial at extratropical latitudes.

At the present time, TOMS observations of total ozone show promise for investigation of exchange processes. The following discussion concentrates on these observations.

## STRAT-TROP EXCHANGE

### 5.2.8.1 Brewer Circulation/ITCZ Exchange/Stratospheric Fountain

The total ozone in the tropics is observed to have a general wavenumber 1 longitudinal variation. The zonal average ozone has a low variability (5-8 Dobsons) and exhibits a shallow minimum located in the winter hemisphere. The latitude of the minimum does not vary with longitude and is confined to within  $15^\circ$  of the equator. At the equinoxes the minimum jumps discontinuously to the opposite hemisphere. This behaviour is different from that of the ITCZ which tends to persist in the northern hemisphere throughout the oceanic areas, except for the western Pacific region where interhemispheric transitions are found. A direct association between the axes of the oceanic ITCZ and total ozone is not found.

The longitude of the minimum of tropical total ozone is, however, stationary and located over the western Pacific ( $150^\circ\text{E}$ ), coincident with the location of the "stratospheric fountain" of Newell and Gould-Stewart (1981), suggesting a possible decrease of lower stratospheric ozone in the fountain region. Alternatively it may only indicate a relation between the tropical tropopause height and total ozone, such as occurs in Figure 5-8.

An analysis of the detailed behaviour of total ozone over the ITCZ shows no relationship except for "superreflectivity" clouds. These clouds have apparent reflectivities greater than 100% and appear in the tropics and in severe storms. They are believed to be ice specularly-reflecting, capped cumulonimbus cloud masses. These clouds show an excess of ozone relative to the surroundings and may indicate subsidence of stratospheric air.

Tropical total ozone also exhibits small scale structure which is organized on scales larger than clouds and cloud masses, but seemingly located at random. Some features persist and migrate meridionally, indicating mass transport of ozone excess or deficit air between the tropics and subtropics. The transport of excess ozone into the tropics is found at Atlantic longitudes while ozone "minima" move out of the tropics at Indonesian longitudes. This behaviour appears to be consistent with the transport diagnosed in Section 5.2.2.2.

### 5.2.8.2 Tropopause Folding near Jet Streams

Aircraft observations of ozone and jet stream structure (Danielsen, 1968; Shapiro, 1980; Shapiro *et al.* 1982) indicate that the folds have typical vertical dimensions of 1-2 km. Recently exchange events with a vertical scale of 3 km have been observed (Figures 5-30 and 5-34). The integral amount of ozone in the fold is estimated to be on the order of 10 Dobsons based on a typical mixing ratio of 0.10 ppmv. This amounts to a 3% change which is well within the precision limits of the instrument. The shape of a fold in plan view can be seen in Figure 5-51, the TOMS data for the aircraft study case of April 20, 1984 described in Section 5.2.6. The fold observed with the airborne LIDAR (Figure 5-43) in the southwestern U.S. is found to coincide with the dark green band (325 - 350 Dobsons) that parallels the steep gradient in the yellow colors along the California-Nevada border. This high gradient band (25 Dobsons/100 km) is located exactly at the jet stream core as observed with the CV 990 aircraft at 310 mb over western Nevada (Figure 5-41).

The polar vortex boundary is another potential location for exchange of air. Polar vortex air masses are identified on TOMS maps by their extremely high total ozone values (450 - 550 Dobsons). The high total ozone would suggest low tropopause heights and, indeed, tropopause pressures of greater than 500 mb are found. The boundaries are also very steep with ozone gradients of 100 Dobsons/500 km typical.

Shapiro and associates investigated these features with aircraft flights across the vortex during the 1983 AGASP experiment. Jet stream winds were found at 300 - 400 mb and stratospheric air in the fold was traced by ozone, potential vorticity, and aerosols to as low as 700 mb (Shapiro, *et al.*, 1984). Other flights during this experiment investigated other folds with similar conclusions. The satellite observations of these features have yet to be investigated.

### 5.2.8.3 Cut-off Lows

In Section 5.2.5, evidence was presented that stratospheric air in cut-off low centres is mixed into the troposphere. TOMS showed an increase of about 50-60 DU associated with the low, and combined with the aircraft ozone data, it could be concluded that much or all of the ozone in this extension was probably mixed into the troposphere.

Cut-off lows always appear as isolated ozone maxima in TOMS maps, thus demonstrating that stratospheric air within the low centre is ozone enriched. In the Bamber *et al.* (1984) study the cut-off low was disrupted by convective activity. It is possible to follow the life cycle of other cut-off lows in the TOMS data. One often sees that a path is established to the main trough after a few days and at least part of the ozone is returned to the system that spawned the cut-off low. In other cases the low centre can be permanently absorbed. At the present time a systematic study of such features has not been made. It is apparent that combining the spatial information and quantitative ozone data in the TOMS maps with conventional radiosonde and aircraft observations and with numerical models will produce a better understanding of the importance of cut-off lows in the exchange budget.

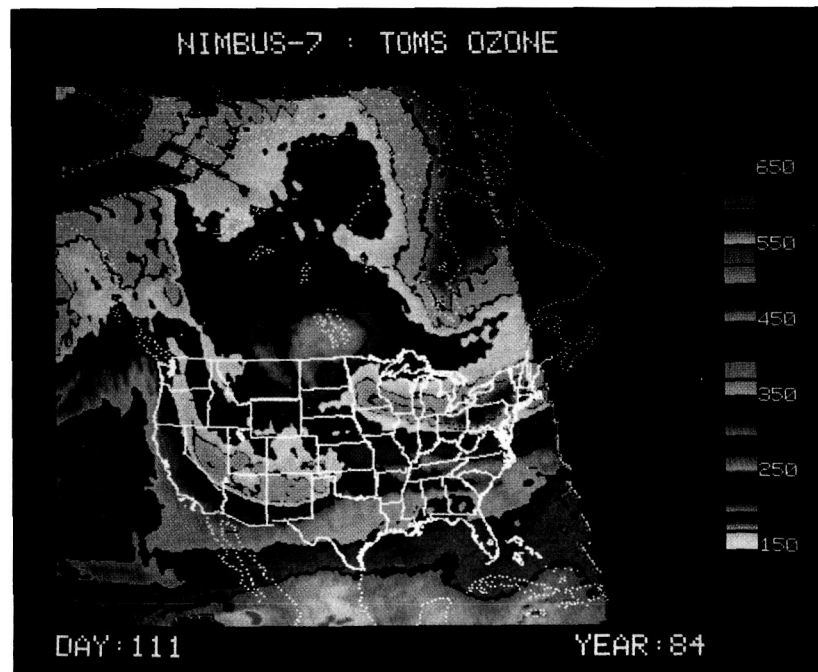


**Figure 5-51.** TOMS map of total ozone during the aircraft experiments over the western United States on 20 April 1984 (see section 5.2.6). Color boundaries are at 25 DU intervals as shown in color scale. The tropopause fold is in the dark green region south and west of the trough which is outlined in yellow color over Nevada and Arizona.

## STRAT-TROP EXCHANGE

### 5.3 LARGE SCALE NUMERICAL MODELLING OF STRATOSPHERE-TROPOSPHERE EXCHANGE

If it is accepted that understanding of the physical nature of the processes effecting exchange across the tropopause is necessary before successful modelling can be attempted, the basic difficulty is apparent from the case studies described in Sections 5.1 and 5.2. In the tropics and in many cases in the extratropics the scale of the individual processes is below the resolution of the global meteorological observing system. There were grounds for encouragement however, in the tropopause folding events reproduced by a limited area operational model, with  $0.9375^\circ \times 0.75^\circ$  longitude-latitude resolution (see Section 5.2.5). Nevertheless, some investigation with general circulation models has been done, because although such models parametrize mesoscale events and cumulonimbus storms, they can resolve the larger scale features of the sea-land contrast and the associated topography, jet streams and the horizontal temperature structure at the tropical tropopause, which arises from the preferential occurrence of the deepest cumulonimbi at longitudes in the western Pacific-Indian Ocean region.

#### 5.3.1 General Circulation Models

One consistent result from general circulation models which transport ozone (usually as a tracer with a parameterized chemistry) is that there is a greater flux from the stratosphere to the troposphere in the Northern than in the Southern Hemisphere. For this reason, and despite the inability of GCMs to adequately resolve the meteorological processes achieving the cross-tropopause flux, a table (5-1) has been given of available general circulation model estimates of the ozone flux to the troposphere. Other estimates of this flux from atmospheric data tend to be of the same general magnitude (Paetzold, 1955; Regener, 1957; Fabian and Junge, 1970; Danielsen and Mohnen, 1977). Figure 5-52 shows a model estimate of the Northern Hemisphere annual mean  $O_3$  cross-tropopause flux and mixing ratio at 500 mb; although these data show that the model is not completely equilibrated, it is nevertheless clear that the maxima are too early, occurring in late winter and early spring. Very recently, Levy *et al.* (1985) have published a more detailed consideration of tropospheric ozone in their GCM; it is discussed in Chapter 4.

(a) GCM estimates of ozone export to the troposphere. There are three model estimates of ozone fluxes from stratosphere to troposphere:

Table 5-1. General circulation model estimates of cross-tropopause  $O_3$  Flux

	NH	SH	
MLM	6.6	3.6	$O_3$ fluxes, $10^{10}$ molecules $cm^{-2} s^{-1}$
GS	4.9	2.5	
AT	3.8	3.0	

The references in the left hand column of Table 5-1 are, in order, Mahlman, Levy and Moxim (1980); Gidel and Shapiro (1979) and Allam and Tuck (1984a, b). The AT figure has not been previously published but was calculated with the same methodology as was used for water vapour in the reference.

The MLM estimate is actually  $O_3$  flux across the 240 mb surface, while the GS estimate assumes that the model zonal mean potential vorticity has a constant ratio to observed zonal mean ozone, and that

this ratio can be used to convert model potential vorticity flux to an ozone flux. The NH annual mean O<sub>3</sub> cross-tropopause flux and mixing ratio at 500 mb, are shown in Figure 5-47 for the AT model. The MLM model had horizontal resolution of 265 km and  $\sigma$  levels at pressures of 500, 315, 190 and 110 mb in the relevant region, while the GS model had 5° × 5° horizontal and 3 km vertical resolution. The AT model had horizontal resolution of ~320 km and similar  $\sigma$  levels to MLM at the relevant altitudes.

It could be argued that if a general circulation model does an acceptable job of getting the large scale dynamics right, the mass flux across the tropopause must be approximately correct, even if the detailed simulation of the synoptic, meso and cloud scale processes involved is poor. Such a view assumes that mass transport by the large scale dynamics is independent of the quality of representation of these smaller scales, and is by no means well established. Also, from the point of view of fluxes of particular chemical species, the case studies of Sections 5.1 and 5.2 show clearly that it is necessary to know the covariance of the species and the motion field on the active scales.

(b) Lagrangian diagnostics of GCM data

Kida (1983a,b) has used a hemispheric GCM, without topography and with annual mean forcing, to obtain trajectories from the 3 velocity components for many thousands of particles for periods of up to 5 years. Model resolution was 3° long × 2.5° lat with 12 levels from the surface to 1 mb, so the results must be dependent upon the treatment of sub grid scale processes. An analysis was used which produced a "spectrum" of ages of air particles in different regions of the model stratosphere. Particles in the tropical stratosphere were younger, and had a narrower spectrum of lifetimes since entry from the troposphere. At the poles, the model air particles were older, with a flat, broad spectrum of ages. Most particles entered the stratosphere across the tropical tropopause, but there was an identifiable fraction which entered the lower mid-latitude stratosphere from the upper tropical troposphere. It is difficult to see how Kida's results can be tested experimentally, since the only particles in the real atmosphere which retain their identity after 5 years in the stratosphere are likely to be N<sub>2</sub> or CF<sub>4</sub> molecules rather than fluid elements.

Allam & Tuck (1984a,b) have examined fluxes of mass and water vapour and associated trajectories across the "tropopause" in a 13-level global general circulation model, with 320 km horizontal resolution and vertical levels (at relevant heights) of 493, 319, 196, 117 and 74 mb. Ozone was available as a tracer, and its cross-tropopause transport calculated; the hemispheric average behaviour over a year is shown in Figure 5-52. Deep tropical convection over the Indian Ocean/Western Pacific and Central American sectors maintained a source of dryness at ~100 mb. Exchange of mass and water vapour occurred above the cores of the subtropical jet stream maxima, between the tropical upper troposphere and lower mid-latitude stratosphere. Some trajectories showed oscillatory behaviour with periods of the right order for inertial instability. A summary of the behaviour seen in all 400 trajectories is as follows.

(i) Within the limits of the model spatial and temporal scales, mixing was sufficiently effective that substantial development of the O<sub>3</sub>-H<sub>2</sub>O ratio of a parcel generally occurred during the 10-day period.

(ii) O<sub>3</sub>-H<sub>2</sub>O ratios developed strikingly around jet streams, particularly at exits and entrances.

(iii) Air parcels frequently underwent decreases in water vapour in the tropics during horizontal motion, especially when this was into the upper troposphere of the equatorial western Pacific; presumably this emphasizes the importance of mixing with drier air.

## STRAT-TROP EXCHANGE

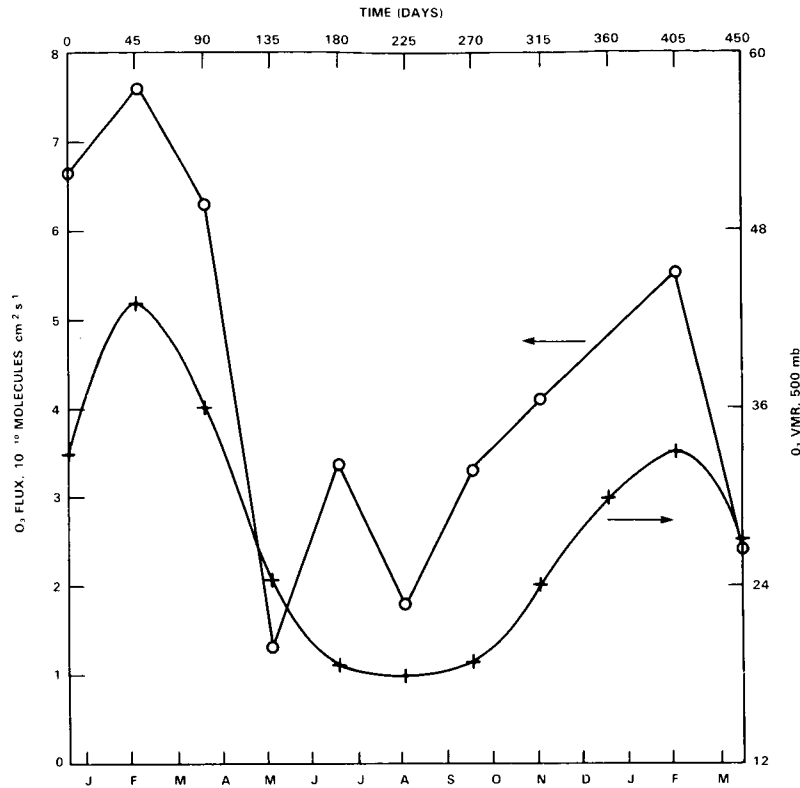


**Figure 5-52.** Northern hemisphere mean ozone flux stratosphere–troposphere (open circles) in the general circulation model described by Allam and Tuck (1984), and 500 mb ozone mixing ratio (crosses). Note that the behaviour is not completely equilibrated, and that the tropospheric ozone maximum occurs in late February.

(iv) There was little development of O<sub>3</sub>-H<sub>2</sub>O covariance in the anticyclonic circulations, particularly in the subtropical highs.

(v) Air entering the equatorial western Pacific region acquired a positive correlation between low values of ozone and low water vapour mixing ratios, presumably because of the co-location of ozone and temperature minima in this region.

(vi) The flow of air from about 100 to 200 mb in the equatorial western Pacific into the right entrance of the Japanese subtropical jet stream, above the core, resulted in low water vapour mixing ratios at the southern flank of the stratospheric Aleutian high, via the left exit.

(vii) Air moved, at about 100 mb, from the southern subtropical jet stream, at about 30°S, to about 15-20°N in a few days, at longitudes 180° to 160°W.

(viii) There were trajectories from subtropical and mid-latitudes at about 100 mb in the Northern Hemisphere which moved equatorward and upward in limited longitudinal zones, transporting relatively high water

vapour mixing ratios to the tropics and so tending to create an increase of water vapour with height above 100 mb. This did not occur in the Southern Hemisphere.

(ix) The proportion of trajectories which oscillated between 'stratosphere' and 'troposphere' was considerably higher than the proportion which directly ascended through the tropical tropopause. This is of course subject to bias in the initial distribution of rings of parcels, and to the difficulty in defining the model tropopause.

This model maintained a negative correlation between ozone and water vapour in the upper troposphere (200 mb level), but showed a positive correlation in the lower tropical stratosphere, with a negative correlation in the lower stratosphere of middle and high latitudes (Allam, Groves and Tuck, 1981). The negative correlations in the troposphere are readily explicable; the positive correlations were attributed to the drying action of deep cumulonimbus upon ozone-poor air from the lower tropical troposphere, a behaviour readily apparent in the time history of ozone and water vapour along appropriate model trajectories. Such predictions have yet to be tested against global scale data, but the lower stratospheric behaviour at high northern latitudes is consistent with old aircraft data obtained by Roach (1962), as may be seen from Figure 5-53.

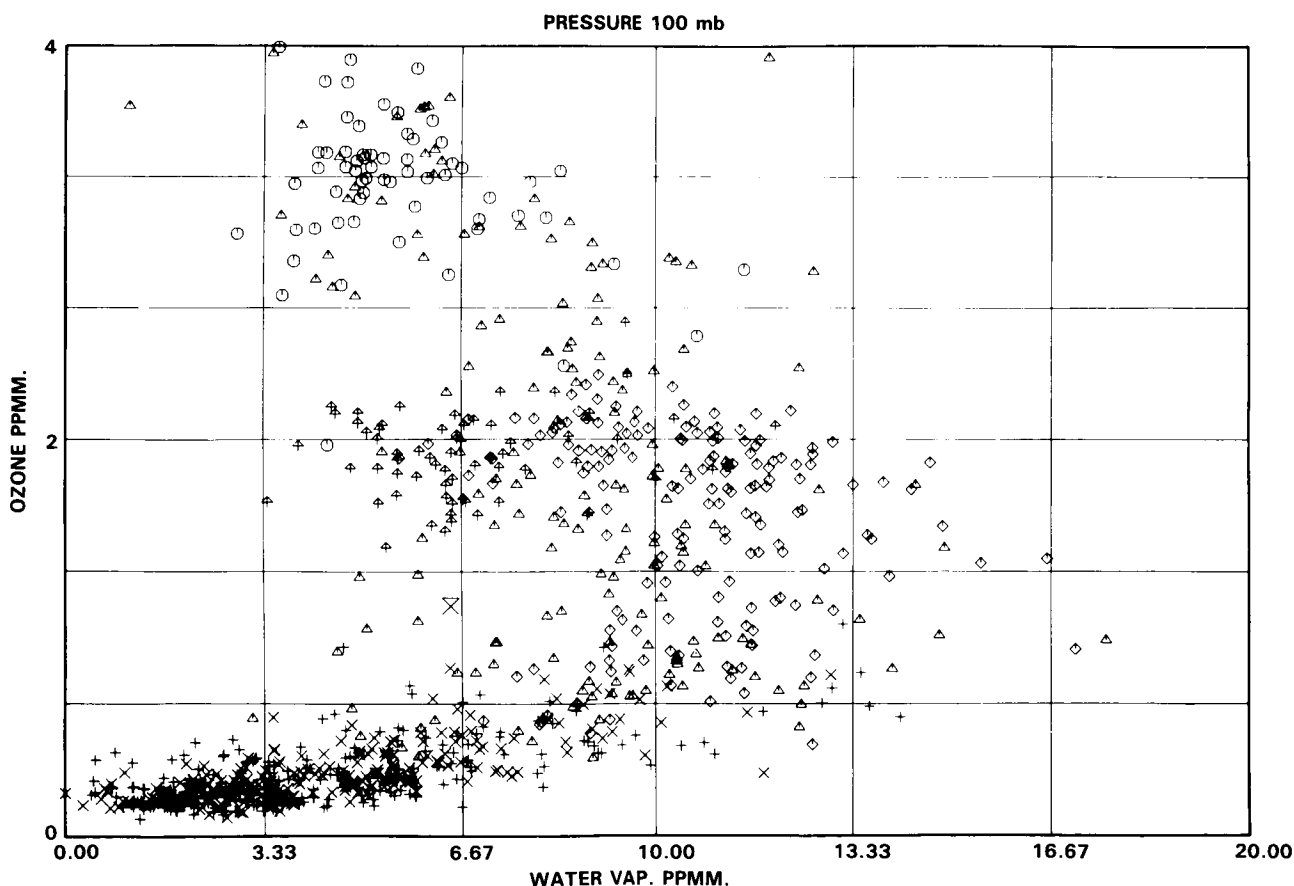


**Figure 5-53.** Ozone-water vapour correlation in the stratosphere. (a) From the general circulation model described by Allam, Groves and Tuck (1981), at 100 mb, January 1st. Circles are gridpoints situated between 90°N and 60°N, diamonds are between 60°N and 30°N, crosses between 30°N and 30°S, tailed triangles between 30°S and 60°S, and triangles are between 60°S and 90°S.

STRAT-TROP EXCHANGE

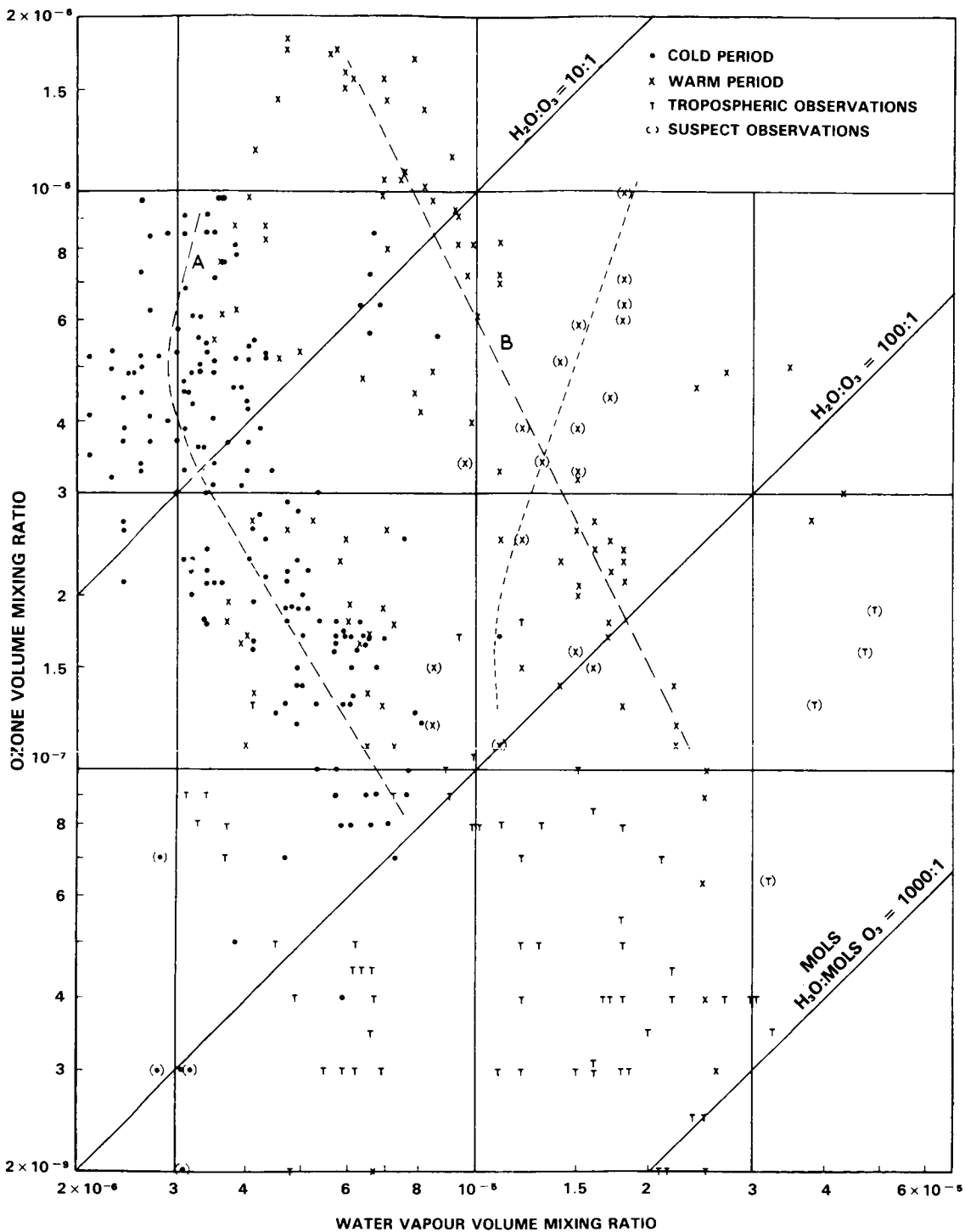


Figure 5-53. (b) from MRF Canberra flights, January-February 1962, 52°N-68°N, Greenwich meridian. Compare negative correlation in stratospheric air with that at high northern latitude points in part (a). From Roach (1962).

A feature common to all general circulation models is the difficulty of defining an objective, realistic tropopause. The representation at high latitudes is often poor, and it is extremely difficult to reproduce a temperature structure at the tropical tropopause which will dry the air there to the correct degree.

### 5.3.2 Operational Weather Forecasting Models

The Met Office global forecast model with levels at 1000, 950, 850, 700, 500, 400, 300, 250, 200, 150, 100, 70, 50 and 30 mb, and with lat.  $\times$  long. resolution  $1.5^\circ \times 1.875^\circ$  failed to produce good wind field analyses on the scale of polar front jet stream, as shown in Figures 5-54 and 5-55. The model's best analysis has the jet core speeds, and the wind shears on either side of it, seriously wrong and an attempt to compute potential vorticity shows that large errors are inherent, and that the horizontal contribution has to be considered. However, the limited area fine mesh of this model, covering  $30^\circ\text{N}$ - $80^\circ\text{N}$  and  $80^\circ\text{W}$ - $30^\circ\text{W}$  with a lat. long. grid of  $0.75^\circ \times 0.9375^\circ$  reproduced the aircraft observed wind shears much better, and in fact resolved a tropopause fold (Figure 5-37), with consistent trajectories, potential vorticity, ozone and water vapour structure. The potential vorticity and water vapour from the model were arrived at independently of the aircraft data, so the correlations between the  $\text{O}_3$  and PV, and between the 2 sets of humidities, are very significant.

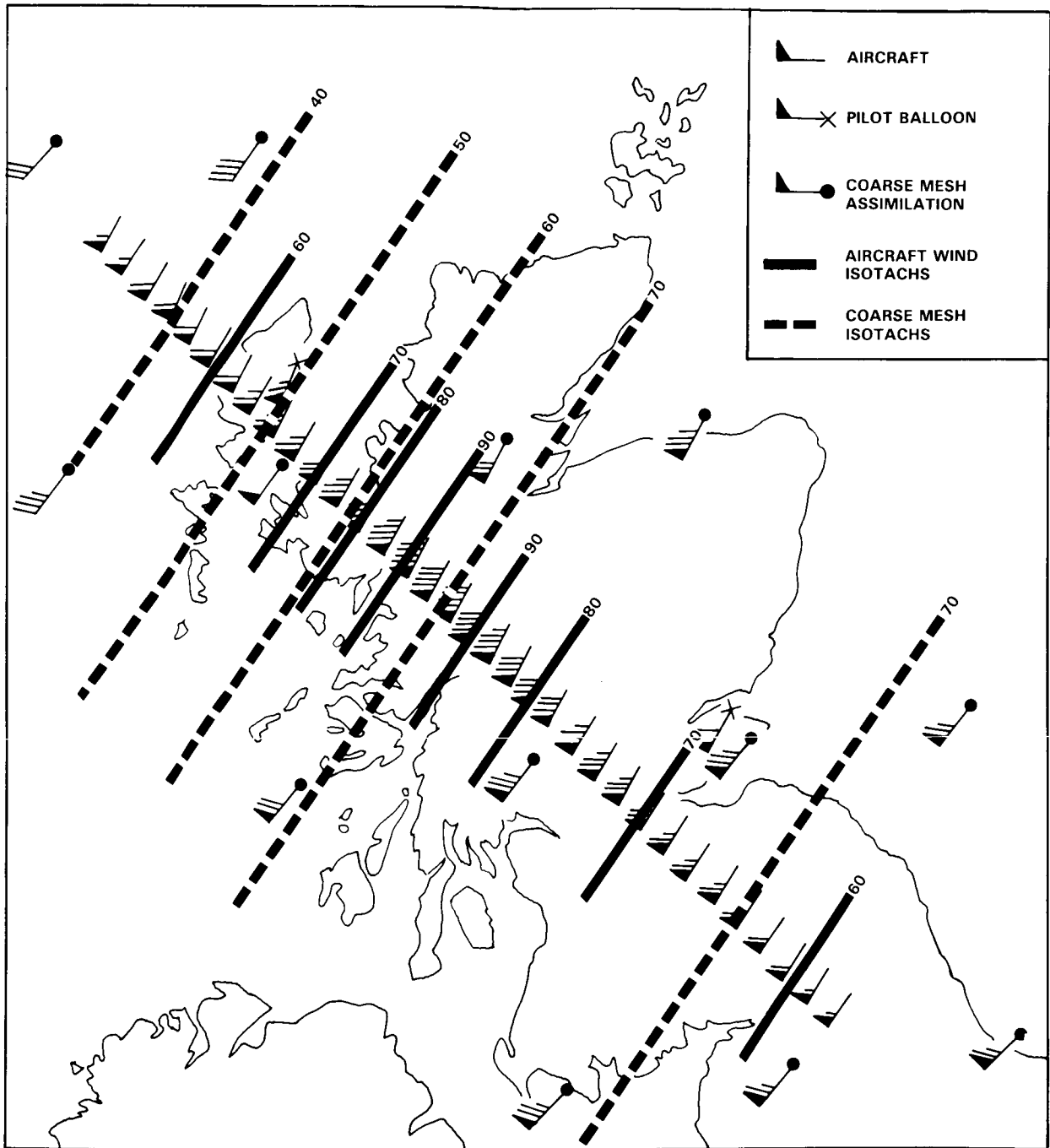
For reasons like those above present estimates of the annual average global transport of  $\text{O}_3$  across the tropopause from general circulation models cannot be considered to be completely reliable, let alone of the structure of the distribution in space and time, which is probably more important than the single number. The fine mesh results, however, give some reason to believe that better estimates will be possible in future.

## 5.4 ASSESSMENT OF STRATOSPHERE-TROPOSPHERE EXCHANGE

In both tropics and extratropics, recent high quality case studies have improved and amplified our detailed understanding of the processes effecting troposphere-stratosphere exchange, while reinforcing the basic correctness of the qualitative, gross mechanisms suggested for ingress by Brewer (1949) and for egress by Reed (1955). These case studies may in future be given global scope by combining them with measurement and analysis systems such as the TOMS observations, and with numerical weather prediction models, one of which has been shown to resolve extratropical tropopause folding events when its lat  $\times$  long resolution was improved from  $1.5^\circ \times 1.875^\circ$  to  $0.75^\circ \times 0.9375^\circ$ . However, for such an approach to work for a specific species, its covariance with potential vorticity in the lower stratosphere and upper troposphere must be known. In the absence of measured profiles of global extent at, above and below tropopause level, a start could be made by preparing correlograms of ozone and potential vorticity from all available data. In the tropics, it is likely to be more difficult to use operational meteorological models to obtain global scale estimates of cross tropopause flux. It may be possible to use satellite imagery of the ice crystal formations associated with deep tropical convection (anvils), but the methodology is not yet established.

Many substantial uncertainties remain. Previous studies used a body count of tropospheric cyclogenesis to compute the mass transfer out of the stratosphere in middle and high latitudes, despite some indications that this was unlikely to be a satisfactory procedure (Mahlman, 1965). Recent studies show that one cut-off low had three exchange events develop in the first three days; it existed as an entity for over 10 days, but no airborne studies were made after day 5. This, and the vertical extent of stratospheric extrusions revealed in some recent studies (3 and even 4 km) suggests that past estimates of ozone transfer to the troposphere may have been too small. Since cut-off lows are often associated with blocking anticyclones,

# STRAT-TROP EXCHANGE



H593 FL180 508MB 1800Z 16 APRIL 1983

**Figure 5-54.** Wind speeds measured from the C130 aircraft compared with the coarse mesh ( $1.5^\circ$  lat  $\times$   $1.875^\circ$  long) assimilation winds. Note the agreement of the aircraft data with the pilot balloon winds, and the model failure to resolve the wind shears. Dashed contours are the model assimilation; solid contours are the aircraft data. The fine mesh ( $0.75^\circ$  lat  $\times$   $0.9375^\circ$  long) did a much better job of reproducing the shears and core velocity.

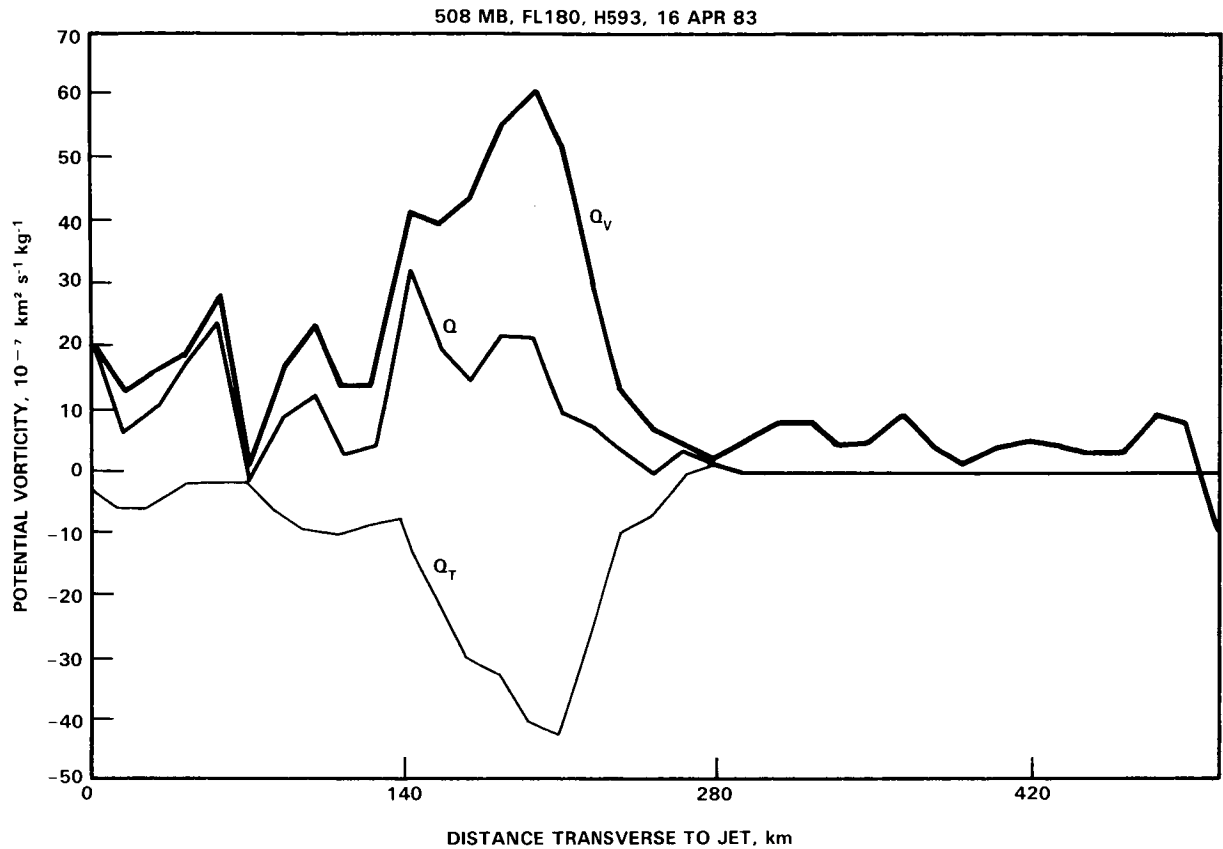


**Figure 5-55.** Potential vorticity from the aircraft winds of Figure 5-54. The vertical,  $Q_v$ , and transverse,  $Q_T$ , contributions to the total potential vorticity  $Q$  are shown. Note that  $Q_v$  is what meteorologists normally call "potential vorticity", and that the transverse component makes an important contribution near the core.

there could be substantial effects on the tropospheric ozone distribution. Blocking anticyclone/cut-off low systems occur preferentially in spring and autumn in the Northern Hemisphere in the NE American seaboard and Icelandic sectors, but in mid summer over the Central Pacific sector. They are also more intense and of longer duration in the Northern than in the Southern Hemisphere, where they are mostly confined to the New Zealand sector. There could thus be a systematic inter-hemispheric difference in tropospheric ozone content, and annual cycle variations which are a function of longitude arising purely from the dynamics of tropopause deformation during upper cyclogenesis. This supposition could be tested by assimilation analyses from a global weather model with adequate resolution (better than  $1^\circ \times 1^\circ$ ) with ozone treated as a tracer, possibly using TOMS data.

There is an apparent difficulty in reconciling the view that air enters the stratosphere solely in the tropics (which arises from recent case studies of water vapour profiles near cumulonimbus anvils in the Panama region) with the factor of 20 or 30 decrease in water vapour mixing ratio which occurs in a few kilometres above the mid-latitude tropopause. This is best resolved by saying that very little air above the hygropause cannot have entered in the tropics, but that air between the hygropause and the tropopause can have been mixed with extratropical tropospheric air moving quasi-horizontally, as suggested by dynamical and general circulation model studies. Whether or not air from this transition layer can be transported

## STRAT-TROP EXCHANGE

upward and equatorward in disturbed conditions, as predicted by a general circulation model, remains to be tested. Close examination of ozone, water vapour and methane profiles above the tropical hygropause is suggested. It is not securely established whether or not there is longitudinal variation in the water vapour mixing ratio at the tropical hygropause level. The matter is important, bearing in mind the potential of the deepest cumulonimbi for rapid vertical transport up to 20 km, with mixing extending up to 3 km higher.

There are two suggested explanations for the positive correlation observed in the stratosphere at and above hygropause level. One is that ozone and the component of water vapour coming from methane oxidation have a common source in the upper stratosphere. A second possibility arises from the general circulation model result of a positive correlation in ozone and water vapour between 30°N and 30°S at 70 mb, with no methane oxidation present. This was explained by deep convection in the western equatorial Pacific region drying ozone-poor air from near the surface.

It is possible that both mechanisms are effective; it might be expected that the first mechanism would give a positive correlation at high values of O<sub>3</sub> and H<sub>2</sub>O, while the second would maintain such a relationship at low values. This hypothesis clearly needs testing.

### 5.4.1 Unresolved Problems

An important unknown is connected with the extent to which tropopause folds are reversible. The data from recent studies in April 1983 and 1985 near the northern British Isles, and from April 1984 over the southwestern United States suggest that purely advective descriptions are incorrect, and that mixing is rapid. Nevertheless in some circumstances folds can be tracked for several days; if the mixed air is transported back to the stratosphere, then some tropospheric air may enter the stratosphere in mid-latitudes.

Both studies with global scale models and results from early aircraft studies in Project Springfield (Danielsen, 1964) suggest that some tropopause folds may split, with the supergeostrophic air to the right of the jet being decelerated and turned to the right, while the subgeostrophic air to the left of the jet is accelerated to the left. The supergeostrophic air descends into the south easterly flow around the upstream anticyclone, and is very unlikely to be reversible in the sense of return to the stratosphere. Such motion by folds has not been studied by aircraft with modern instrumentation, but is suggested by TOMS total ozone patterns in some troughs. Such volumes of air could reveal interesting chemical evolution. It is the subgeostrophic air which could re-enter the stratosphere. Figure 5-56 illustrates the splitting process.

There is a possible difficulty in need of resolution between the interpretation of the amplifying baroclinic wave given in Section 5.2.3.2 and the local dynamical constraint of potential vorticity conservation. It is shown that in such waves, subtropical air is transported poleward on isentropic surfaces that span the subtropical troposphere and the polar stratosphere, and that this transport exceeds that of polar air equatorward on the same surfaces. However, if the tropopause is advected with the air, exchange is not necessarily implied. The decrease in the water vapour profile, by roughly a factor of 30 within less than a scale height above the mid-latitude tropopause, argues that exchange does occur, but it is not clear how the large increase in potential vorticity needed to change tropospheric air into stratospheric air is achieved. In this context, the roles of radiative transfer and the presence of high cloud (cirrus), which occurs frequently in the warm sector of baroclinic lows, need examination; it may be also that the radiative time scale for the relaxation of cut-off highs which have moved to higher latitudes, as suggested in Section 5.2.3.2, needs further study. The time scales in actual cases have not as yet been established. There is one case study (Shapiro *et al.*, 1980), where in a split jet structure, tropospheric air with anticyclonic vorticity (i.e., low

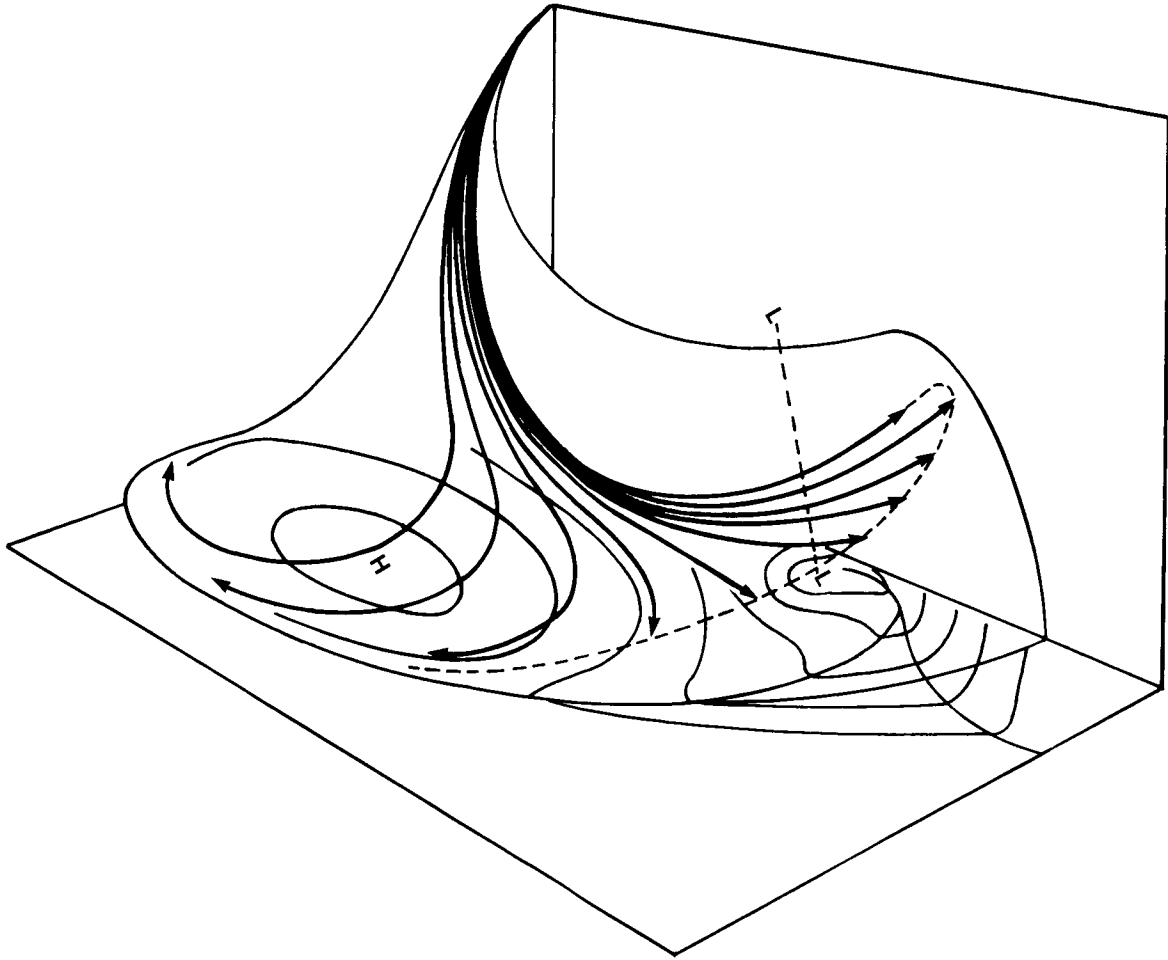


**Figure 5-56.** Schematic of trajectories of air extruded in a tropopause fold, relative to surface pressure pattern. The orthogonal planes are to lend a three-dimensional appearance. The air curving anticyclonically and downwards is unlikely to return to the stratosphere. The upward moving, cyclonically curved trajectories could return to the stratosphere, subject to constraints imposed by mixing processes.

potential vorticity) did move into the stratosphere, but which left open the question of how long it could stay there. Exchange from troposphere to stratosphere near jet streams needs more examination experimentally.

#### 5.4.2 Recommended Future Studies

There have as yet been no studies of exchange at the subtropical jet streams. In view of the considerable differences between such jets and polar front jet streams (see for example Newton and Trevisan, 1984), and the general circulation model results which suggest that partial inertial oscillations in the STJ could play a role in stratosphere-troposphere exchange, such studies are required, particularly of the E Eurasian jet stream in winter and spring.

It is not certain how much of the stratospheric air in cut-off lows is mixed into the troposphere after the system becomes isolated from the polar vortex. Similarly, the posited return of upper tropospheric

## STRAT-TROP EXCHANGE

air in baroclinic cyclogenesis to the stratosphere has not been characterized by detailed aircraft studies. A combination of upward looking DIAL ozone profiles and dropsondes to get  $u$ ,  $v$ ,  $w$ ,  $T$ ,  $P$  and humidity would be valuable, particularly in association with TOMS ozone mapping, which provides the means for a global extrapolation of local studies of each of the exchange processes.

Investigation of the largest cumulonimbus storms, in the equatorial W Pacific Indian Ocean sector, the Bay of Bengal and at mid-latitudes in summer is required. The simple experiment of Barrett *et al.* (1973) could be very informative if repeated with modern instrumentation. It is also necessary to see if there is a widespread, thin layer of ice crystals in the region of low tropical tropopause temperatures (Figure 5-5).

There is also a clear need to examine the nitrogen oxide content of the air injected into the stratosphere by large Cb, and also that left behind by dissipating anvils. The ability of Cb to rapidly transport air from near the surface to tropopause level suggests that the whole range of the chemical composition of their inflow and outflow may need characterization. It is possible that suggestions made in 1976 that lightning may be an important source of  $\text{NO}_x$  for the lower stratosphere are correct, but better measurements are required.

There are instances in the literature where studies of the flow over mountains has revealed extremely steep slopes in the isentropes in the upper troposphere and lower stratosphere. Such situations should be investigated on a case study basis; the Himalayas and the Andes are outstanding examples of course.

Finally, if the global distribution of ozone flux across the tropopause is required in detail, satellite profiles in the lower stratosphere and upper troposphere will be required ultimately, as a check on techniques using global weather prediction models and potential vorticity.